Dynamic Modeling of Target's Cooling Systems

Maximilian Cahlin

Thesis for the degree of Master of Science in Engineering
Division of Thermal Power Engineering
Department of Energy Sciences
Faculty of Engineering | Lund University

Dynamic Modeling of Target's Cooling Systems

Maximilian Cahlin

June 2021, Lund

This degree project for the degree of Master of Science in Engineering has been conducted at the Division of Thermal Power Engineering, Department of Energy Sciences, Faculty of Engineering, Lund University, and at ESS.

Supervisor at the Division of Thermal Power Engineering was Associate Professor Marcus Thern
Supervisor at ESS was Jaime Arriagada
Examiner at Lund University was Professor Jens Klingmann

Thesis for the Degree of Master of Science in Engineering

ISRN LUTMDN/TMHP-21/5478-SE

ISSN 0282-1990

Division of Thermal Power Engineering
Department of Energy Sciences
Faculty of Engineering, Lund University
Box 118, 221 00 Lund
Sweden

www.energy.lth.se

Abstract

The thermal energy generated from the spallation process in the ESS facility must be cooled by cooling systems in order to ensure safe operation of the facility. It is of interest to understand what operating conditions of the cooling systems will ensure this safety for both stationary conditions and transient events.

A part of the water cooling system in ESS was modeled in Dymola with the aid of the free Modelica Standard Library and the Buildings Library. Component models such as a pipe segment, a gas and liquid separation tank, a delay tank and a heated component have been constructed. The component models were verified with manufacturer data or known and well-proven mathematical calculations but could not be validated with data from the actual cooling system since it is yet to be in operation. With the system model, normal operation and disturbance cases were simulated. The disturbance cases have been simulated in order to analyze what operating conditions will trigger an alarm and also discern the duration from the introduction of a disturbance to the triggering of an alarm. The temperature transients in the cooling system could be simulated, however the pressure transients could not due to convergence issues.

Acknowledgements

My deepest gratitude goes to my supervisor at ESS, Jaime Arriagada, for his guidance and support. His advice and encouragement has been an incredible help. I would like to thank Per Nilsson at ESS for his help and advice regarding dynamic modeling and for his interest in the thesis. I would also like to thank the staff at the Target Division for their warm welcome and their knowledge and ESS for providing a workplace and funding of the thesis. It was interesting to follow the construction and progress of the ESS facility during my time at ESS.

Finally, I would like to thank my supervisor at LTH, Associate Professor Marcus Thern for his academic advice and my examiner, Professor Jens Klingmann for his review of the thesis.

Contents

List of figures

List of tables

Nomenclature

Symbols

ρ	Density	kg/m^3
A	Area	m^2
v	Velocity	m/s
t	Time	s
x	Spatial coordinate along the fluid flow direction	m
p	Pressure	Pa
F_f	Pipe friction	N/m
g	Gravitational acceleration	m/s^2
z	Spatial coordinate along the gravity direction	m
u	Specific internal energy	J/kg
k	Thermal conductivity	W/mK
T	Temperature	K
$\dot{Q}$	Heat transfer rate	W
w	Width	m
d	Diameter	m
K	Loss coefficient	-
n	Quantity	-
Δp	Pressure drop	Pa
$\dot{m}$	Mass flow rate	kg/s
f_T	Friction factor	-
θ	Angle	°
k_{vs}	Flow coefficient of a valve at maximum opening with a pressure differential of 1 bar	m^3/h
k_{vv}	Flow coefficient of an obstruction with a pressure drop of 1 bar	m^3/h
C	Heat capacity	J/K
c_p	Specific heat capacity	J/kgK
m	Mass	kg
π	Pi	-
l	Length	m
h	Convective heat transfer coefficient	W/m^{2}K
V	Volume	m^3
α	Angle	°
ζ	Resistance coefficient	-
λ	Friction coefficient	-
$\varepsilon_0{}^{-Re}$	Coefficient	-

ζ_{φ}	Coefficient	-
ζ_0	Coefficient	-
A_f	Flow area of obstructions cross-section	m^2
A_g	Area of obstructions front cross-section	m^2
$H2$	High alarm limit	-
$L2$	Low alarm limit	-
ε	Heat transfer effectiveness	-
Z	Ratio of minimum and maximum flow rate capacity	-
FR	Type of flow in the heat exchanger, ex counter flow, cross flow etc.	-
H	Height	m
$\dot{V}$	Volumetric flow rate	m^3/h
ρ_0	Reference density, density of water at 4 °C and 1 atmosphere	kg/m^3
N	Pump speed	rpm
ζ	Eigenvalue	-
η	Eigenvector	-
B	Constant	-
a	Constant	-
c	Proportional gain	-
τ	Time constant	s
y	Variable	-
L	Water level	m

Subscripts

i	Inner
o	Outer
l	Liquid
s	Solid
0	Previous
n	Nominal
∞	Ambient
w	Wall
E	Elbow
R	Reducer
T	T-junction
V	Valve
tot	Total
large	Large
small	Small

Abbreviations

ESS	European Spallation Source
MSL	Modelica Standard Library
P&ID	Piping and instrumentation diagram
GLS	Gas and liquid separation
HSV	Hand shut-off valve
YSV	Actuator shut-off valve
FSV	Flow safety valve
FCV	Flow control valve
HCV	Hand control valve
PLC	Programmable logic controller
ESDIRK	Explicit singly diagonal implicit Runge-Kutta
PFD	Process flow diagram
P	Pump
TE	Temperature sensor
PSZ	Pressure switch
HX	Heat exchanger

1 Introduction

1.1 Background

The European Spallation Source (ESS) is a European Research Infrastructure Consortium, who are in cooperation with Skanska, constructing a research facility based on a neutron source in Lund, Sweden. The objective of the facility is to generate neutrons for neutron scattering in different instruments. The neutron beams at ESS will be up to 100 times brighter than existing facilities [1]. The scattering of the neutrons from the investigated samples at ESS can give researchers information on a molecular and atomic level. The facility can enable new opportunities for scientific discovery in fields such as material science, life science, energy and environmental technology [2]. The Data Management and Software Centre is located in Copenhagen, Denmark. The objective of the center is to handle and analyze scientific data from the ESS instruments.

Construction of the research facility began in 2014 and it is estimated that the ESS User Program will commence in 2023, allowing between 2000-3000 scientists to conduct experiments at the facility [2][3]. In 2013 the total construction cost was estimated to 1,843 billion Euros [4]. In January 2020 the project completion is at 65 % with 507 employees from 56 nations working together to strive for the set goal [3]. An aerial view of the ESS facility is shown in Figure 1.1.

Figure 1.1: Aerial view of the ESS construction site [5].

ESS is formed by three main subsystems: Accelerator, Target and Instruments. At the beginning of the linear accelerator, an ion source containing hydrogen gas is present. Fast varying electromagnetic fields heat the hydrogen gas resulting in evaporation of electrons from the

hydrogen molecules, leaving a proton plasma in the ion source. The protons are then guided to the accelerator beam line, which is under vacuum. The accelerator beam line consists of piping and accelerator structures. Magnets around the piping between the accelerator structures focuses and guides the proton beam in the intended direction while the accelerator structures accelerate the proton beam. The proton beam will pass through the proton beam window, which purpose is to separate two atmospheres at different pressures, before entering the Monolith [6]. The purpose of the Monolith is to shield against the ionizing radiation that arises due to the spallation of the neutrons [7]. Before contact with the rotating target wheel the proton beam will reach 96 % of the speed of light [7]. The proton beam consists of 2.86 ms long proton pulses at a frequency of 14 Hz and has an average beam power of 5 MW [8]. The rotating wheel with a diameter of 2.6 m, a mass of 4900 kg and a rotation of 23.33 rpm consists of around 7000 tungsten blocks encased in steel shielding [7]. When the proton beam comes in contact with the rotating target wheel, neutrons are spallated from the tungsten bricks. The proton beam will be in contact with the target wheel for about 4% of the total operation time [8]. The spallated neutrons are then slowed down to appropriate energy levels by the moderators and reflected by the reflectors to different instruments through 42 beam ports consisting of guides, optics and filters [7]. The thermal energy generated from the spallation process must be cooled down in a series of cooling systems in order to prevent components such as the rotating wheel, moderators, reflectors among others from getting damaged. A cross section view of the Monolith is shown in Figure 1.2.

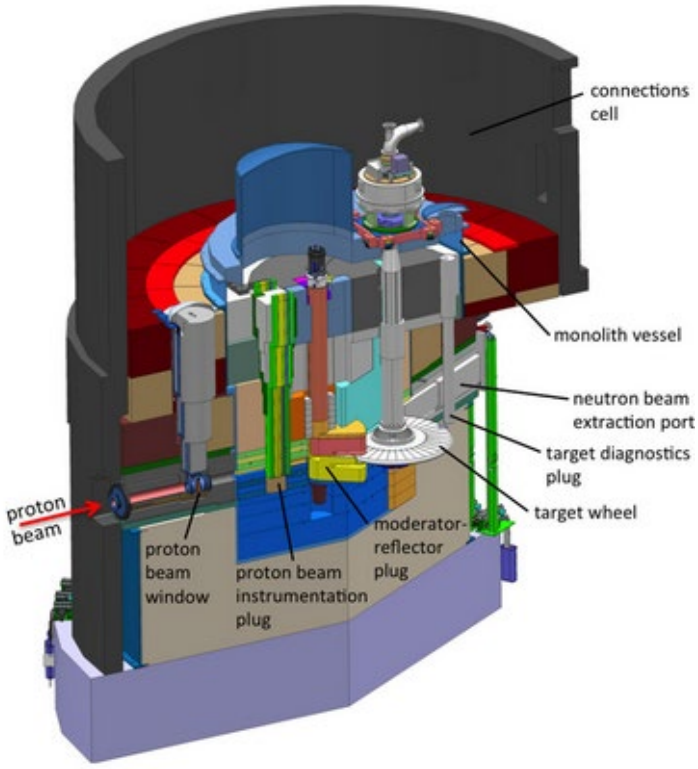

Figure 1.2: Cross section view of the Monolith [9].

1.2 Objective

Dymola models have been developed for the cooling systems by using commercial libraries. These models have been used during the basic and detailed engineering design phase for dimensioning of main equipment. There is a however a desire to obtain improved models in order to use them for several other applications. There is also a desire that the improved models are constructed from free component libraries to avoid the economic cost of maintaining the commercial libraries. The objective is therefore to develop improved Dymola models on the cooling systems based on the Modelica Standard Library (MSL), to verify them and use them to run simulations and studies on normal and non-normal operating conditions, transient conditions and accident analysis.

The existing models will be studied and used as reference in order to develop improved models. The models to be improved are specific component models such as heat exchangers, pumps and delay tanks. They will be upgraded with data made available from the ESS partners and suppliers. The models will be verified against experimental or calculated data as much as possible.

The specific simulations that will be performed are: normal operational modes, start and stop, pump trip in different cooling systems and accident analysis.

1.3 Disposition

The disposition of the report is shown below.

Dynamic modeling – A brief introduction to dynamic modeling is given.

Programs – The programs used are presented.

Cooling Systems – The cooling systems in ESS are described.

Modeling – The system modeling procedure is presented. Thereafter, the function of each component is described before the modeling procedure of the component is given.

Verification and validation – The verification and validation of component models are presented.

Simulation set-up – The set-up of the simulations is presented.

Results – The results of each case study are shown and discussed.

Discussion – A general discussion and challenges are discussed.

Conclusion – The most important conclusions are presented.

Future work – Recommendations for future work are given.

1.4 Dynamic modeling

Both the steady-state behavior and the transient behavior of a cooling system is of interest during the design phase. During nominal steady-state operation, process variables at each point in the cooling system are constant. When a disturbance is introduced to the cooling system, a transient occurs until a new steady-state is reached. During transients the process variables alter with time, therefore the time variables need to be added to the balance equations to be able to simulate the transient behavior of the cooling system. Dynamic modeling of the cooling systems is performed in order to analyze how the process variables in the cooling systems respond to disturbances. Normal disturbances include operations such as a change in opening of a control valve and a change in rotational speed of a pump. Unexpected disturbances include sudden pump trips or sudden leakages. Disturbance scenarios can be simulated in order to analyze if and when alarm limits of the sensors have been exceeded. With the results, alarm limits of the sensors can be adjusted and operational procedures can be altered to ensure that the cooling systems will operate in safe conditions.

The balance equations used by the Modelica Standard Library are given by equations (1.1) - (1.4) [10].

Mass balance:
$$\frac{\partial(\rho A)}{\partial t} + \frac{\partial(\rho A v)}{\partial x} = 0 \tag{1.1}$$

Momentum balance:
$$\frac{\partial(\rho v A)}{\partial t} + \frac{\partial(\rho v^2 A)}{\partial x} = -A\frac{\partial(p)}{\partial x} - F_f - A\rho g\frac{\partial z}{\partial x} \tag{1.2}$$

Energy balance 1:
$$\frac{\partial(\rho\left(u + \frac{v^2}{2}\right)A)}{\partial t} + \frac{\partial(\rho v\left(u + \frac{p}{\rho} + \frac{v^2}{2}\right)A)}{\partial x} = -A\rho\frac{\partial z}{\partial x} + \frac{\partial}{\partial x}\left(kA\frac{\partial T}{\partial x}\right) + \dot{Q}_e \tag{1.3}$$

Energy balance 2:
$$\frac{\partial(\rho u A)}{\partial t} + \frac{\partial\left(\rho v\left(u + \frac{p}{\rho}\right)A\right)}{\partial x} = vA\frac{\partial p}{\partial x} + vF_f\frac{\partial}{\partial x}\left(kA\frac{\partial T}{\partial x}\right) + \dot{Q}_e \tag{1.4}$$

For a control volume with dynamic balance equations, the energy, mass and momentum in a control volume can alter with time. To gain a better understanding of the dynamic balance equations a simple example is presented, comparing the dynamic results with the steady-state results.

A control volume has an inlet and an outlet with a constant volume. The inlet mass flow rate is constant and the control volume is insulated, suddenly the fluid temperature at the inlet increases from 20 °C to 50 °C. The dynamic and steady-state results of the control volume temperature are shown in Figure 1.3. In the dynamic case, the control volume temperature is a function of time due to the accumulation of energy in the control volume. For the given boundary and initial conditions,

the time it takes to reach steady state in the control volume depends on the mass and the specific heat capacity of the fluid. The control volume can be more complex by including the mass and specific heat capacity of the walls, convection between the fluid and the wall and convection between the wall and the ambient. With a dynamic energy balance, the thermal inertia of a fluid and wall is included in the simulations, making it possible to capture the time delay of a temperature sensor.

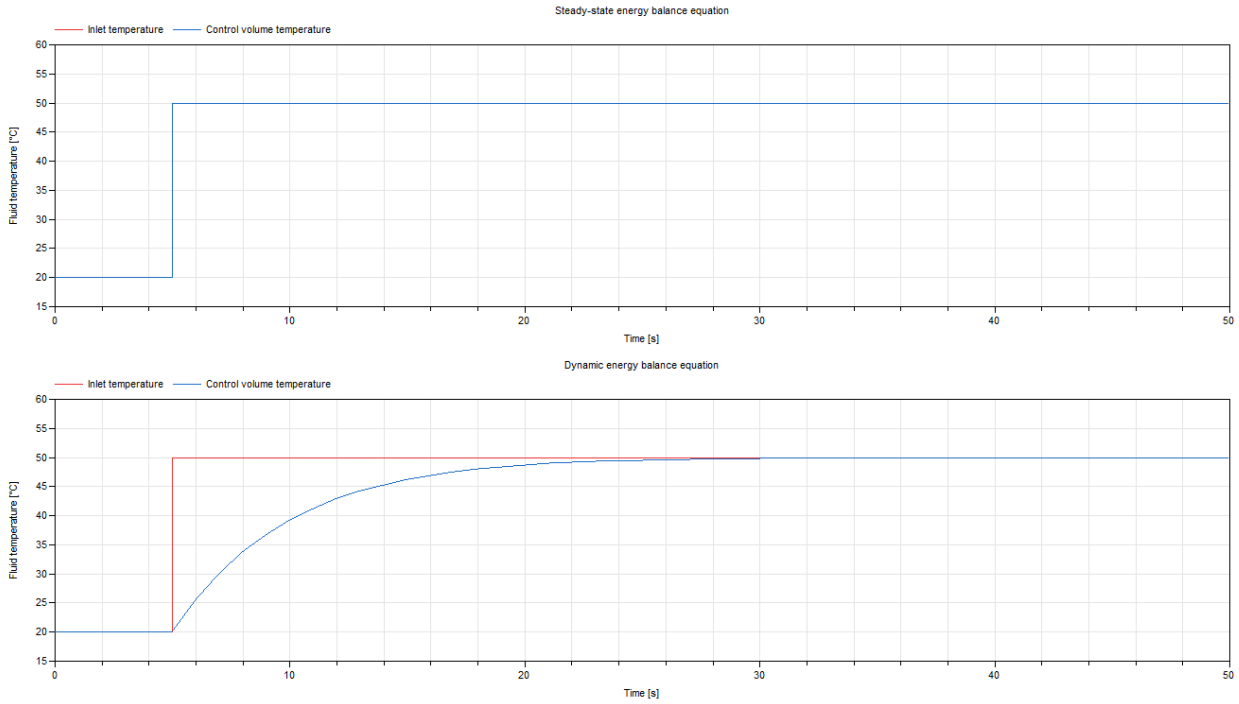

Figure 1.3: The control volume temperature with a steady-state and dynamic energy balance equation.

The dynamic and steady-state results of the control volume mass are shown in Figure 1.4. When the inlet fluid temperature suddenly increases from 20 °C to 50 °C, the control volume temperature will be a function of time for the dynamic energy balance. As the control volume temperature increases, the density will decrease. As the water volume in the control volume is assumed constant, the mass of the control volume will decrease with time for the dynamic mass balance. With a dynamic mass balance, the fluid mass in pipes as a function of time can be captured. Level changes of tanks can also be captured due to an increase of fluid mass in the tank.

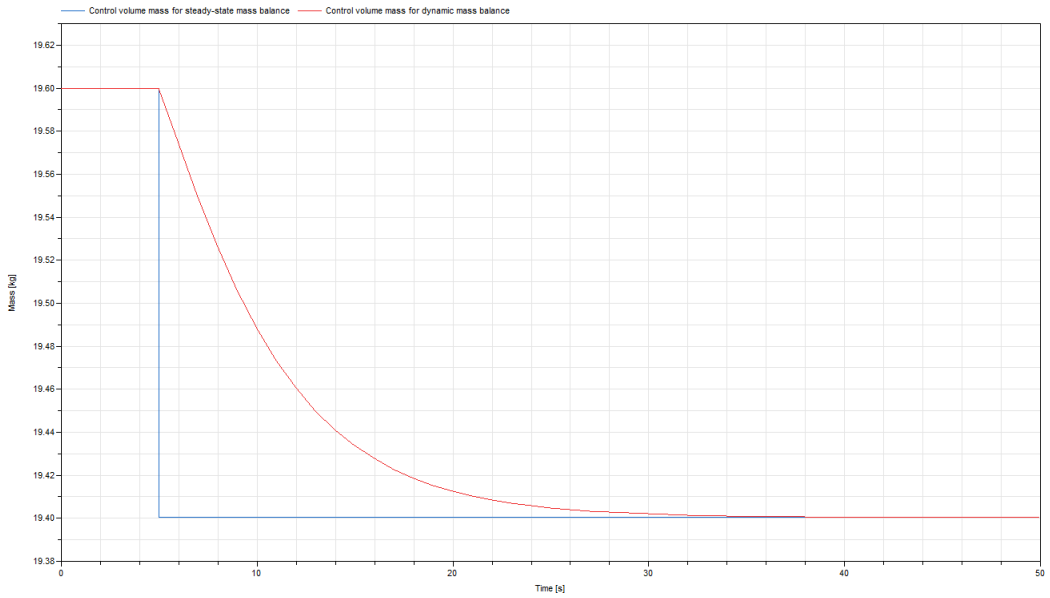

Figure 1.4: The mass of a control volume with a steady-state and dynamic mass balance equation.

As the inlet mass flow rate is kept constant and the control volume density decreases, the fluid of the control volume must accelerate. A pressure wave is created and after a period of time a lower steady-state pressure is achieved. This is because some static pressure is converted to dynamic pressure. The steady-state and dynamic results of the mean velocity and the pressure of the control volume is shown in Figure 1.5 and Figure 1.6 respectively. With a dynamic momentum balance, fluid decelerations and pressure surges due to sudden disturbances such as pump trip and valve closing can be captured.

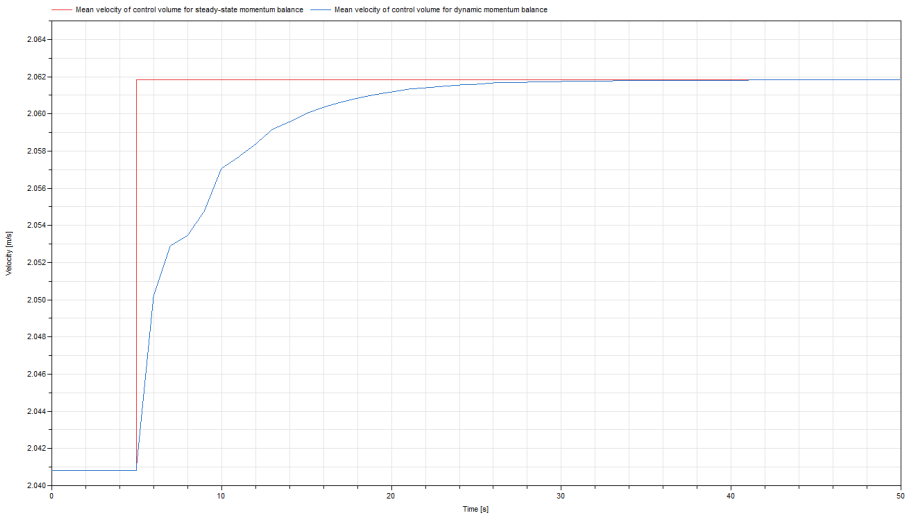

Figure 1.5: Mean velocity in a control volume with a steady-state and dynamic momentum balance.

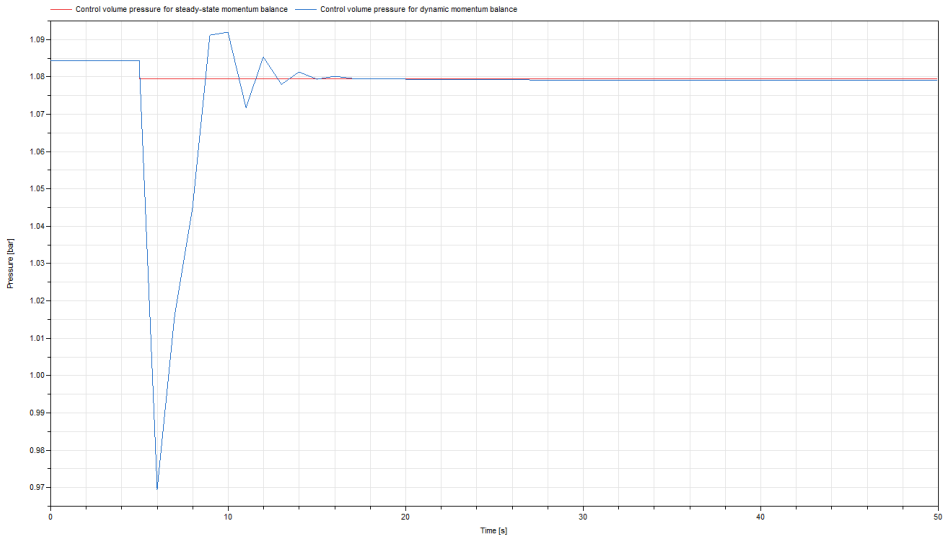

Figure 1.6: Control volume pressure in a control volume with a steady-state and dynamic momentum balance.

1.5 Programs

The dynamic modeling and simulation of the cooling systems is performed in Dymola, a modeling and simulation environment provided by Dassault Systèmes [11]. It is suitable for modeling over multiple engineering domains such as thermodynamics, heat transfer, fluid mechanics and control theory. Tasks are performed in the modeling and simulation tabs of the program. Models can be created from graphical and textual editors. The component models can be user-defined or retrieved from existing model libraries. The simulations of the created models are performed and the results are plotted in the simulation tab.

The Modelica language is an object-oriented and equation-based modeling language used for modeling large and complex physical systems. The Modelica language is developed by the non-profit and non-governmental organization Modelica Association [12]. The organization also develops and maintains the Modelica Standard Library (MSL), a free component model library which consists of a wide variety of component models from engineering fields such as thermodynamics, fluid dynamics, control theory and mechanics [12]. Mathematical and logical operations are also included in the MSL. The system models are constructed from component models in the MSL and the free and open-source Buildings library developed by Lawrence Berkeley National Library [13]. The code generated in Dymola is compiled by C Compiler Visual C++ 2010 Express Edition.

The measurements of the three-dimensional models of the cooling systems are performed in Autodesk Navisworks Freedom 2020.

For mathematical computations done in order to verify component models, Microsoft Excel 2016 is used.

2 Cooling systems

There are three levels of cooling systems in ESS. An overview of the cooling systems and their interfaces are shown in Figure 2.1. The levels are separated from each other by heat exchangers, which is shown as an interface in Figure 2.1.

There are primary cooling systems which cool specific Target components, intermediate cooling systems and the central utility building cooling systems. The heat recovered in the central utility building cooling systems is transferred to the district heating network. Different mediums are used in the cooling systems. Most of the cooling systems use water as cooling medium while one cooling system use helium in the gaseous phase as cooling medium.

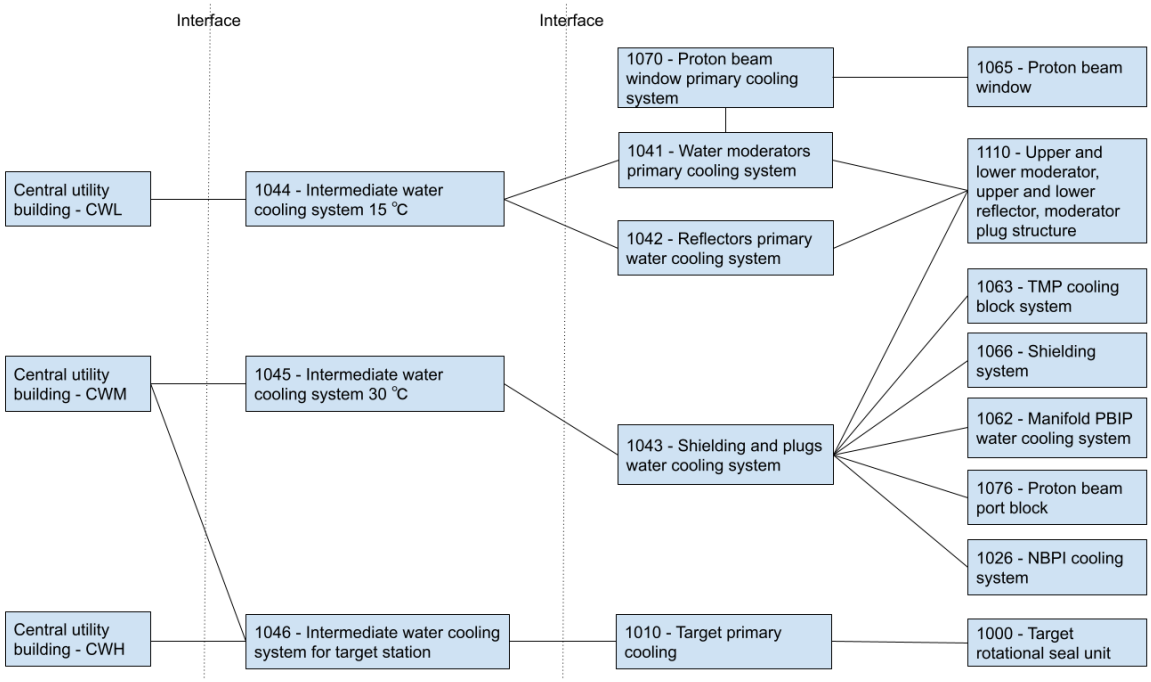

Figure 2.1: Overview of all the cooling systems.

2.1 Primary water cooling systems

The objective of system 1010 is to cool the rotating target wheel consisting of 36 sectors of around 7000 tungsten blocks [7]. The rotating target wheel is cooled by gaseous helium circulating around the tungsten blocks. The heat is removed from the system by three tube and shell heat exchangers located in series. The third heat exchanger is located downstream two parallel circulators in order to transfer heat produced by the active circulator. One of the circulators is redundant in order to increase the availability of the cooling system. Filters are placed at both the inlet and the outlet of system 1000 to avoid clogging of particles in the target wheel and particle contamination of system 1010 [14].

The objective of system 1043 is to cool six different systems with a total of 11 separate pipelines cooling these systems. The main components in system 1043, listed in the direction of the flow, include a gas and liquid separation vessel open towards the atmosphere, a plate heat exchanger, two centrifugal pumps in parallel while one pump is redundant, a delay tank and a filter [15].

The objective of system 1042 is to cool the upper and lower reflectors. The main components in system 1042, listed in the direction of the flow, include a gas and liquid separation vessel open towards the atmosphere, a plate heat exchanger, centrifugal pumps in parallel while one pump is redundant, a delay tank and a filter [16].

The objective of system 1041 is to cool system 1100 and system 1070. Furthermore, the objective of system 1070 is to cool system 1065. All the previous named systems are described in more detail in chapter 2.6.

2.2 Intermediate water cooling systems

The objective of system 1044 is to cool systems 1041 and 1042. In system 1044 the cooling flow to system 1041 and 1042 is extracted at the same connection point in the closed loop. The main components in system 1044, listed in the direction of the flow, include an expansion vessel open towards the atmosphere, a centrifugal pump, a plate heat exchanger and a filter [17].

The objective of system 1045 is to cool system 1043. The construction of system 1045 is similar to system 1044. The main components in system 1044, listed in the direction of the flow, include a level tank open towards the atmosphere, a centrifugal pump, a plate heat exchanger and a filter [18].

The objective of system 1046 is to cool system 1010. System 1046 consists of three almost identical closed water cooling loops. For each closed loop, the cooling flow flows through a separate heat exchanger located in system 1010. All three heat exchangers in system 1010 are located in series. The flow in closed water cooling loop 1 flows through the first heat exchanger in system 1010, the flow in closed water cooling loop 2 flows through the second heat exchanger downstream in system 1010 and the flow in closed water cooling loop 3 flows through the third heat exchanger downstream in system 1010. Closed water cooling loop 1 is cooled by the central utility building CWH water cooling loop while closed water cooling loops 2 and 3 are cooled by central utility building CWM water cooling loop. The main equipment in every closed water cooling loop, listed in the direction of the flow, include a gas and liquid separation tank, a plate heat exchanger and a centrifugal pump [19].

2.3 Central utility building

Three closed water cooling loops from the central utility building cool the three intermediate water cooling systems via heat exchangers in the intermediate water cooling systems. The fluid temperature from CWL to system 1044 is 8°C and the heat transfer rate at the interface is 400 kW [20]. The fluid temperature from CWM to system 1045 is 25°C and the heat transfer rate at the interface is 2025 kW [20]. The fluid temperature from CWH to system 1046 is 50°C and the heat transfer rate at the interface is 2750 kW [20].

2.4 Location

The central utility building is located a few hundred meters from the target station building and the intermediate and primary water cooling systems are located in the target utility rooms. The utility rooms are located next to the connection cell on the opposite side from where the proton beam hits the target wheel. The target wheel, moderators and reflectors are located inside the monolith vessel which is in turn located inside the connection cell [21]. The utility rooms are located on two floors: on the bottom floor the heat exchangers and pumps are located and on the top floor the gas and liquid separation tanks and delay tanks are located [22]. The location of each cooling system is shown in Figure 2.2.

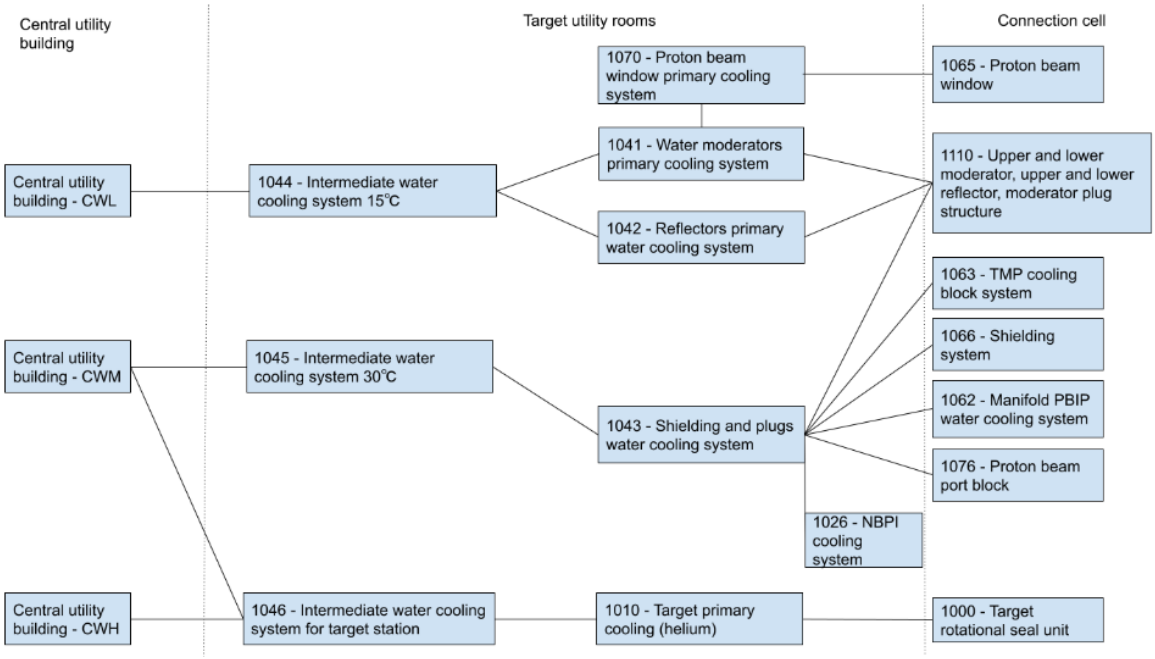

Figure 2.2: Location of the cooling systems.

2.5 Safety systems

The warning and alarms limits of the controllers and sensors in the cooling systems are a part of a safety system called Basic Process Control. It is the first safety level and its purpose is to assure safe operation in order to avoid damaging components in the cooling systems. This safety system is implemented in the PLC in all the cooling systems. Two more safety systems exist which monitor more crucial process values in the entire ESS facility. The second and third safety level is called the Machine Protection System and the Target Safety System respectively.

2.6 Systems to be modeled

The cooling systems to be modelled are systems 1041, 1070, 1110 and 1065. The functional description and the control logic of the cooling systems will be described.

2.6.1 Description of systems

System 1041 is a closed loop circulation system which uses demineralized water as cooling medium. The function of system 1041 is to ensure heat transfer from the upper and lower moderator and the proton beam window to system 1044 via a plate heat exchanger. One hermetic centrifugal pump in system 1041 circulates the water and is controlled by a frequency converter. A parallel pump is included in system 1041 to improve the availability of the system. The gas and liquid separation tank is a tank which functions as a pressurizer in the closed circuit and as a degasser of the products of the water radiolysis. It is also designed to retain water for a specified duration. The delay tank is designed to retain the water for a specified duration to ensure the radioactive decay of radionuclides with a short half-life. The function of the filter is to retain larger particles after the assembly and maintenance. The filter cartridge is not used in operation however the filter housing is still present in the closed system. The control valves regulate the flow to the cooling objects, the check valves prevent backward flow and the hand valves are used during maintenance. The transmitters transmit process variables and eventual warning or alarms to the operator to ensure that the cooling systems operate in safe conditions. System 1041 should form a barrier to prevent spreading radioactive substances between the cooled components and system 1044. This is guaranteed by having a lower pressure at the hot side of the heat exchanger in system 1041 relative to the pressure at the cold side of the heat exchanger [23].

Cooling flow is diverted to system 1070 from a connection point in system 1041 upstream the pumps. In system 1070 a pump aids in the circulation of the flow to and from the proton beam window in system 1065. The entire system 1065 is located in the connection cell. There are two separate flows to the proton beam window, the objective of one flow is to cool the proton beam window and the frame which it is attached to, whereas the objective of the other flow is to cool the two flanges at both sides of the proton beam window. The flow is finally connected back to system 1041 at a connection point downstream the delay tank [24].

Four separate flows are present to and from the moderators in system 1110. Two flows are needed for each moderator, where each flow cools half a moderator. The entire system 1110 is located in the connection cell [25].

The circulating flow needs to be continuously purified, resulting in a fraction of the flow being diverted downstream the pumps in system 1041 and adjoined upstream the pumps [26].

The cooling systems consists of a gas and liquid separation tank, a plate heat exchanger, two pairs of hermetic centrifugal pumps, pipelines, valves, controllers, sensors, transmitters and a delay tank [26][24][25] [27]. The components in the cooling system are described in the chapter 4. Simplified drawings based on the P&IDs of systems 1041 and 1070 are shown in Figure 2.3 and Figure 2.4 respectively while and a view of the three-dimensional models of systems 1041, 1070, 1110 and 1065 is shown in Figure 2.5 [26][22].

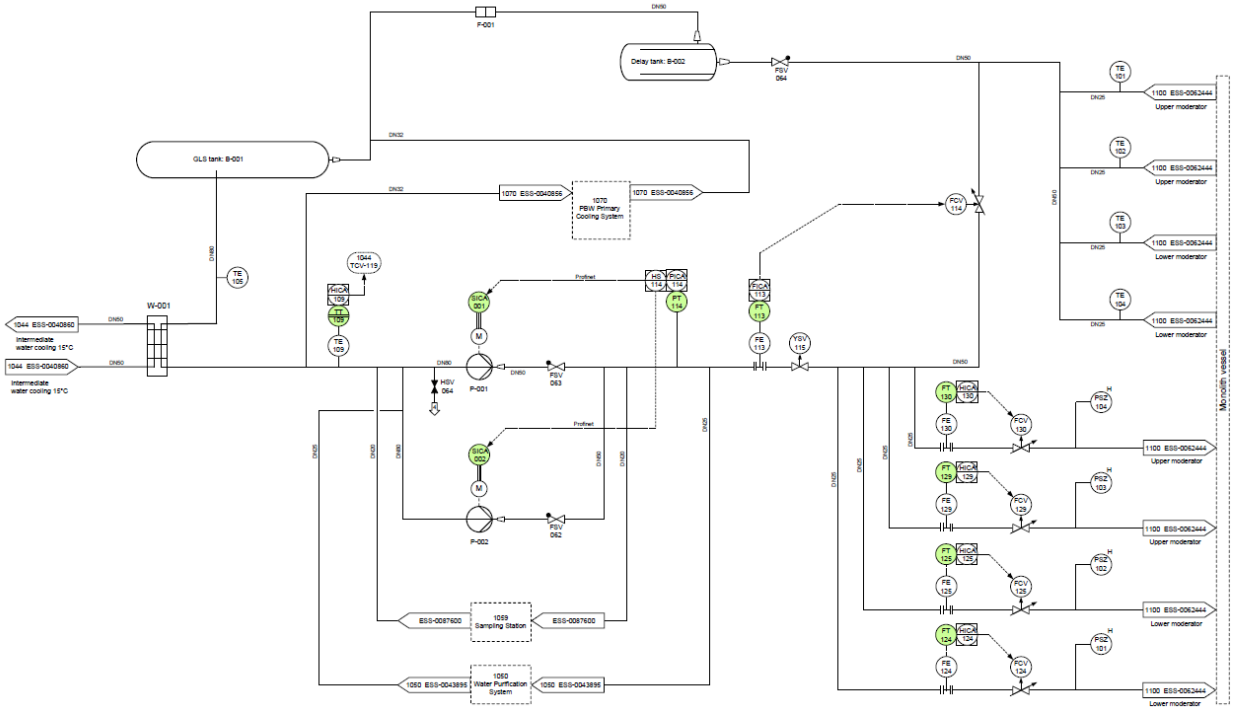

Figure 2.3: Simplified drawing of system 1041 based on the P&ID of system 1041 [26].

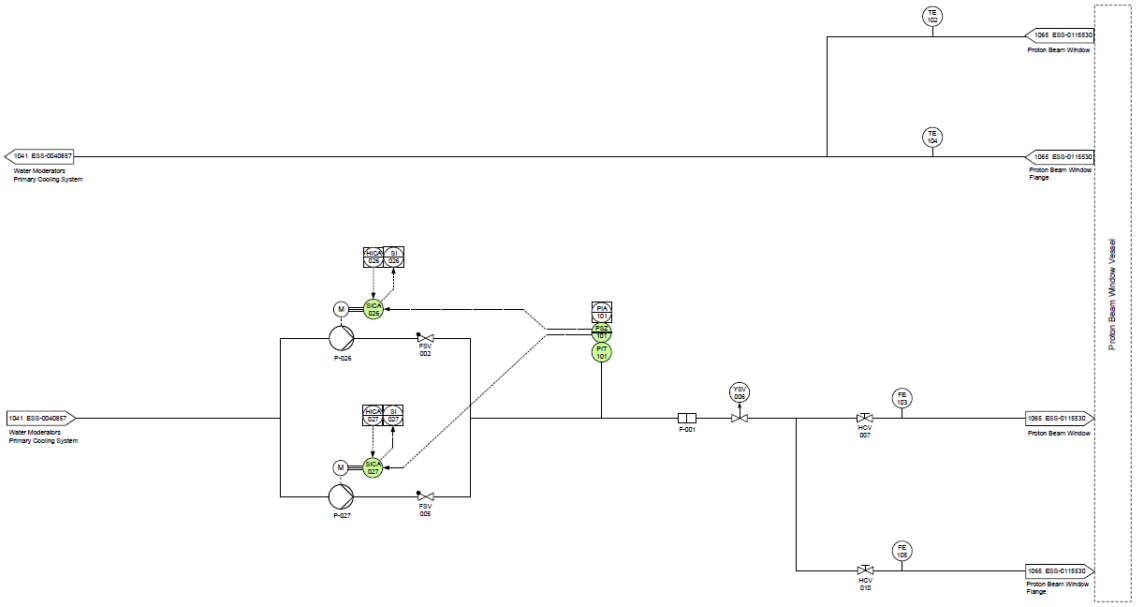

Figure 2.4: Simplified drawing of system 1070 based on the P&ID of system 1070 [24].

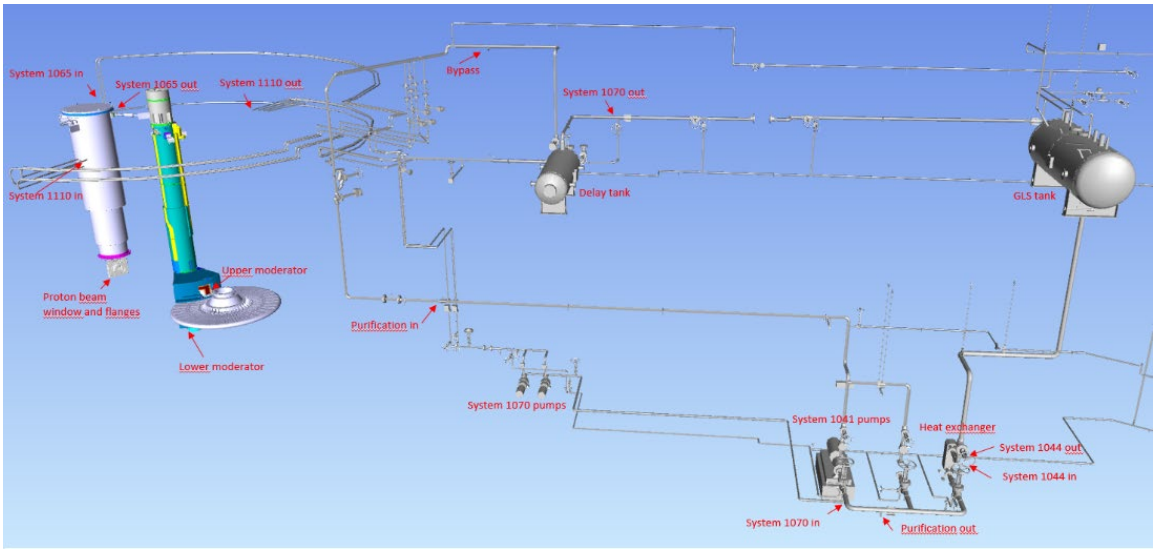

Figure 2.5: View of three-dimensional models of systems 1041, 1070, 1110 and 1065 [22].

2.6.2 States

During the operation of the ESS facility the cooling systems will enter different States. The program logic in the PLC declares which State each cooling system should enter. Each State has a set of sequences that are executed in a specified order and time. The States described briefly below are defined fully in [28]. Some assumptions are made in regards to which order sequences are

executed, but this will be clarified after the commissioning. The States of interest for the dynamic modeling of the cooling systems are:

- Off
- Standby
- Starting
- Running
- Stopping
- Fault

2.6.2.1 Off

This State is used for shut-down of the system and longer stops. Pumps in systems 1041 and 1070 are off, all controllers are off and all actuated valves are put in fail-safe position. The fail-safe positions of the actuated valves in systems 1041 and 1070 are shown in Table 2.1. The hand control valves 1070-HCV-007 and 1070-HCV-010 in system 1070 are not actuated valves, the openings are set during commissioning and are then kept at these given values [6].

Table 2.1: Fail-safe positions of actuated valves in systems 1041 and 1070.

	1041-FCV-114	1041-FCV-124	1041-FCV-124	1041-FCV-125	1041-FCV-129	1041-FCV-130	1070-YSV-006
Fail-safe position							

Valve open in fail-safe Valve closed in fail-safe

2.6.2.2 Standby

This state is used when it is expected that the cooling system will operate on short notice. The temperature controller 1041-HICA-109 is on, allowing water from the intermediate cooling system to flow through the cold side of the plate heat exchanger 1041-W-001. It is assumed that the flow ramps up linearly from zero to operational flow. Thereafter, a pump in system 1041 ramps up to a reduced speed while the flow controller 1041-FIC-113 is on, ensuring a minimum circulating flow in the main loop and the controllers FIC-124, FIC-125, FIC-129 and FIC-130 are on, cooling the moderators at reduced flow. At the same time the water purification controller is on, allowing water to flow through the water purification system. It is assumed that the flow to the water purification system ramps up linearly from zero to operational flow.

The State is complete when the pump in system 1041 has reached its reduced speed and the pump in system 1070 has reached its operational speed. Additionally, a minimum flow in the main loop has been established and a specified time has elapsed in the Standby State.

2.6.2.3 Starting

During this State the process values such as temperature, flow, and pressure of the cooling systems are allowed to come into steady-state. The pump in system 1041 is ramped up to operational speed. The state is complete when steady-state is reached and the pressure of 1041-PDICA-114 is within its warning limits.

2.6.2.4 Running

During this State the proton beam is on and hitting the rotating target wheel. The cooling systems are cooling the moderators and the proton beam window and transferring the heat to the intermediate water cooling system.

2.6.2.5 Stopping

During this State the cooling systems are being stopped. Water is still circulating through the moderators and the proton beam window, to remove the residual heat after the proton beam is off. The pump in system 1041 is running at reduced speed while the speed of the pump in system 1070 is kept at operational speed. The State is complete when a specified amount of time has elapsed in this State. This is to ensure that sufficient amount of residual heat has been removed.

2.6.2.6 Fault

An alarm qualifying for the transition to State Fault or an operation intervention forces the cooling systems into State Fault. Water is still circulating through the moderators and the proton beam window, to remove the residual heat after the proton beam is off. In this State the system is put in a fail-safe mode and an alarm is sent to the operator indicating that there is a problem in the operation of the cooling systems that needs to be solved. In this State the speed of the pump in system 1041 is reduced while the speed of the pump in system 1070 is kept at operational speed. The state is complete when a specified amount of time has elapsed in this State. This is to ensure that sufficient amount of residual heat has been removed.

3 Modeling

The modeling of the cooling systems is performed in Dymola. When constructing large system models it is important to organize the package in Dymola. The package is organized with the following sub packages.

- `Components`
- `ComponentsTest`
- `SubSystems`
- `SubSystemsTest`
- `System`
- `SystemTest`
- `SystemSimulations`

Components that are modified from the MSL and the Buildings library are stored in the `Components` package. All the components used in the entire system are tested in the `ComponentsTest` package. Subsystems are constructed and stored in the `SubSystem` package and tested in the `SubSystemTest` package. The subsystems are connected to create the entire system and this system is stored in the System package and the system tests are stored in the `SystemTest` package. All the different simulations of the system model are stored in the `SystemSimulations` package.

3.1 Modeling strategy

When constructing large subsystems, it is beneficial to start with simple open loop fluid systems. Open loop fluid systems have boundary conditions at the inlet and outlet of the system model. The simple open loop fluid systems can start with a pressure boundary model at the inlet and outlet and a pump model in between them. After a simple open fluid system is constructed, the fluid system is closed with the addition of the MSL model `OpenTank`. For every new component addition to the closed loop fluid system, a simulation should be performed to assure that the model converges. This approach simplifies the debugging of the system if the simulation is not successful. When the system model is as accurately described as possible with MSL components and able to converge, the system model can be developed further. The system model is further developed by the modification of the MSL and Buildings models to describe the real components more accurately.

Before the modified component models are incorporated in the subsystems they need to be tested to assure that they behave as expected for different input values. The modified component models are then incorporated in the subsystem models and the subsystem models are subsequently tested to determine if they converge. The entire system model is then tested to determine if it converges with the new changes.

3.2 Modeling guidelines

When convergence of large system models fail it can be hard to discern what the underlying issue is. In many cases component model tests converge, but the incorporation of several component models to a closed system model increases the complexity and suddenly the system model does not converge. When constructing fluid system models in Dymola some guidelines can be followed in order to build robust and converging models.

Components in Dymola can be organized into two categories; volume and flow models. In volume models the energy and mass balances are formulated and the pressure and temperature are defined as state variables. The MSL models `OpenTank`, `TeeJunctionVolume` and `Boundary_pT` are volume models. In flow resistance models the momentum balance is formulated and the mass flow rate is defined as a state variable. The mass flow rate in the flow resistance model is calculated from the pressure drop across the model. The MSL model `SimpleGenericOrifice`, `ValveIncompressible` and `MassFlowSource_T` are flow resistance models. In the MSL model `DynamicPipe`, both volume and flow resistance models are present and the order in which they appear in the model can be configured via the `modelStructure` parameter. To increase the chances for convergence the components should be positioned in a staggered grid structure as volume model – flow model – volume model [29]. Connecting two flow resistance models together lead to large nonlinear systems which is due to the pressure at the connection being unknown. To calculate the pressure the solver needs to iterate at every time step [29]. Connecting two volume models together lead to high-index differential algebraic equations which are due to temperatures at the ports of the two models not being equal at the connection and iteration is required by the solver to equalize the two temperatures [29].

Closing of the fluid system with the incorporation of the MSL component `OpenTank` can cause circular equalities for the mass flow rate to arise, leaving the pressure undetermined. To solve this the mass balance in the tank is altered to `Fixedinitial` [30].

When modeling fluid systems with incompressible medium models, only one component model which sets the reference static pressure in the system and accounts for the fluid expansion can be incorporated in order to avoid singularities in the model [31]. In closed loop system models the MSL model `OpenTank` can be incorporated to solve these issues. The ambient pressure and the water level of the tank sets the static pressure at the tank inlet and outlet and the water level is allowed to increase and decrease in order to account for fluid expansion due to temperature changes.

3.3 Debugging

Even after following the modeling guidelines of the previous chapter, the performance can still be low and convergence failures can still occur. When simulations fail, error messages are shown and are the first thing to look at. Usually the quickest way to find an error is to first find out at what time and in which component model the simulation failed. In many cases though it is still unclear what the underlying issue is. Some debugging options and translation options are available in Dymola to simplify the process and increase the possibility of finding the errors. The translation window is available in **simulation window of Dymola -> Simulation -> Setup -> Translation** and the debugging window is available in **simulation window of Dymola -> Simulation -> Setup -> Debugging.** The translation and debug window is shown in Figure 3.1, with the ticked parameters being used to aid in finding errors and enhancing simulation performance. The wanted debugging parameters need to be ticked before the simulation in order for them to function during debugging.

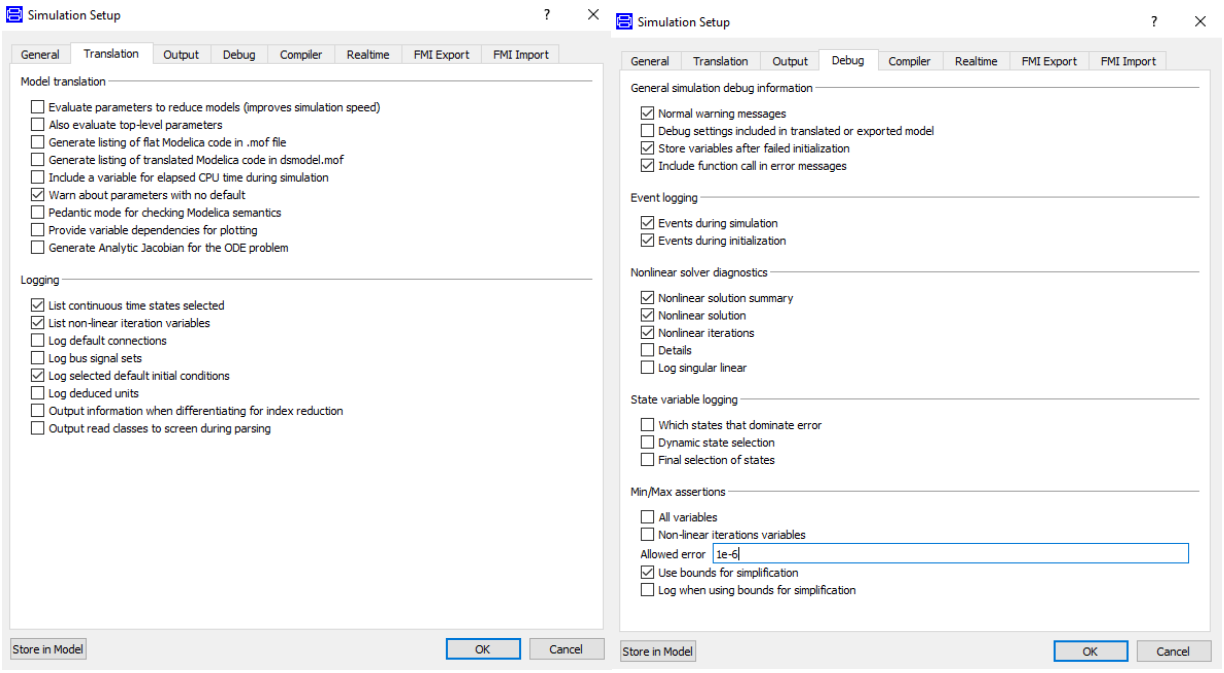

Figure 3.1: Translation and debugging window of Dymola.

By logging selected default initial conditions and storing variables after a failed initialization, an overview of the initial conditions and variables can be created, making it easier to analyze if some variables have unphysical values.

In many cases the solver is not able to solve the nonlinear system of equations. When debugging, the number of nonlinear equations can be retrieved as well as the nonlinear iteration variables and their initial values. At the time the initialization or simulation does fail, it can be helpful to investigate what is happening in the nonlinear system of equations and to the nonlinear variables.

Performance issues and errors can arise during events in the simulation. The event logging can help visualize what events that occur in the model and which expressions that are creating them. In events some variables become discontinuous and can be introduced with if and when statements. The event logging is visualized by right clicking on the simulation result in the **Variable Browser** and selecting **Analyze numerics**.

3.4 System model

The final system model is constructed from the four subsystems 1041, 1070, 1110 and 1065 and the top view is shown in Figure 3.2.

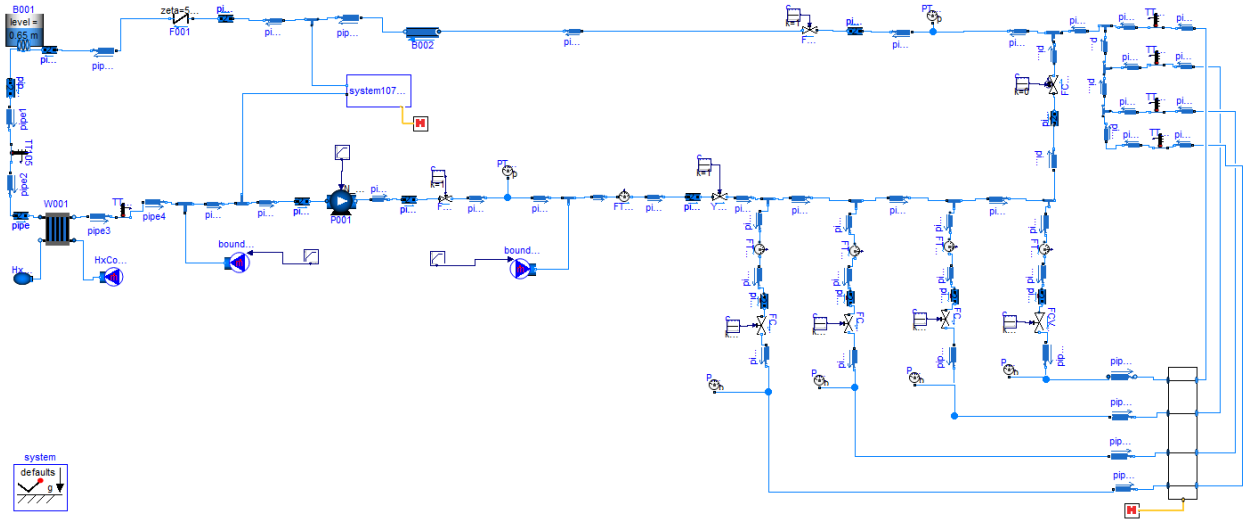

Figure 3.2: Final system model.

The four subsystems are shown in Figure 3.3 - Figure 3.6.

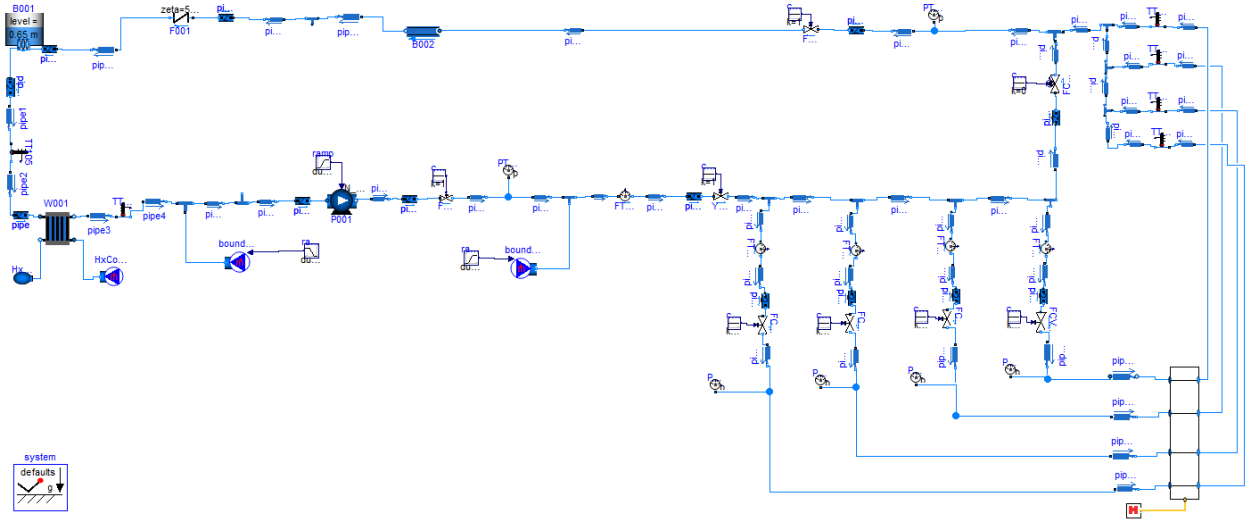

Figure 3.3: Model of system 1041 connected to systems 1070 and 1110.

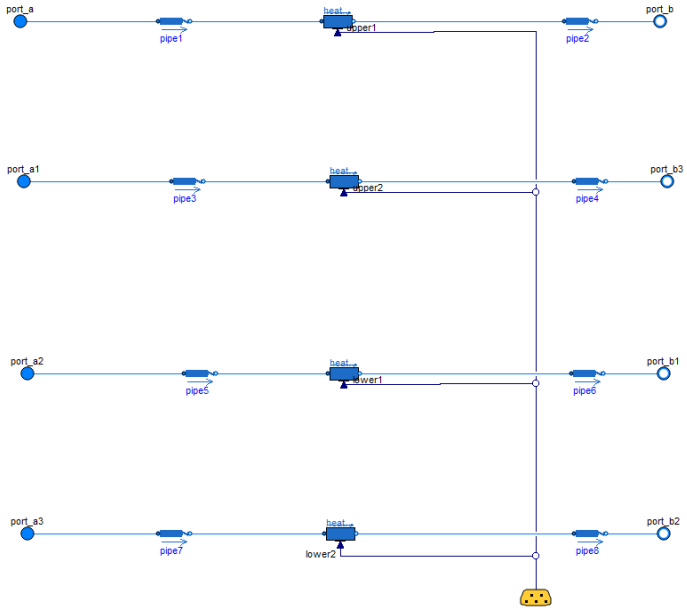

Figure 3.4: Model of system 1110.

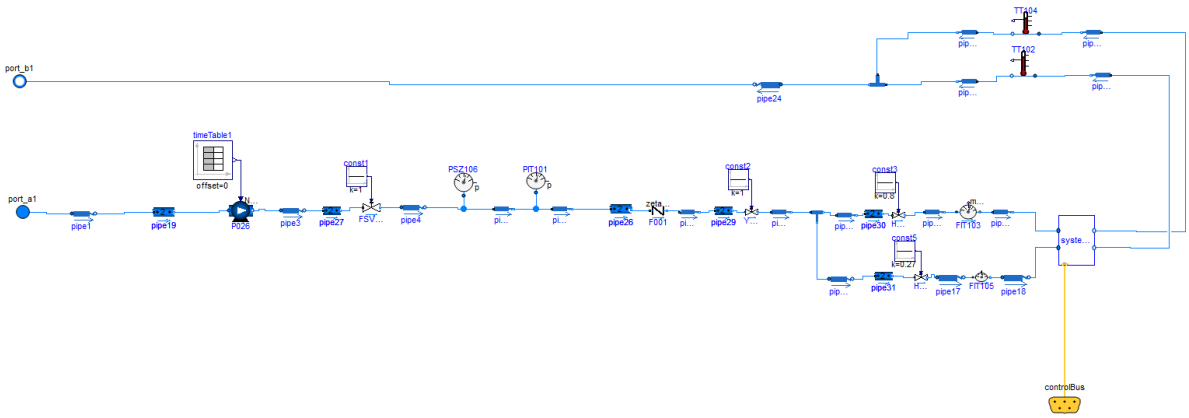

Figure 3.5: Model of system 1070.

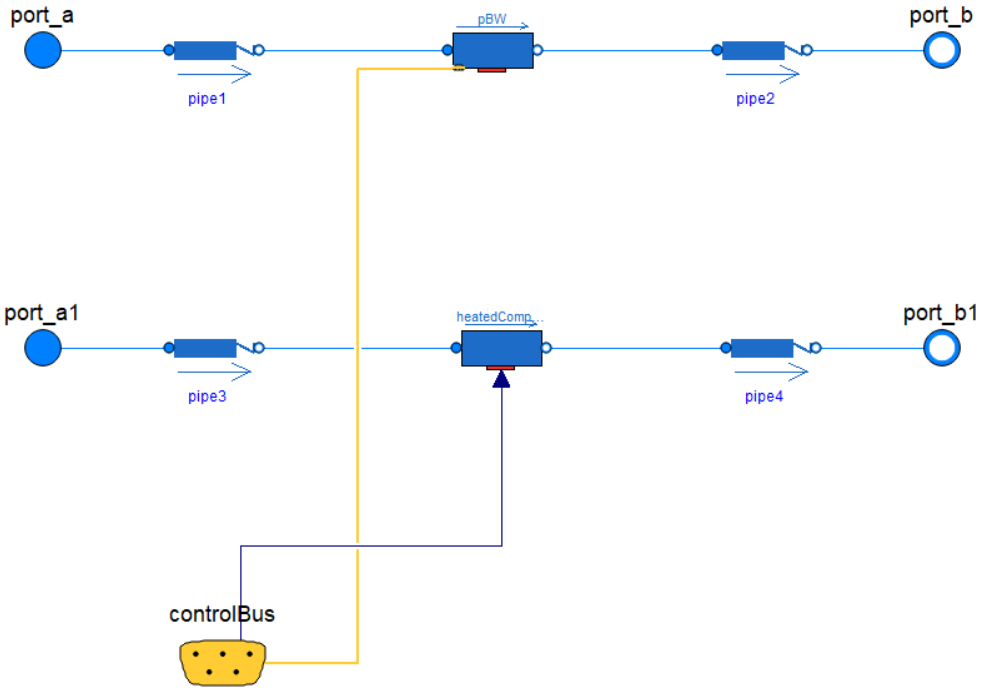

Figure 3.6: Model of system 1065.

The layout of the subsystems is constructed to resemble the corresponding P&IDs. The parallel pumps are however not included in the subsystem models 1041 and 1070 as they are only in stand-by during operation and neglecting these reduces the complexity of the subsystem models. Several components are included in the subsystem models. It is deemed necessary to model the system at this accuracy in order to locate the sensors and valves at the correct positions.

3.5 Initialization

To increase the chances of convergence for a system model, appropriate start values for the iteration variables such as pressure, temperature and mass flow rate need to be set.

The start value of temperature is set at the ambient temperature in all component models. To achieve appropriate start values for pressure and mass flow rate in every component model, subsystem 1041 is opened up with the creation of two open loop models and subsystem 1070 is opened up with the creation of one open loop model.

For subsystem 1041, the GLS tank and the pump is replaced with a pressure boundary and a mass flow rate boundary respectively. The first open loop model is constructed between the GLS tank outlet and the pump inlet and the second open loop model is constructed between the pump outlet and the GLS tank inlet. For a given pressure set at the pressure boundary and a given starting mass flow rate set at the mass flow rate boundary, the pressure and the mass flow rate at each component model inlet and outlet is determined. The open loop model between the GLS tank and the pump

inlet is shown in Figure 3.7 while the open loop model between the pump outlet and the GLS tank is shown in Figure 3.8.

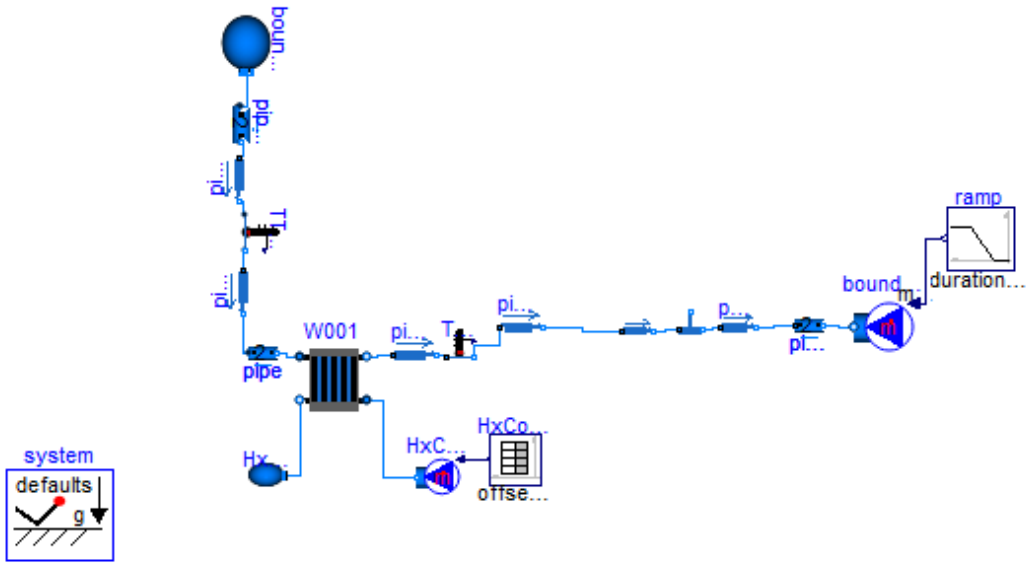

Figure 3.7: Open loop model between the GLS tank outlet and the pump inlet in system 1041.

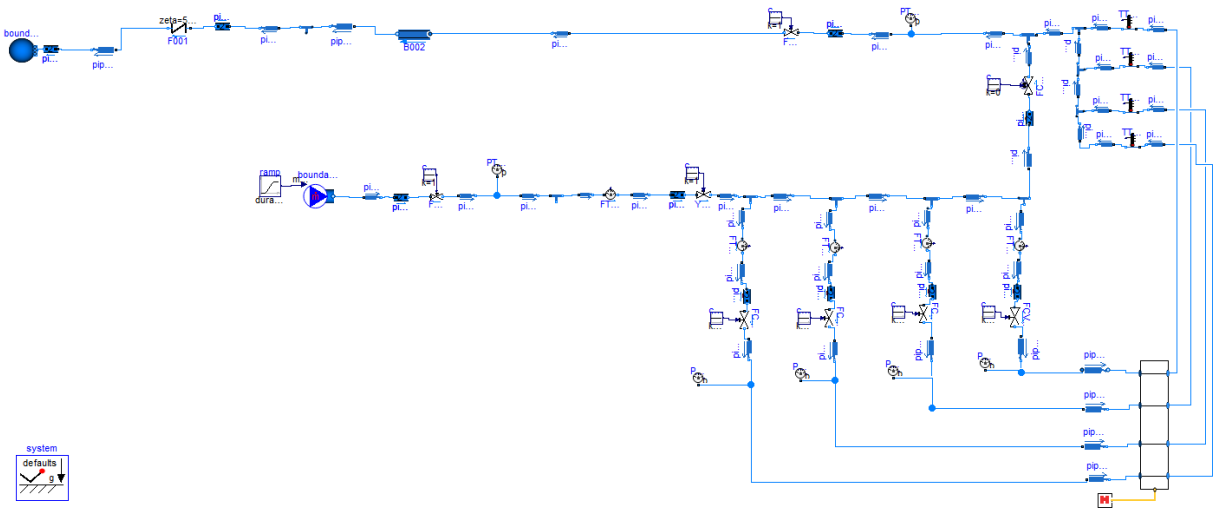

Figure 3.8: Open loop model between the pump outlet and the GLS tank inlet in system 1041.

After the pressure distribution in subsystem 1041 is computed from the two open loop models, the inlet and outlet pressure boundaries of subsystem 1070 can be determined. From the open loop model of system 1070, seen in Figure 3.9, the pressure and mass flow rate at each component model inlet and outlet in subsystem 1070 is determined.

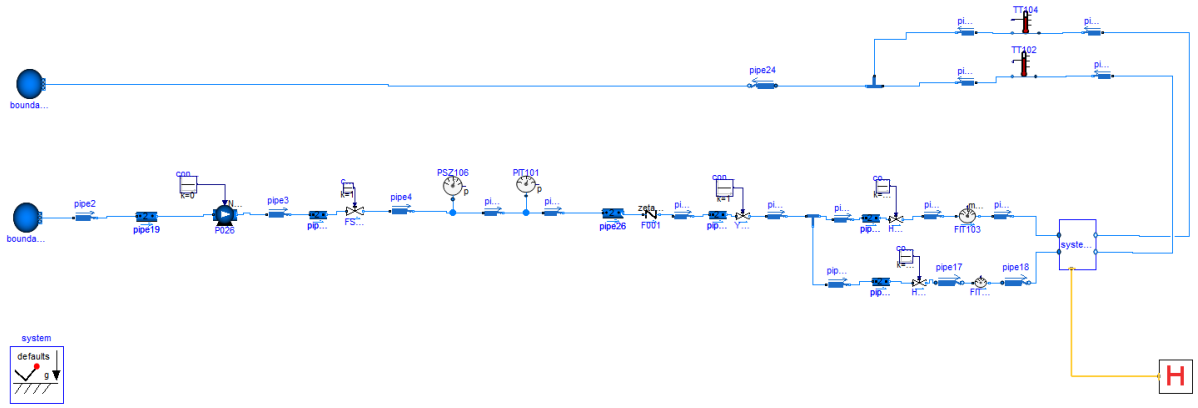

Figure 3.9: Open loop model of system 1070.

As the starting mass flow rate and the starting inlet and outlet pressures of the pumps in subsystem 1041 and 1070 now are known from the previous tests, the starting pump speed is determined through pump tests. In the pump tests, the pump inlet pressure and the mass flow rate is set. The pump speed is ramped up linearly until the known pump outlet pressure is achieved. A pump test model is shown in Figure 3.10.

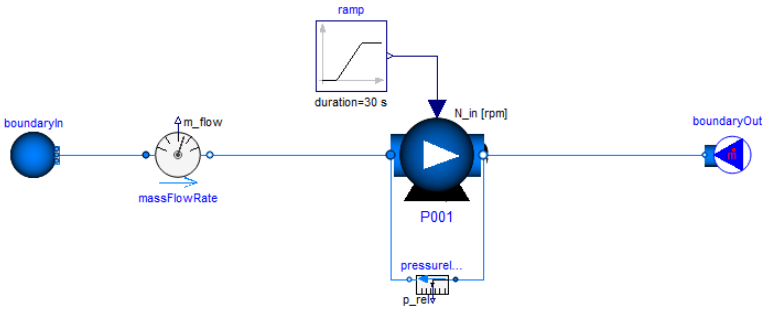

Figure 3.10: Test model to find the starting pump speed.

When the mass flow rate distribution, the pressure distribution and the pump speeds are computed from the open loop models, they are subsequently put in as starting values for the component models in the closed loop subsystems. An excerpt of the parameter window of the pipe segment model containing the starting values of process variables is shown in Figure 3.11.

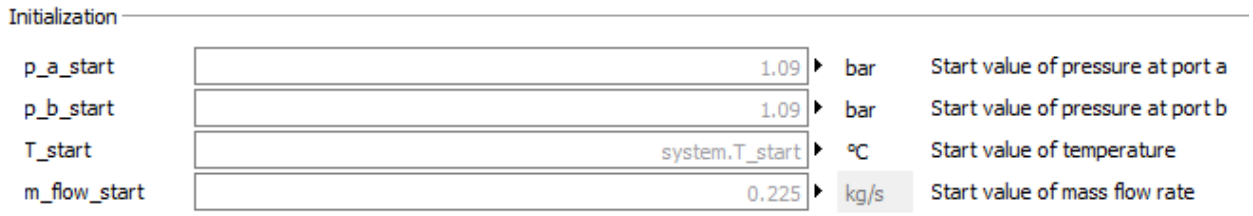

Figure 3.11: Excerpt of the parameter window of the pipe segment model containing the starting values of process variables.

3.6 Nominal operation

Most data regarding the cooling systems is known, however some assumptions have to be made. The operating speed of the pumps and the operational opening of the hand control valves in subsystems 1070 are not specified. The pump speeds and the opening of the valves are adjusted to achieve the nominal flow distribution and the defined pressure drop across each control valve as specified in each cooling system's PFD [32][33]. The set pump speeds and openings of the control valves will in turn set the operational pressure distribution in the cooling systems. The final adjusted parameter values, to achieve nominal flow in the cooling systems, are listed in Table 3.1.

Table 3.1: Values of operational pump speeds and valve openings.

Parameter	**Value**
Operational pump speed of 1041-P-001	2542 rpm
Operational pump speed of 1070-P-026	3613 rpm
Operational opening of 1041-FCV-124	35.2 %
Operational opening of 1041-FCV-125	35.2 %
Operational opening of 1041-FCV-129	35.2 %
Operational opening of 1041-FCV-130	35.2 %
Operational opening of 1070-HCV-007	54.1 %
Operational opening of 1070-FCV-010	24.1 %

3.7 Component models

For each type of component in the cooling systems, the function of the component and the design data is described prior to the modeling discussion. Thereafter a table is illustrated, listing the most important parameters that can be assigned to the component model.

3.7.1 Atmosphere

The surrounding atmosphere is modeled with the outer component model called `system` where the ambient temperature and pressure is set. The ambient temperature and pressure is set to 20 °C and 1.01325 bar respectively. In the system component model the formulation of the energy, mass and momentum balances are set and the default start value of the temperature in the component models is chosen. All start values of pressure and mass flow rates are set in the component models. The entire cooling system is initialized at the ambient temperature of 20 °C and for mass flow rates over zero in subsystems 1041 and 1110. These start values are set since it facilitates the initialization of the simulation as mass flow rates starting too close to zero in the entire system model can cause singularities.

3.7.2 Medium

The medium used in the cooling systems is demineralized water. The medium is modeled with the medium model `WaterIF97_pT` since the medium should only exist in the liquid phase. The thermodynamic properties of the medium can be calculated in the liquid and gas regions according to the IAPWS-IF97 standard. The thermodynamic properties are calculated from the pressure and temperature of the medium. The medium model calculates always the following quantities:

- Pressure
- Temperature
- Density
- Specific internal energy
- Specific enthalpy

3.7.3 Pipe segment

In the report a pipe segment is defined as the collective name of the piping, elbows, reducers and hand shut-off valves that are situated between two components such as pumps, tanks, T-junctions, sensors, check valves and control valves. The piping and fittings of the cooling systems is made of seamless stainless steel 1.4404 and are connected with each other through butt welding [34]. The piping is constructed in compliance with the European standard EN 10220 and most elbows, reducers and T-junctions are constructed in compliance with the European standard EN 10253-4 [34]. The elbows are of Type A and 3D construction while the reducers and T-junctions are of type A construction [34]. The elbows are used to change the direction of the flow while the reducers are used to change the size of the piping. The hand shut-off valves in the cooling systems is a globe type of valve and are used to separate components from the cooling system and to allow for drainage of the system during maintenance. During operation of the cooling systems the hand shut-off valves in the main loops are fully open.

The geometrical values of the pipe segments are obtained from the P&IDs and the 3D models of the cooling systems. The nominal diameter of the pipe segments is specified on the PI&Ds of the cooling systems and the corresponding outer diameter and wall thickness is retrieved from the

European standard EN 10220. The internal diameter of the pipe segments can then be calculated by equation (3.1).

$$d_i = d_o - 2w \tag{3.1}$$

The cooling system layout can be seen in the three-dimensional model. The lengths and heights of the pipe segments are measured and the number of elbows, reducers, T-junctions and hand shut-off valves in each pipe segment are counted. When measuring the lengths and heights of the pipe segments some simplifications are made at the elbows. The length of an elbow is simplified with the measurement of two straight lines instead of one curved line. The measuring tool in Naviswork Freedom 2019 is shown in Figure 3.12.

Figure 3.12: Measuring tool in Naviswork Freedom 2019.

The pipe segments are modeled with the MSL models `DynamicPipe`, `SimpleGenericOriface`, `ThermalCollector` and `FixedTemperature` while the models `HeatCapacitorArray` and `ConvectionArray` are created by ESS from the MSL models `HeatCapacitor` and `Convection`. The pipe segment model is shown in Figure 3.13.

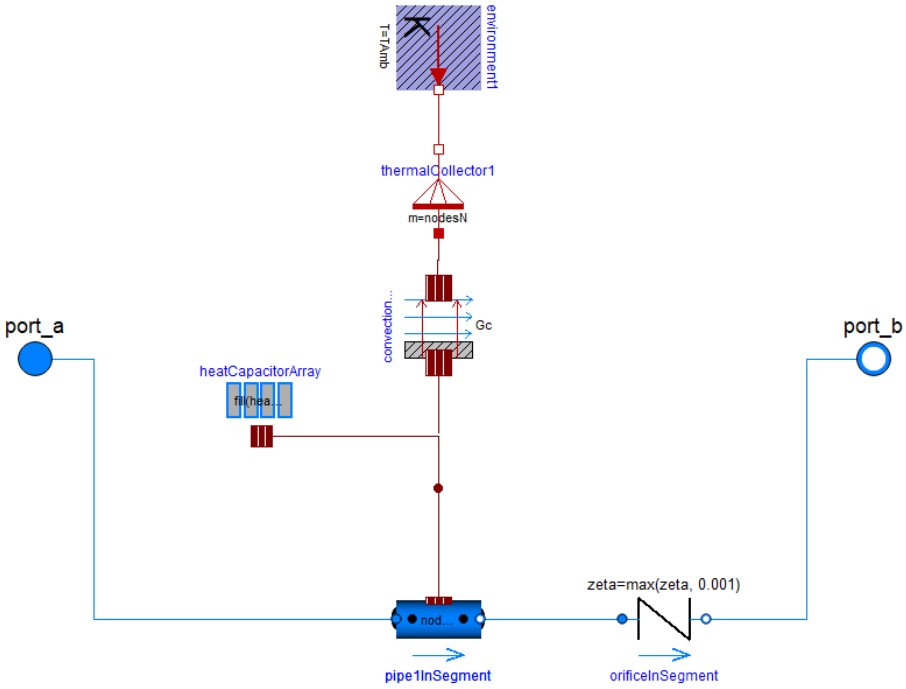

Figure 3.13: Pipe segment model.

The model `DynamicPipe` models a straight pipe with distributed mass, energy and momentum balances for one-dimensional flow. The partial differential equations are treated with the finite volume method and the staggered grid scheme is used for the momentum balances. The pipe can be split into a defined number of equally spaced segments along the flow path with the `nNodes` parameter. For all the pipe segments in the system model, the parameter `nNodes` is equal to two. The `modelStructure` parameter determines how the mass, energy and momentum balances are lumped in the model. The default values in the model are set to two nodes and a modelstructure of: volume model – flow model – volume model. With this configuration the energy and mass balances are lumped at the ports of the pipe and the momentum balance is lumped between the two ports. The inner diameter, thickness, length, height and surface roughness of each pipe segment are quantified in `DynamicPipe`. As the pipes are new and made of seamless steel, the absolute surface roughness is estimated to 0.025 mm [35].

The model `SimpleGenericOriface` models the pressure losses that arise from the elbows, T-junctions, hand-shut-off valves and reducers. All individual component loss coefficients are summed up to a total loss coefficient as seen in equation (3.2).

$$K_{tot} = n_E K_E + n_R K_R + n_T K_T + n_V K_V \tag{3.2}$$

The pressure loss across the `SimpleGenericOriface` model is given by equation (3.3) [36].

$$\Delta p = \frac{8K_{tot}}{\pi^2 {d_i}^4 \rho} \dot{m}^2 \tag{3.3}$$

For elbows and T-junctions, the loss coefficient can be approximated as a function of the friction factor. The friction factor is in turn a function of the Reynolds number and the relative surface roughness. For simplification the friction factor is assumed to be constant, which is true for turbulent flow and a constant relative surface roughness. During the transients in most of the disturbance cases studied the flow will be in the turbulent region. Errors will however arise during the start-up and shut-down case studies and the pump trip case studies, since the flow will be laminar during a few seconds when the mass flow rate is close to zero. The friction factor is given for different pipe sizes in Table 3.2 [37].

Table 3.2: Friction factors for different pipe sizes.

Nominal size	DN25	DN32	DN50	DN80
Friction factor (f_T)	0.023	0.022	0.019	0.018

The loss coefficient of an elbow is equal to the sum of the friction coefficient and the local fluid resistance coefficient [35]. Most elbows in the cooling systems have a turning angle of 90°, but there also exists a few elbows that have other turning angles. For simplification all elbows are set to 90°, which is a conservative simplification since lower degree elbows generate smaller pressure drops. According to EN-10253-4, for DN25, DN32, DN50 and DN80 elbows, the curvature radius and inner diameter ratio is $1 < \frac{r}{d_i} < 1.5$. As a conservative simplification, the ratio is set to $\frac{r}{d} = 1$ for all nominal diameters of elbows, since elbows with smaller curvature radius and inner diameter ratios generate larger pressure drops. With the simplifications of 90° elbows and $\frac{r}{d} = 1$, the loss coefficient of an elbow is given by equation (3.4) [37].

$$K_E = 20 f_T \tag{3.4}$$

The pressure loss in the elbows which arise due to the friction coefficient is already captured by the specification of the total pipe segment length, which includes the lengths of the elbows. Due to this the friction coefficient of the elbow is specified twice resulting in an error which leads to a larger value of the loss coefficient. The friction coefficient of an elbow is however small compared to the local fluid resistance coefficient of an elbow resulting in a small error which is deemed acceptable.

The loss coefficient of a T-junction is dependent on the friction factor and the type of flow. The medium can either flow through the line or the branch of the T-junction. The loss coefficient for line flow is given by equation (3.5) and the loss coefficient for branch flow is given by equation (3.6) [37].

$$K_T = 20 f_T \tag{3.5}$$

$$K_T = 60 f_T \tag{3.6}$$

For reducers, the loss coefficient is a function of the angle. The angle can be computed using Pythagoras theorem since the length and the small and large diameter of the reducer is known, as seen in equation (3.7).

$$\theta = 2\tan^{-1}\left(\frac{d_2 - d_1}{2l}\right) \tag{3.7}$$

The loss coefficient is computed for gradual expansions by equations (3.8) and (3.9) [37] .

$$\theta < 45°:\ K_R = \frac{2.6\left(\sin\frac{\theta}{2}\right)\left(1 - \left(\frac{d_1}{d_2}\right)^2\right)^2}{\left(\frac{d_1}{d_2}\right)^4} \tag{3.8}$$

$$45° < \theta < 180°:\ K_R = \frac{\left(1 - \left(\frac{d_1}{d_2}\right)^2\right)^2}{\left(\frac{d_1}{d_2}\right)^4} \tag{3.9}$$

The loss coefficient is computed for gradual contractions by equations (3.10) and (3.11) [37].

$$\theta < 45°:\ K_R = \frac{0.8\left(\sin\frac{\theta}{2}\right)\left(1 - \left(\frac{d_1}{d_2}\right)^2\right)^2}{\left(\frac{d_1}{d_2}\right)^4} \tag{3.10}$$

$$45° < \theta < 180°:\ K_R = \frac{0.5\left(1 - \left(\frac{d_1}{d_2}\right)^2\right)^2\sqrt{\sin\frac{\theta}{2}}}{\left(\frac{d_1}{d_2}\right)^4} \tag{3.11}$$

Since the hand shut-off valves are always fully open during operation, they are simplified with the `SimpleGenericOriface` model. The k_{vs} values for the hand shut-off valves with specified nominal diameters in system 1041 are shown in Table 3.3 and the k_{vs} values for hand-shut off valves with specified nominal diameters in system 1070 are shown in Table 3.4 [38][39].

Table 3.3: K_{vs} values of hand shut-off valves in system 1041.

Nominal diameter of hand-shut off valves	**k_{vs}**
DN50	40
DN80	113

Table 3.4: K_{vs} values of hand shut-off valves in system 1070.

Nominal diameter of hand-shut off valves	**k_{vs}**
DN25	7.1795
DN32	15.57

The k_{vs} value expresses the flow rate through a valve at maximum opening and a pressure differential of 1 bar [40]. Since the medium is water, the pressure differential can be determined by equation (3.12) [41].

$$\Delta p = \left(\frac{\rho}{\rho_0}\right)\left(\frac{\dot{V}}{k_{vs}}\right)^2 \cdot 10^5 \tag{3.12}$$

The reference density ρ_0 is usually chosen to be the density of water at 4 °C [42]. The volume flow rate can be written as

$$\dot{V} = \frac{3600\dot{m}}{\rho} \tag{3.13}$$

The pressure differential can also be determined by equation (3.14) [36].

$$\Delta p = \frac{8K_v}{\pi^2 {d_i}^4 \rho}\dot{m}^2 \tag{3.14}$$

Combining equations (3.12) - (3.14), the loss coefficient of the hand shut-off valve is given by equation (3.15).

$$K_V = \frac{3600^2 \cdot 10^5 \cdot \pi^2 {d_i}^4}{8\rho_0 {K_{vs}}^2} \tag{3.15}$$

The model `HeatCapacitorArray` models the heat capacity of the pipe segment wall and assumes a uniform temperature. A uniform temperature of the pipe wall in the radial direction is assumed since the pipe wall thickness is small and the pipe wall conductivity is high. The heat capacity describes the energy storage capabilities of a component. The heat capacity of the pipe wall segment can be viewed as the energy required to raise the temperature of the pipe wall segment by one degree. The heat capacity of the pipe segment wall is given by equation (3.16).

$$C = c_p m \tag{3.16}$$

The specific heat capacity at constant pressure c_p and the mass m are used as inputs to the model. The specific heat capacity at constant pressure varies with temperature. The pipe walls are in normal operation affected by water temperatures between 20-30°C and pressure variations between 1-5.2 bar(a)[32]. These temperature variations will not affect the specific heat capacity at constant

pressure significantly, therefore the specific heat capacity at constant pressure is assumed to be constant. The specific heat capacity at constant pressure is chosen at the temperature of 20°C and has a value of 500 $\frac{J}{kgK}$ [43]. Since the temperature in the model is a state variable, a start temperature value must be assigned to the model. This value is set equal to the ambient temperature of 20°C.

As the pipe wall is made of stainless steel 1.4404, the density amounts to 8000 $\frac{kg}{m^3}$ [34] [43]. As the outer diameter is retrieved from the European standard EN 10220, the inner diameter from equation (3.1) and the length from measurements in the three-dimensional model, the mass of the pipe wall segment can be calculated by equation (3.17).

$$m = \rho V = \frac{\rho \pi l \left(d_o{}^2 - d_i{}^2\right)}{4} \tag{3.17}$$

As mentioned earlier, the `HeatCapacitorArray` model is modified from the MSL model `HeatCapacitor`. The reason for this is that the `HeatCapacitorArray` model, unlike the `HeatCapacitor` model, is able to divide the total heat capacity of the pipe wall segment among the number of elements in the `DynamicPipe` model, thus creating an array of heat capacities spatially along the pipe segment. The same reasoning is applied to the creation of the `ConvectionArray` model.

The convective heat transfer between the pipe segment wall and the surrounding air is modelled with the `ConvectionArray` model. Natural convection occurs between the pipe segment wall and the surrounding air. The convective heat transfer from the pipe segment to the ambient can be expressed by equation (3.18).

$$\dot{Q} = Ah(T_\infty - T_w) \tag{3.18}$$

The temperature of the pipe wall segment and the surrounding air is assumed to be uniform and the heat transfer area is the outer pipe wall area. The convective heat transfer coefficient h is a variable that depends on the geometry of the solid, the flow field and the properties of the fluid [44]. As it is assumed that the surrounding air is kept at a constant temperature of 20 °C and only natural convection occurs, the convective heat transfer coefficient is assumed to be constant. A convective heat transfer coefficient of 5 W/m^{2}K is chosen since the convective heat transfer coefficient of air is between 2.5-25 W/m^{2}K [45].

Convective heat transfer between the fluid and the inner pipe wall is modeled by setting the `use_HeatTransfer` to `true` under the `Assumptions` tab of the `DynamicPipe` model. The convective heat transfer coefficient is computed locally in the `DynamicPipe` model by setting `HeatTransfer` to `LocalPipeFlowHeatTransfer`.

The input to the pipe segment model is listed in Table 3.5, where the displayed values are constant for all the pipe segments in the cooling systems and the input of the empty value fields vary for each individual pipe segment.

Table 3.5: Input to the pipe segment model.

Input	Value	Source
Model structure		
Model structure []	-	
Initialization		
Starting pressure at inlet [bar]	-	
Starting pressure at outlet [bar]	-	
Starting temperature [°C]	20	
Starting mass flow rate [kg/s]	-	
Geometry		
Pipe inner diameter [m]	-	
Pipe wall thickness [m]	-	
Length [m]	-	
Height [m]	-	
Absolute surface roughness [mm]	0.0025	[35]
Thermal		
Ambient temperature [°C]	20	
Convective heat transfer coefficient [W/ m^2K]	5	[45]
Pipe wall density [kg/m^3]	8000	[43]
Pipe wall specific heat capacity [J/kgK]	500	[43]
Discrete losses		
Friction factor for turbulent flow []	-	
Bends		
Number of bends []	-	
Hand shut-off valves		
Number of hand shut-off valves []	-	
K_{vs} value []	-	
Tees		
Number of tees with flow through line []	-	
Number of tees with flow through branch []	-	
Reducer/Expander		
Number of expanders []	-	
Number of reducers []	-	
Length of the expander/reducer [m]	-	

Inner diameter upstream/downstream the expander/reducer [m]	-	
Lengthwise discretization		
Number of nodes []	2	

3.7.4 Actuator shut-off valve

The actuator shut-off valves (YSV) are fully open during normal operation, but if the cooling systems reach unsafe operation they can abruptly close to save components from getting damaged. By having the ability to close the YSV after an event, the YSV is modeled with the MSL model `ValveIncompressible`. It is assumed that no heat is lost to the ambient and changes in kinetic energy is neglected.

To determine the nominal operating point of the YSV, the nominal mass flow rate and the nominal pressure drop need to be specified. Since water is the medium and the nominal mass flow rate and the K_{vs} value are known, the nominal pressure drop over the valve can be determined by equation (3.14). The nominal opening of the component model is set to 1 with a constant input signal of value 1 connected to the valve, indicating that the valve is fully open. The input to the YSV models is shown in Table 3.6.

Table 3.6: Input to the YSV models.

Input	**1041-YSV-115**	**1070-YSV-006**
Flow coefficient K_{vs} []	40 [38]	7.1795 [39]
Nominal mass flow rate [kg/s]	4 [28]	0.8 [28]
Nominal pressure drop [bar]	0.13	0.121
Nominal opening []	1	1

3.7.5 Flow safety valve

The purpose of the flow safety valve (FSV) is to prevent backflow in the piping. For the FSV, the MSL model `ValveIncompressible` is used. The FSVs are modelled to be fully open during operation with the nominal opening position of the FSV set to fully open. A constant input signal with the value 1 is connected to the FSV, indicating that the FSV is fully open. The `ValveIncompressible` model is modeled as a FSV by setting the `checkvalve` to true under the `Assumption` tab. The backward flow is prevented when the downstream pressure is larger than the upstream pressure of the FSV. It is assumed that no heat is lost to the ambient and changes in kinetic energy is neglected. The nominal pressure drop across the FSV is determined by equation (3.14). The input to the flow safety valve models is shown in Table 3.7.

Table 3.7: Input to the FSV models.

Input	**1041-FSV-062**	**1041-FSV-064**	**1070-FSV-002**
Flow coefficient k_{vv} []	31 [46]	31 [46]	15.57 [39]
Nominal mass flow rate [kg/s]	5.1 [28]	4 [28]	0.8 [28]
Nominal pressure drop [bar]	0.354	0.217	0.028
Nominal opening []	1	1	1

3.7.6 Flow control valve and hand control valve

The flow control valve (FCV) is a globe type of valve which can be controlled with an electric, hydraulic or pneumatic drive. If the opening of the valve is regulated by hand, it is instead called a hand control valve (HCV). In the water cooling systems, the control valves are either controlled by hand or with a pneumatic drive. If the control valve is controlled by hand, the opening of the control valve is adjusted by hand at the commissioning to obtain the desired flow rate downstream the control valve during operation. For control valves with pneumatic drives the opening of the control valves can be adjusted during operation to achieve the given set-point of a process variable. Pneumatic drives operate the control valves faster than hydraulic drives but the possible power output is lower, making pneumatic drives more suitable for smaller control valves.

Both the FCVs and the HCVs are modelled with the MSL model `ValveIncompressible`. With this model, the input signal can control the valve position of the control valve. The valve position ranges from 0-1, where 0 is fully closed. The valve characteristics can be set in the model and it describes the flow capacity as a function of the valve opening at a constant pressure drop across the valve [47]. As all FCVs have a linear valve characteristic, the flow capacity is proportional to the opening of the valve (document D Andersson 2020 Nov 11) [39].

The valve opening is adjusted until the nominal pressure drops are achieved for the nominal mass flow rates through the control valves. The input to the control valve models is listed in Table 3.8.

Table 3.8: Input to the control valve models.

Filter	1041-FCV-114	1041-FCV-124 1041-FCV-125 1041-FCV-129 1041-FCV-130	1070-HCV-007	1070-HCV-010
Valve characteristic []	Linear (document D Andersson 2020 Nov 11)	Linear (document D Andersson 2020 Nov 11)	Linear [39]	Linear [39]

Flow coefficient k_{vv} [m^3/h]	10 (document D Andersson 2020 Nov 11)	8.3 (document D Andersson 2020 Nov 11)	4.2385 [39]	4.2385 [39]
Nominal mass flow rate [kg/s]	0 [28]	1 [28]	0.55 [28]	0.25 [28]
Nominal pressure drop [bar]	0	1.55 [32]	0.78	0.75 [33]
Nominal opening []	0	0.352	0.541	0.241

3.7.7 Filter

The function of the filter is to retain large particles so that they do not damage components in the cooling systems. The large particles either enter the cooling systems after installation or maintenance or they arise due to component wear in the cooling systems. As a discrete pressure drop arises across the filter, the filter is modeled with the MSL model `SimpleGenericOriface`. For a given mass flow rate, the pressure drop across the filter in system 1041 can be determined from [48]. For a filter with a nominal diameter of DN25, the pressure drop can't be determined from [48]. The K_v value of the filter in system 1070 is assumed by finding a similar filter by the same manufacturer that has a printed K_v value for a filter with a nominal diameter of DN25. The nominal pressure drop across the filter in system 1070 is given by equation (3.12).

The nominal diameter, mass flow rate, pressure drop and K_v value for the filters in systems 1041 and 1070 are shown in Table 3.9. The inner diameter, nominal mass flow rate and pressure drop are used as input to the component model. For mass flow rates deviating from the nominal operating point, a quadratic correlation between the pressure drop and mass flow rate is utilized.

Table 3.9: Nominal diameter, mass flow rate and pressure drop across the filters in systems 1041 and 1070 .

Filter	**Nominal diameter of filter**	**Nominal mass flow rate [kg/s]**	**Flow coefficient k_{vv} [m^3/h]**	**Nominal pressure drop [bar]**
1070-F-001	DN25	0.8 [6]	17.8 [49]	0.026
1041-F-001	DN80	4.8 [23]	-	0.021 [48]

3.7.8 Gas and liquid separation tank

The gas and liquid separation (GLS) tank is a horizontal cylindrical tank which is filled to 70% of the total volume of the tank [28]. The purpose of the tank is to withhold the medium for 300 seconds to allow for most gases of hydrogen and oxygen, produced from the radiolysis, to be separated from the medium [28]. The gases rise to the upper gaseous space of the gas and liquid separation tank and is thereafter transported to a radiolysis gas treatment system. The tank also acts as a

pressurizer in the cooling system and should always provide the centrifugal pumps with medium during operation, thus avoiding gas to enter the centrifugal pumps. The three-dimensional model of the GLS tank is shown in Figure 3.14.

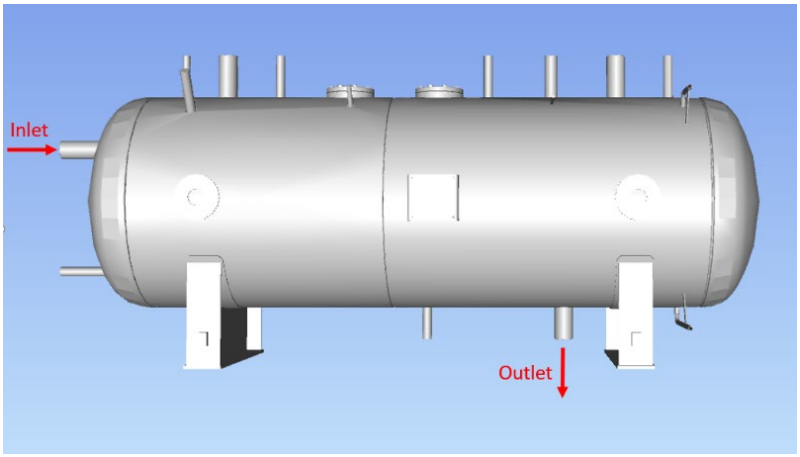

Figure 3.14: Three-dimensional model of the GLS tank [22].

The GLS tank is modeled with a modified MSL model `OpenTank` including the `HeatCapacitor`,`Convection` and `FixedTemperature` MSL models in order to include the heat capacity of the tank and the heat loss from the tank. The `OpenTank` model is modified to a horizontal cylindrical tank from the previously vertical cylindrical tank. The horizontal cylindrical tank is a simplification since the actual tank is cylindrical with torispherical heads at both ends. This simplification is done in order to simplify the calculation of the heat transfer area and nominal water level of the tank. It is assumed that the tank is filled with a single medium having a density higher than the ambient medium, the medium has uniform temperature and density and no medium leaves through the top of the tank. The GLS tank model is shown in Figure 3.15.

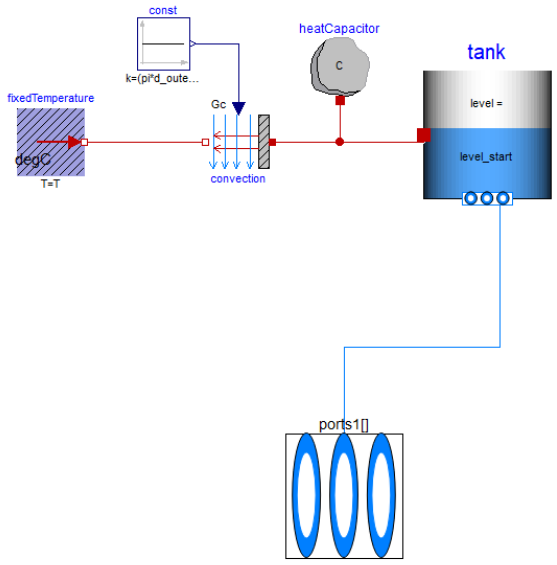

Figure 3.15: GLS tank model.

For given values of the total volume and the inner diameter of the tank, the corresponding inner tank length can be computed by equation (3.19).

$$l_i = \frac{4V}{\pi {d_i}^2} \tag{3.19}$$

As the GLS tank is modeled with the modified MSL component model `OpenTank`, the tank pressure is fixed and not variable as it will be during operation. As the operating pressure is estimated to be in the pressure range of 1.0-1.5 bar, the operating tank pressure is assumed to be constant at 1.2 bar [32].

The nominal water volume of the GLS tank is 70% of the total volume [28]. With this specification, the nominal water level of the tank can be calculated and set as an input to the model. This nominal water level together with the tank pressure will set the pressure at the inlet and outlet of the tank. A simplified cross section of the GLS tank is illustrated in Figure 3.16.

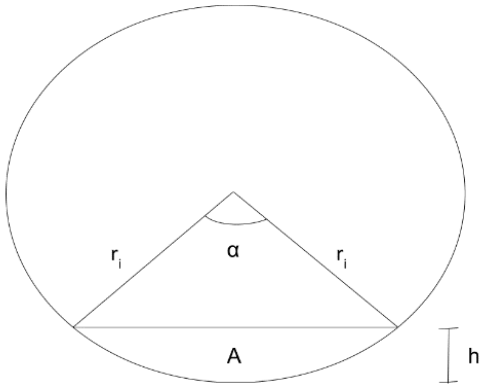

Figure 3.16: Simplified cross section of the GLS tank.

The cross sectional area of the tank under water at a tank volume of 70% is given by equations (3.20) and (3.21) [50].

$$A = \frac{V_{70\%}}{l_i} \tag{3.20}$$

$$A = \frac{{d_i}^2}{8}(\alpha - \sin\alpha) \tag{3.21}$$

Combining equations (3.20) and (3.21), yields equation (3.22).

$$\alpha - \sin\alpha = \frac{8V_{70\%}}{{d_i}^2 l_i} \tag{3.22}$$

Equation (3.22) is solved numerically using the Newton Raphson method. With the angle α now determined, the water level can be computed by equation (3.23) [50].

$$h = \frac{d_i}{2}\left(1 - \cos\frac{\alpha}{2}\right) \tag{3.23}$$

The tank inlet has a nominal diameter of DN80 and is situated 0.75 m over the tank bottom while the tank out has a nominal diameter of DN80 and is situated 0 m over the tank bottom [51].

For fixed values of the cross area radius and length of the GLS tank, the water volume of the tank can be written as a function of the water level, as seen in equation (3.24) [52] .

$$V = \left(r^2 \cos^{-1}\left(\frac{r-L}{r}\right) - (r - level)\sqrt{2r \cdot L - h^2}\right) l \tag{3.24}$$

The heat transfer area between the water and the tank wall is calculated by equation (3.25) [50][52]. For simplification the heat transfer area is chosen to be the contact area between the water and the

tank wall only, since the convective heat transfer coefficient for water is higher than for gases. The convective heat transfer coefficient is challenging to compute, since it depends on several factors. A test is performed on a horizontal cylindrical pipe with similar boundary conditions as the GLS tank has during nominal operation, such as the inlet mass flow rate and the temperature of the tank medium. With this test, a convective heat transfer coefficient is computed to approximately 50 W/m^2K and is set as the convective heat transfer coefficient in the GLS tank model.

$$A_i = 2\cos^{-1}\left(1 - \frac{L}{r}\right) rl + 2r^2 \cos^{-1}\left(\frac{r-L}{r}\right) - (r-L)\sqrt{2r \cdot L - h^2} \tag{3.25}$$

The heat capacity of the tank is calculated by equation (3.16). The specific heat capacity at constant pressure c_p and the mass m are used as inputs to the model. Since the GLS tank is mostly made of the same material as the piping, the specific heat capacity of the tank wall at constant pressure is set equal to the pipe walls specific heat capacity at constant pressure [53][43]. The mass of the tank walls amounts to 890 kg [51]. For simplification, the water and the tank wall are modeled as separate heat capacities with uniform temperatures. In reality however, the water will be hotter at smaller water depths since water heated from the moderators enters the GLS tank above water level and hotter water will have lower density. As the water will be in contact with the tank wall, the tank wall temperature will be higher at lower water depths. At the top of the tank, gases of hydrogen and oxygen exist. As the convective heat transfer coefficient is lower between a gas and a solid than between a liquid and a solid, the tank wall temperature in contact with the gases will be lower than the tank wall temperature in contact with the liquid medium, but as previously stated the heat transfer rate between the gases and the tank wall are neglected.

Heat transfer occurs between the GLS tank and the surrounding air. Natural convection is assumed between the GLS tank and the surrounding air. The convective heat transfer rate from the tank to the ambient is calculated by equation (3.18). The temperature of the GLS tank and the surrounding air is assumed to be uniform and the heat transfer area is the outer tank area. The convective heat transfer coefficient is set equal to convective heat transfer coefficient of the piping. With a given tank wall thickness, the outer diameter and outer length of the tank can be calculated [51]. The outer area of the tank is approximated by equation (3.26).

$$A_o = \frac{\pi d_o (d_o + 2l_o)}{2} \tag{3.26}$$

The input to the GLS tank model is listed in Table 3.10.

Table 3.10: Input to the GLS tank model.

Input	**Value**	**Source**
Initialization		
Starting temperature of water volume [°C]	20	

Geometry		
Number of ports []	2	
Diameter of tank [m]	0.98	[51]
Total tank volume [m^3]	2.266	[51]
Tank thickness [m]	0.01	[51]
Nominal operating point		
Tank pressure [bar]	1.2	
Water level [m]	0.65	
Thermal		
Mass of tank excluding water [kg]	890	[51]
Specific heat capacity of the GLS tank [J/kgK]	500	[43]
Convective heat transfer coefficient between the tank wall and the ambient [W/m^2K]	5	[45]
Convective heat transfer coefficient between the tank fluid and the tank wall [W/m^2K]	50	
Ambient temperature [°C]	20	

3.7.9 Delay tank

The delay tank is a horizontal cylindrical tank with a smaller volume than the gas and liquid separation tank and is entirely filled with water. The inner design of the delay tank is such that flow paths are created with the flow being diverted so that it travels approximately two lengths of the tank before reaching the outlet of the tank. The purpose of this design is to provide a specified time delay to the flow to ensure that N-16 gamma radiation has decayed before reaching the gas and liquid separation tank. A three-dimensional drawing of the delay tank is shown in Figure 3.17.

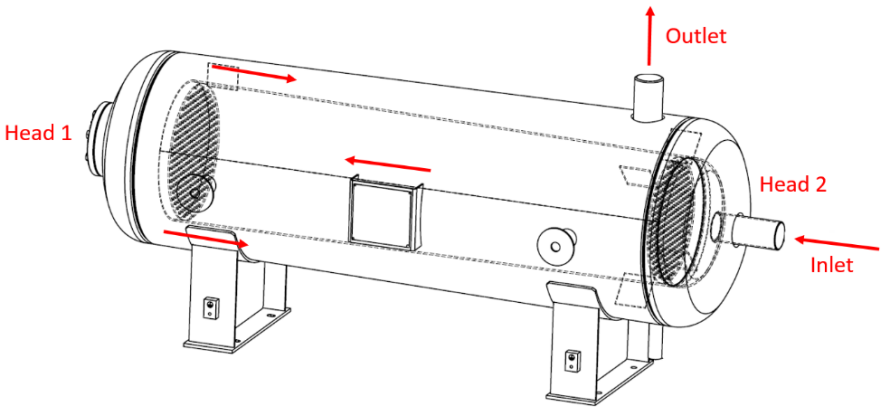

Figure 3.17: Three-dimensional drawing of the delay tank [54].

Since flow paths exist in the entirely water filled delay tank, it is more appropriate to model the delay tank as a pipe using the `DynamicPipe` model and modeling the heat capacity of the delay tank and heat transfer from the delay tank using the `HeatCapacitorArray` and `ConvectionArray` models respectively. The discrete losses are modeled with the `SimpleGenericOrifice` model. The fluid in the delay tank model is assumed to flow uniformly through the inner shell before turning at a mean flow path into the outer shell. It is assumed that the entire flow will flow through the second delay tank head before exiting the delay tank. The delay tank model is shown in Figure 3.18.

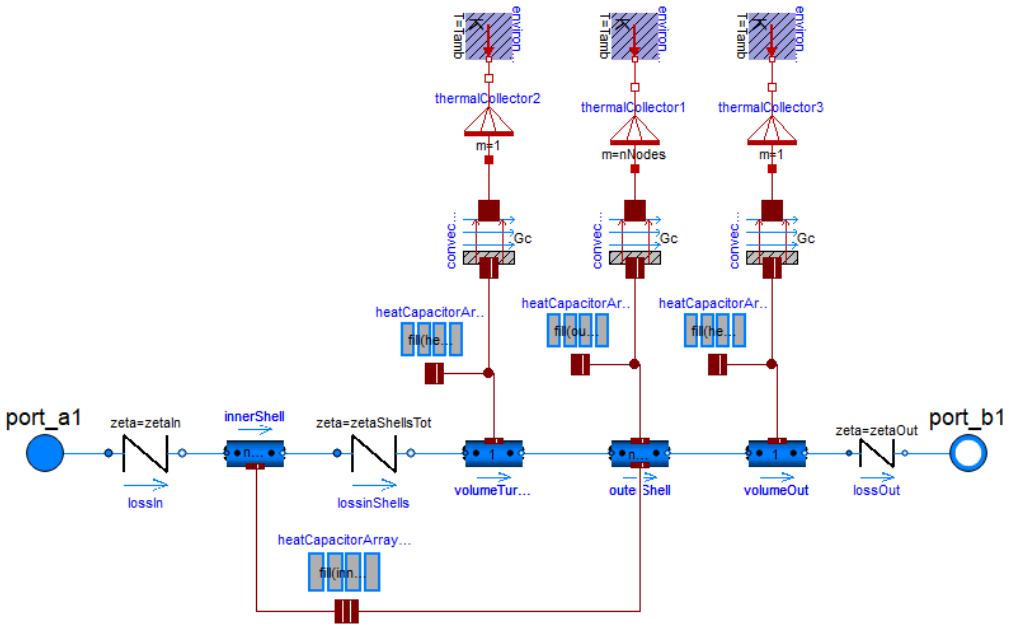

Figure 3.18: Delay tank model.

When the flow enters the delay tank, a sudden expansion of the flow occurs due to the increase in flow area. A pressure drop will occur due to this sudden expansion of flow and for an assumed uniform velocity the resistance coefficient is $\zeta = 1$ [35]. The loss is modeled in the first `SimpleGenericOrifice` model in Figure 3.18.

The flow will thereafter flow through a perforated plate before entering the inner shell and exit through a perforated plate. The flow will then turn 180° before entering the outer shell. It is assumed that the perforated plates are sharp-edged. As the perforated plate thickness and inner diameter of an orifice ratio $\frac{th}{d_i} > 0.015$ and the Reynolds number through the perforated plate at nominal flow and below is $Re < 10^5$, the resistance coefficient of a perforated plate can be computed by equation (3.27) [35]. The coefficients in equation (3.27) are determined from graphs in [35]. ζ_φ is a function of the Reynolds number and the cross-section coefficient, $\varepsilon_0{}^{-Re}$ is a function of the Reynolds

number and ζ_0 is a function of the cross-section coefficient and the ratio of the thickness of the perforated plate and the inner diameter of a orifice.

$$\zeta = \frac{\left(\zeta_\varphi + \varepsilon_0{}^{-Re}\zeta_0 + \lambda\frac{th}{d_i}\right)}{\left(\frac{A_f}{A_g}\right)^2} \tag{3.27}$$

To compute the resistance coefficient of the turn of the flow, the turn of the flow is seen as a sharp-edged elbow of 180° with equal inlet and outlet sections. This is greatly simplified and will thus yield a resistance coefficient with a large level of uncertainty. The pressure drop associated with the turning of the flow will be approximately a factor of 100 lower than the pressure drop associated with the expansion of the fluid and will therefore have a smaller impact on the total pressure drop across the delay tank. The resistance coefficient is computed by equation (3.28) [35]. The coefficients in equation (3.28) are determined from graphs in [35]. k_Δ is a function of the Reynolds number, C_1 is a function of the geometry of the inlet area and ζ_l is a function of the ratio of the inlet diameter and the distance between the inlet and the outlet as well as the ratio of the diameter at the turn of flow and the inlet diameter [35].

$$\zeta = k_\Delta C_1 \zeta_l \tag{3.28}$$

The losses due to the perforated sheets and the turn of the flow are lumped together in a `SimpleGenericOrifice` model and the inner shell is modeled as a `DynamicPipe` model. The outer shell is also modeled as a `DynamicPipe` model but as the cross section area of the outer shell is annular, the input will be different. For the outer shell; the cross section area, the inner perimeter and the outer perimeter is calculated in the delay tank model. The inner diameter of the inner and outer shell is not constant, however in the model, the mean inner diameter of the inner and outer shell is chosen.

The fluid volumes at the two heads of the delay tank are modeled with the `DynamicPipe` model, but for these models the pipe length is assumed to be the approximate path length of the flow and the heat transfer area is modified to correspond to the heat transfer area of the delay tank heads. The inner diameter is assumed to be constant. The inner diameter of the flow path of head 1 is assumed to be the inner diameter of the inner shell exit, and the inner diameter of the flow path of head 2 is assumed to be the inner diameter of the outer shell exit.

When the flow exits the delay tank, a sudden compression of the flow occurs due to the decrease in flow area. A pressure drop will occur due to this sudden compression of flow and for an assumed uniform velocity the resistance coefficient ζ = 0.5 [35]. The loss is modeled in the last `SimpleGenericOrifice` model in Figure 3.18.

The inner shell wall, outer shell wall and the ends of the delay tank are modeled as separate heat capacitors. Convection occurs between the fluid in the inner shell and the inner shell wall and

between the inner shell wall and the fluid in the outer shell. For the fluid in the outer shell and at the ends of the delay tank, convection is modeled to the outer tank walls. Finally, convection is modeled between the outer tank walls and the ambient.

The input to the delay tank model is listed in Table 3.11.

Table 3.11: Input to the delay tank model.

Input	Value	Source
Initialization		
Starting pressure at inlet [bar]	1.259	
Starting pressure at outlet [bar]	1.22	
Starting temperature of water volume [°C]	20	
Starting mass flow rate [kg/s]	0.3	
Shell Geometry		
Length of inner shell [m]	1.7	[55]
Inner diameter of inner shell [m]	0.4132	[55]
Thickness of inner shell wall [m]	0.005	[55]
Length of outer shell [m]	1.7	[56]
Inner diameter of outer shell [m]	0.609	[56]
Thickness of outer shell wall [m]	0.008	[56]
Head geometry		
Mean length of flow path at head 1 [m]	0.18	[57]
Mean diameter of flow path at head 1 [m]	0.584	[57]
Wall thickness at head 1 [m]	0.008	[57]
Mean length of flow path at head 2 [m]	0.20	[57]
Mean diameter of flow path at head 2 [m]	0.634	[57]
Wall thickness at head 2 [m]	0.010	[57]
Inlet/Outlet geometry		
Inlet diameter [m]	0.0817	[57]
Outlet diameter [m]	0.0777	[57]
Thermal		
Specific heat capacity of the delay tank walls [J/kgK]	500	[43]
Mass of inner shell [kg]	101.15	[58]
Mass of outer shell [kg]	205.95	[58]
Mass of head 1 [kg]	23.8	[58]
Mass of head 2 [kg]	38.1	[58]
Convective heat transfer coefficient from the delay tank walls to the ambient [W/m^2K]	5	[45]
Ambient temperature [°C]	20	
Loss		
Resistance coefficient at inlet [-]	1	[35]

Resistance coefficient at outlet [-]	0.5	[35]
Resistance coefficient at perforated plates [-]	97	[35]
Resistance coefficient at the turning of the flow [-]	8.1	[35]
Lengthwise discretization		
Number of nodes for each shell []	2	

3.7.10 T-junction

The purpose of the T-junction is to converge flow from branching pipes to a main pipe or to diverge flow from a main pipe to branching pipes. The T-junctions are modeled with the MSL model `TeeJunctionVolume`. A volume is defined in the model and it is chosen to be 0.01 m^3 for all T-junctions in the cooling system. Due to the volume definition, mixing will occur in the model. The pressure losses that arise due to T-junctions are included in the pipe segment model. For the chosen T-junction model, the initial pressure and temperature in the volume needs to be defined.

3.7.11 Sensors

The sensors objective is to measure process values such temperature, pressure and flow in the cooling system. A signal is then sent to a transmitter, which through manipulation, sends a standardized signal with a current of 4-20 mA to either an indicator or a PLC. In the PLC, an analogous alarm is triggered if the measured process value gets too high (exceeding the high alarm limit H2), or gets too low (exceeding the low alarm limit L2), for a specified duration. When an alarm is triggered, either the operator is required to intervene to prevent the cooling system to go to State Fault or the system is automatically sent to State Fault. The action taken depends on which sensor that has triggered the alarm. Most alarm limits are set as a deviation in % from the set-point value of the measured process value. When a process value exceeds an alarm limit it needs to be exceeded during a specified duration before the alarm is triggered. This duration is called the on-delay. The on-delay is implemented to avoid the triggering of an alarm when a sudden surge of a process value occurs before reaching safe process values again.

In the cooling system there are four different sensors present. These are temperature, flow, pressure and quality sensors. The quality sensor measures the conductivity of the water. This sensor is omitted from the modelling since the conductivity of the water is not a variable of interest in the case studies.

3.7.11.1 Temperature sensor

Resistance temperature detectors are used to monitor the water temperature in the cooling system (Email L Rosberg 6 Nov 2020). The temperature can be monitored with the aid of a specified temperature and electric resistance relationship of a detector element. A current is sent through the sensor and the change in electric resistance of the detector element is measured and subsequently converted to the change in temperature of the detector element [59]. The resistance temperature detector is inserted into a thermowell to protect the device and also allow for easy access during

operation. The thermowell is a tube with a closed end in contact with the fluid in the cooling system and an open end where the resistance temperature detector is inserted.

The temperature sensor is modeled with the Buildings library model `TemperatureTwoPort` in order to model the time delay of a temperature sensor. A time delay will arise from when a specified temperature in the fluid is reached until the sensor measures the same temperature. This time delay arises due to the heat transfer process from the fluid to the sensor. The time delay is affected by the design of the sensor and thermowell and the flow conditions. Since no data regarding the time constant of the temperature sensors are available, the time constant is assumed. The time constant is assumed to be constant and equal for all the temperature sensors at their nominal mass flow rates. The time constant is chosen to generate a response time of 20 seconds for the nominal mass flow rate at the sensor (Email L Rosberg 11 Oct 2020).The response time is defined as the time required for the sensor to read 99,3 % of the step change in fluid temperature [60]. The measured temperature converges to the incoming fluid temperature using a first order differential equation. The mass flow rate is taken into account for the time constant. For deviations of the mass flow rate from the nominal mass flow rate, the time constant will be inversely proportional to the mass flow rate. The warning and alarm limits are specified in the model in order to visualize when process values have exceeded sensor limits, when analyzing simulation results. The starting temperature of the temperature sensor model is set at the ambient temperature.

The input to the temperature sensor model is listed in Table 3.12, where the displayed values are constant for all the components in the cooling system and the input for the empty fields vary for each individual temperature sensor.

Table 3.12: Input to the temperature sensor model.

Input	**Value**
Initialization	
Type of initialization	Initialization with initial states
Starting temperature	20 °C
Nominal condition	
Nominal mass flow	-
Time constant	4
Warning/alarm limits	
Set-point	-
H2 alarm	-
H1 warning	-
L1 warning	-
L2 alarm	-

3.7.11.2 Pressure sensor and pressure switch

A pressure sensor monitors the pressure while a pressure switch is a switch which sends a signal when two electrical contacts come in physical contact. The pressure sensors and pressure switches are connected to the cooling system by a short branched pipe. The pressure sensor monitors the pressure through piezoelectric technology while the pressure switch is mechanical and calibrated so the two electrical contacts come in physical contact when the set-point pressure of the pressure switch is reached (Email L Rosberg 3 Feb 2021). In the cooling system, the pressure switches are hardwired to a mechanism which will decrease the pump speed when the set-point pressure at the pressure switch is reached [28].

The pressure sensors and the pressure switches are modeled with the MSL model `PressureSensor`. No pressure loss is assumed across the sensor. The respond time of the sensors is relatively fast resulting in no delay time being assumed. The warning and alarm limits are specified in the pressure model in order to visualize when process values have exceeded sensor limits, when analyzing simulation results. The input to the model is listed in Table 3.13.

Table 3.13: Input to the pressure model.

Input
Set-point
H2 alarm
H1 warning
L1 warning
L2 alarm

3.7.11.3 Flow sensor

In-line ultrasonic flowmeters are utilized to monitor the flow in the cooling system (Email L Rosberg 28 Jan 2021). The flowmeters are modeled with the MSL model component `massFlowRate`. As no obstruction is placed inside the piping for the flowmeters, no pressure loss is assumed. The respond time of the sensors is relatively fast resulting in no delay time being assumed. The warning and alarm limits are specified in the components in order to visualize when process values have exceeded sensor limits, when analyzing simulation results. The input to the model is listed in Table 3.14.

Table 3.14: Input to the flow sensor model.

Input
Set-point
H2 alarm
H1 warning
L1 warning
L2 alarm

3.7.12 Heated component

The heated components refer to the objects that are heated up and need to be cooled by the cooling system. The heated components in the cooling system are the upper and lower thermal moderator, the proton beam window and the proton beam window flanges.

The objective of the thermal moderators is to slow down the spallated neutrons to appropriate energy levels [7]. The thermal moderators consist of a moderator over and under the target wheel and they are called the upper and lower thermal moderator. Two fluid inlets and outlets exist for each moderator. The thermal moderator can simply be described as an aluminum disk with several cooling water channels in it. The target wheel and the upper and lower thermal moderator are shown in Figure 3.19 while a detailed drawing of the upper thermal moderator is shown in Figure 3.20.

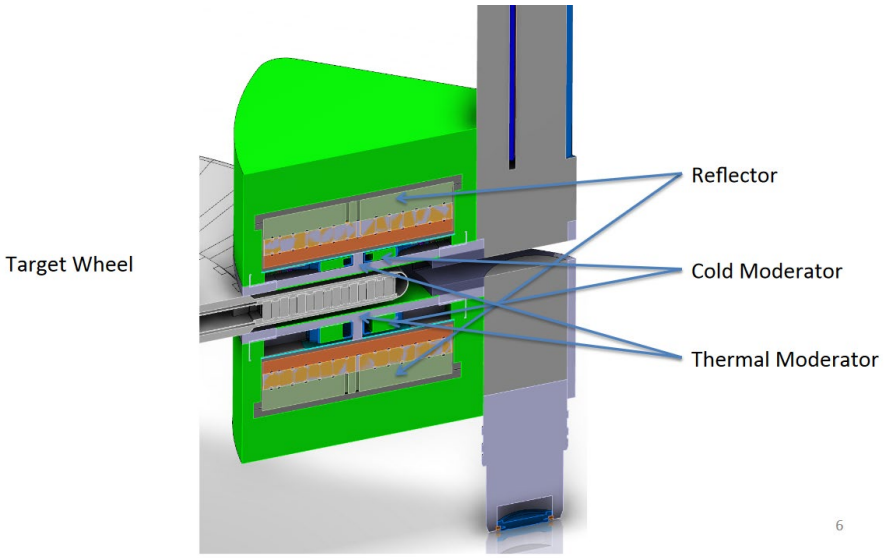

Figure 3.19: Target wheel and the thermal moderators, cold moderators and reflectors [61].

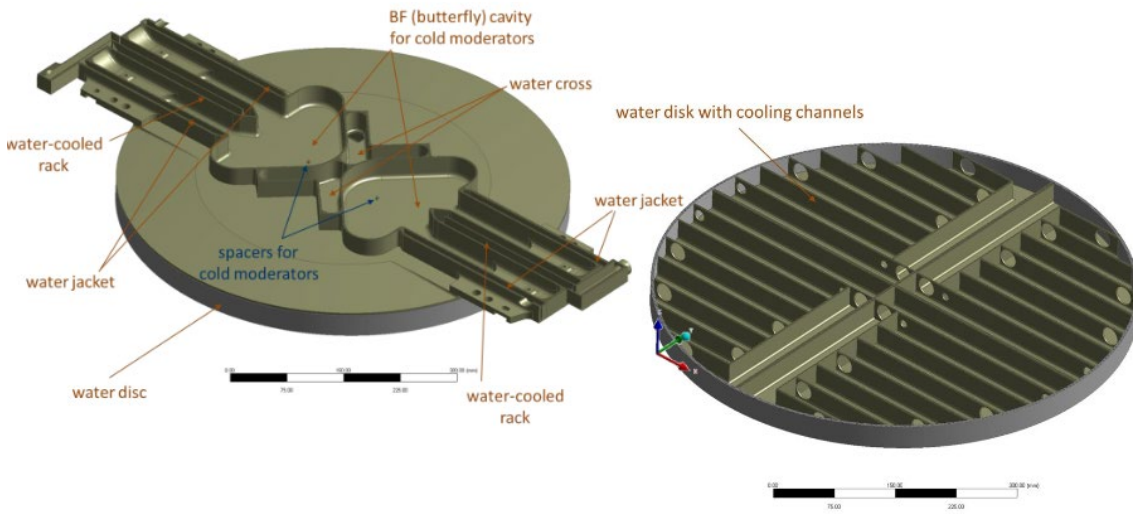

Figure 3.20: Detailed drawing of the upper thermal moderator [62].

The objective of the proton beam window is to separate the vacuum atmosphere in the accelerator tube and the sub-pressure atmosphere in the Monolith Vessel and simultaneously permit the proton beam to cross through the proton beam window [63]. The proton beam window consists of two thin aluminum plates separated by a cooling channel and is coupled to an aluminum frame. The proton beam window and frame is in turn assembled to stainless steel flanges, which will aid in preserving vacuum atmosphere in the accelerator tube. The proton beam window, frame and flanges are shown in Figure 3.21.

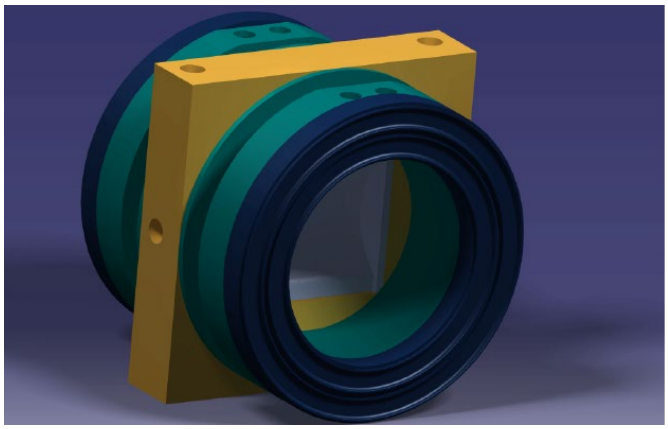

Figure 3.21: Proton beam window, frame and flanges [63].

The heated components are modeled with the MSL models `DynamicPipe` and `SimpleGenericOriface` and the ESS modified models `HeatCapacitorArray` and `PrescribedHeatFlowArray`. A heat input to the heated component is defined. This heat is transferred to the solid parts of the heated components and through convection the heat is transferred to the fluid. The PBW is modeled with more detail; the piping at the frame inlet, proton beam window and the frame outlet are modeled individually with individual heat capacities and

heat loads. The heated component model and the PBW model is shown in Figure 3.22 and Figure 3.23 respectively.

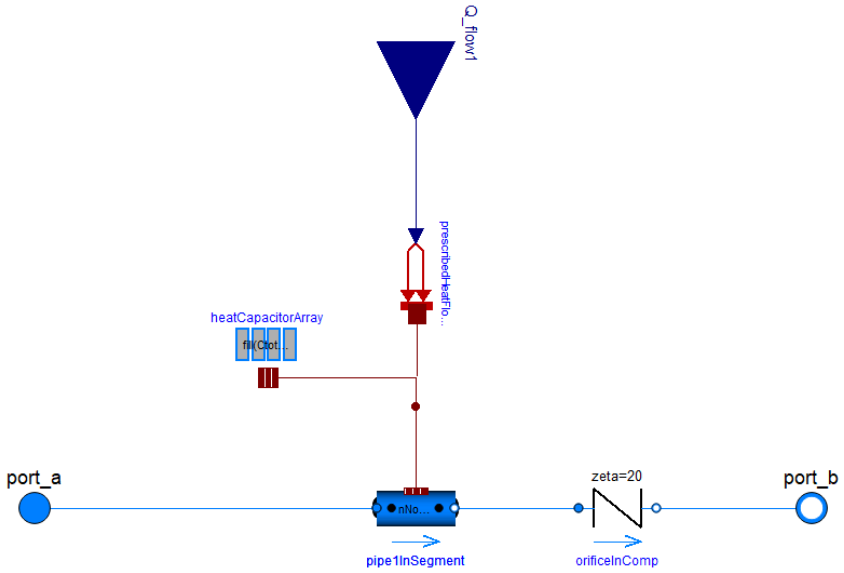

Figure 3.22: Heated component model.

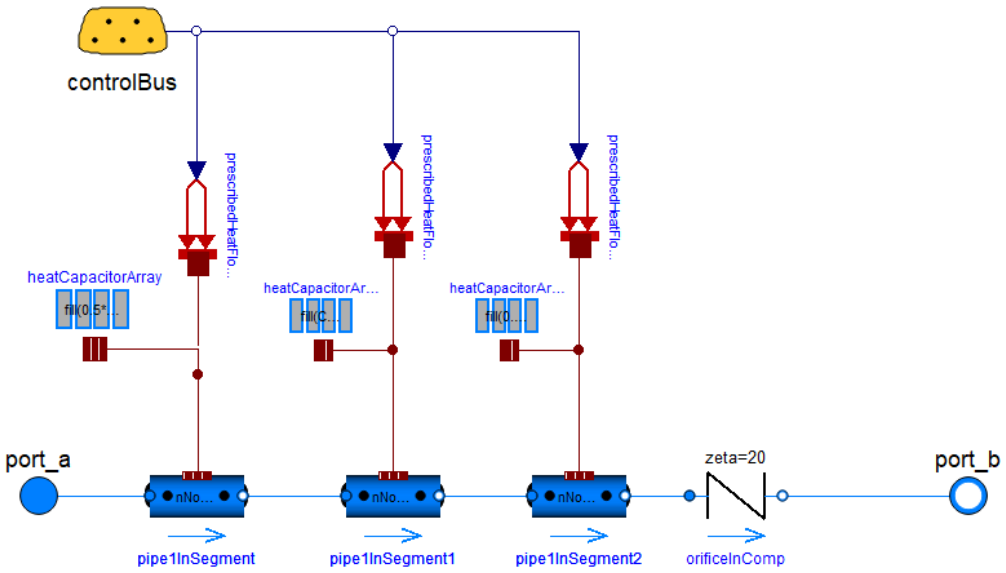

Figure 3.23: PBW model.

The piping lengths in the proton beam window and the proton beam window flanges in system 1065 are estimated in Naviswork Freedom 2020. The measurement of the piping lengths in the proton beam window and the proton beam window flanges are shown in Figure 3.24 and Figure 3.25 respectively.

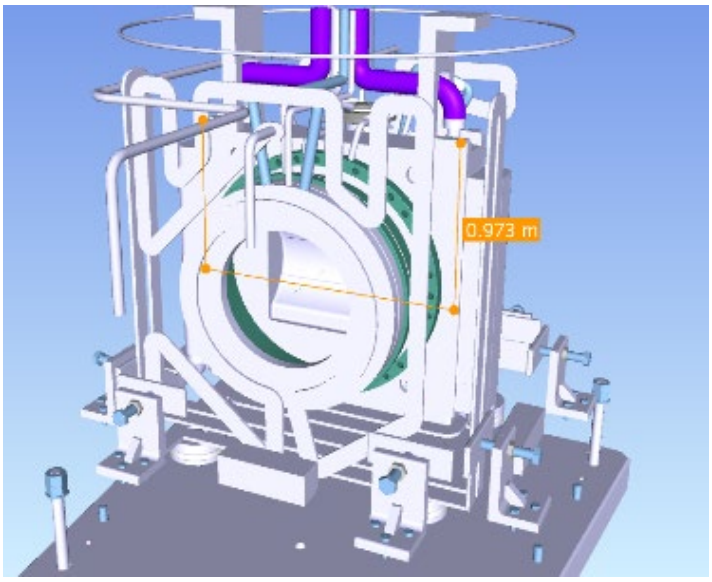

Figure 3.24: Measurement of the piping length in the proton beam window [22].

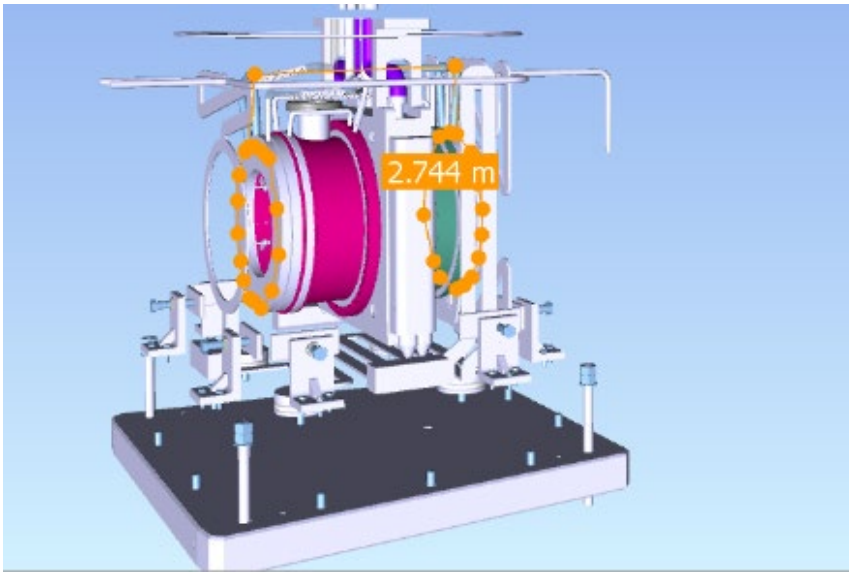

Figure 3.25: Measurement of the piping length of the proton beam window flanges [22].

The piping length in each moderator is difficult to measure, however the water volume of each moderator is specified and as a simplification the length is adjusted to correspond to this volume. The water volume of the moderators and piping lengths of all the heated components is listed in Table 3.15.

Table 3.15: Water volume of the moderators and the piping lengths in all the cooled components.

Component model	**Water volume [m^3]**	**Piping length [m]**
Upper moderator	0.0135 [64]	21.2
Lower moderator	0.0148 [64]	23.2

Proton beam window	-	0.2
Proton beam window frame inlet		0.4
Proton beam window frame outlet		0.4
Proton beam window flanges	-	2.8

The nominal pressure drop across the subsystems 1110 and 1065 is known. The nominal pressure drops across the heated component models are then calibrated to result in the correct nominal pressure drops at nominal flow across the subsystems. The nominal pressure drops across subsystems 1110 and 1065 are listed in Table 3.16.

Table 3.16: Nominal pressure drop across subsystems 1110 and 1065.

Subsystem	**Nominal pressure drop [bar]**
Subsystem 1110	0.75 [25]
Subsystem 1065	0.85 [65]

For subsystem 1110, the mass of the moderators can be computed from the known volume and density of the moderators. There are different aluminum materials in the moderators, however one of the materials make up the largest volume of each moderator and thus it is assumed that each moderator is constructed entirely from this material [62]. For subsystem 1065, the mass of the proton beam window and frame is specified while the mass of the proton beam window flanges is calculated with the multiplication of the volume with the density. As the material of the proton beam window flanges is specified as stainless steel, it is assumed that the flanges have the same material as the piping [66]. The volume of the proton beam flanges is computed with data available in the drawings of the proton beam window flanges [67]. It is assumed that the heat capacity and density of the heated components are constant. Different properties of the heated components are listed in Table 3.17.

Table 3.17: Properties of the heated components.

Component	**Material**	**Heat capacity [J/kgK]**	**Density [kg/m^3]**	**Volume [m^3]**	**Mass [kg]**
Upper moderator	Al 6061-T6 [62]	896 [68]	2700 [68]	0.00411 [64]	11.10
Lower moderator	Al 6061-T6 [62]	896 [68]	2700 [68]	0.0031 [64]	8.37
Proton beam window	Al6061-T6 [66]	896 [68]	2700 [68]	-	0.47 [67]

Proton beam window frame	Al6061-T6 [66]	896 [68]	2700 [68]	-	13.31 [67]
Proton beam window flanges	Stainless steel 1.4404	500 [43]	8000 [43]	0.0231 [67]	184.8

The input to the heated component models and the PBW model is shown in Table 3.18, where the displayed values are constant for all the components in the cooling systems and the input for the empty fields vary for each individual component.

Table 3.18: Input to the heated component model and the PBW model.

Input	**Value**
Initialization	
Starting pressure at inlet [bar]	-
Starting pressure at outlet [bar]	-
Starting temperature [°C]	20
Starting mass flow rate [kg/s]	-
Geometry	
Length [m]	-
Inner diameter [m]	-
Height [m]	-
Discrete loss	
Nominal mass flow rate [kg/s]	-
Nominal pressure drop [bar]	-
Thermal	
Mass of component exluding water [kg]	-
Specific heat capacity of component [J/kgK]	-
Lengthwise discretization	
Number of nodes []	4

3.7.13 Heat exchanger

The heat exchanger is a welded plate heat exchanger with the two fluids flowing in counter flow. The objective of the heat exchanger is to transfer heat from the moderators and the proton beam window to the intermediate cooling system. Since the heat exchanger is a plate heat exchanger, the heat exchanger model `PlateHeatExchangerEffectivnessNTU` in the Buildings library is used. It does not model heat transfer due to condensation but this is no issue since the mediums on both sides should always be in the liquid phase. No heat capacity is assumed in the walls between the hot and cold fluid. The heat transfer rate is defined by equation (3.29).

$$\dot{Q} = \varepsilon \dot{Q}_{max} \tag{3.29}$$

The heat transfer effectiveness is in turn defined by equation (3.30).

$$\varepsilon = f(Z, NTU, FR) \tag{3.30}$$

The convective heat transfer coefficients of the two flows in the heat exchanger are proportional to $\left(\frac{\dot{m}}{\dot{m}_n}\right)^p$, where $p = 0.8$. The input to the heat exchanger model is listed in Table 3.19 [69].

Table 3.19: Input to the heat exchanger model.

Input	**Value**
Configuration []	Cross flow
Nominal condition	
Nominal mass flow rate in hot side[kg/s]	4.8
Nominal mass flow rate in cold side [kg/s]	4.8
Pressure drop in hot side [bar]	0.23
Pressure drop in cold side [bar]	0.415
Nominal thermal performance	
Nominal heat transfer [kW]	170.8
Nominal temperature at hot side inlet[°C]	28.5
Nominal temperature at cold side inlet [°C]	15

3.7.14 Pump

The pumps are hermetic centrifugal pumps which can be controlled by frequency converters. During normal operation the pump speeds are constant. The pumps purpose is to circulate a cooling medium to ensure an adequate cooling of the moderator and proton beam window and all components in the cooling system. To ensure this cooling flow the pump must produce a pump head to overcome the frictional losses in the cooling system.

The pumps are modeled as a centrifugal pump with ideally controlled rotational speed with the MSL model `PrescribedPump`. The input signal is used to specify the rotational speed of the pump. The pump speed ramping at start-up, shut-down and faults is listed in Table 3.20. It shall be noted though that the start-up procedures will have to be adapted through linear interpolation for a pump speed over zero, since a starting pump speed of zero results in convergence failures.

Table 3.20: Ramping of pump speeds at different events.

Start-up	30 seconds linear increase of pump speed from zero to operational speed.
Shut-down	30 seconds linear decrease of pump speed from operational speed to zero.
Fault	5 second linear decrease of pump speed from operational speed to zero.

The pump curve at nominal speed and density is incorporated in the pump model. These values are retrieved from the manufacturer specification. A number of points on the pump curve need to be determined and set into the pump model, which then interpolates the points to a pump curve. Different points on the pump curve are selected as well as the number of points, in order to determine which configuration is the most accurate while still keeping the computation low.

Four specific points on the pump curve are chosen as this results in an accurate interpolated pump curve by the pump model. An interpolated curve is plotted over the manufacturers pump curve and the points are altered until a reasonable accuracy of the interpolated pump curve is achieved. Through the similarity laws the component model can generate pump curves at different pump speeds and densities. The points on the pump curve chosen as inputs for the pumps in systems 1041 and 1070 are shown in Figure 3.26 and Figure 3.27 respectively, where the y-axis shows the pump head and the x-axis shows the volume flow rate through the pump.

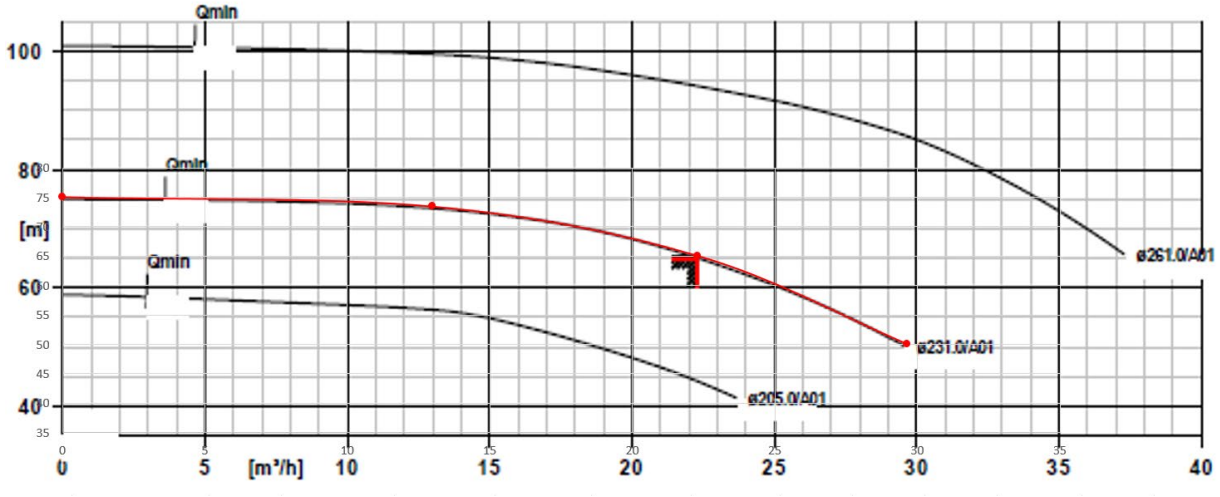

Figure 3.26: Four points on the pump curve chosen as inputs to the pump model in system 1041 [70].

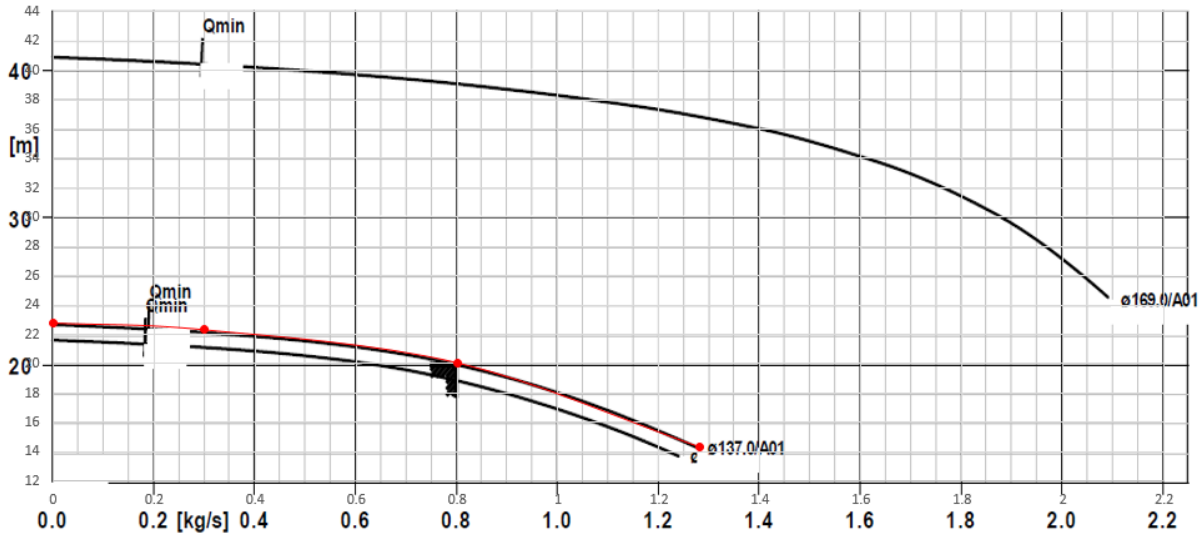

Figure 3.27: Four points on the pump curve chosen as inputs to the pump model in system 1070 [71].

At a constant pump speed the efficiency of the pump varies with flow. The efficiency increases with flow until it reaches a maximum, for larger flows the efficiency drops again. For flows close to the maximum point the efficiency is roughly constant. For simplification, the pumps are assumed to have a constant efficiency with a value equal to the maximum efficiency of the pump at nominal pump speed. The simplification will not affect the total heat input to the cooling system significantly, the heat input to the cooling system from the pumps at nominal pump speeds and mass flow rates will amount to approximately 2% of the total heat input [32][33]. The input to the pump models is listed in Table 3.21 [70][71].

Table 3.21: Input to the pump models.

Input	**1041-P-001**	**1070-P-026**
1041-P-001		
Flow characteristic	Polynomial curve based on four operational points	Polynomial curve based on four operational points
Nominal rotational speed for flow characteristic [rpm]	2971	2961
Operational speed [rpm]	2542	3613
Nominal fluid density for flow characteristic [kg/m^3]	998	998
Efficiency [%]	38	19

3.7.15 Proton beam

The proton beam is modeled with the MSL model `CombiTimeTable`. This timetable specifies the heat input to the cooled components as a function of time. The connection between the MSL

model CombiTimeTable and the MSL model `PrescribedHeatFlow` in the heated components is constructed through connections to MSL models `ControlBus`. By using the `ControlBus` model, connections across subsystem model boundaries are allowed. The `CombiTimeTable` interpolates between the operational points set as inputs to the proton beam model. Since the interest is to analyze how the cooling systems responds to disturbances at normal operation, the heat input by the proton beam is simplified. The heat input to the heated component models is increased from zero to operational power in a one second ramp at a specified time. Heat inputs to the PBW frame inlet, PBW and PBW frame outlet are retrieved from [63], however more recent calculations computed a higher total heat input to the PBW and frame [72]. The heat inputs to the PBW frame inlet, PBW and PBW frame outlet are approximated with the multiplication with a factor to achieve the total heat input as seen in [72].The heat input to each heated component model is shown in Table 3.22 [32][33][63][72].

Table 3.22: Heat input to the cooled component models.

Component	**Heat input [kW]**
Upper moderator inlet 1	40
Upper moderator inlet 2	40
Lower moderator inlet 1	40
Lower moderator inlet 2	40
Proton beam window frame inlet	0.4
Proton beam window	4.4
Proton beam window frame outlet	0.4
Proton beam window flanges	1

4 Verification and validation

The verification and validation of the models is important to ensure that the simulation results can be trusted.

The aim of the verification is to confirm that the models have been implemented in a correct way. A wide-proven commercially available software, Dymola, and the Modelica Standard Library and Buildings Library, developed and tested by developers around the world, are chosen to guarantee the correctness of the underlying equations and component models in the libraries. Furthermore, an expert from Modelon, a Lund-based company which develop advanced Modelica models, has given advice in how to correctly implement models in the software environment. The component models that have been developed in Dymola are verified with manufacturer data or known and proven mathematical calculations performed in Excel.

The aim of the validation is to check the accuracy of the models compared to the real systems. As the real systems are not in operation yet, no operational data is available for comparison. The validation can however be performed in the future, once the systems have been commissioned.

4.1 Pipe segment

Several components such as piping, elbows, hand shut-off valves, T-junctions and reducers are integrated in the developed pipe segment model. In order to verify all the integrated components simultaneously, the pipe segment model tested included one of every integrated component. First the pressure drop across the pipe segment as a function of mass flow rate is verified, thereafter, the temperature of the pipe segment walls and the temperature of the fluid as a function of time is verified.

4.1.1 Pressure drop verification

The implementation of the model used to simulate the pressure drop across the pipe segment as a function of mass flow rate is depicted in Figure 4.1. The model results are then compared to the results obtained from the mathematical calculations, which are explained in the following paragraphs.

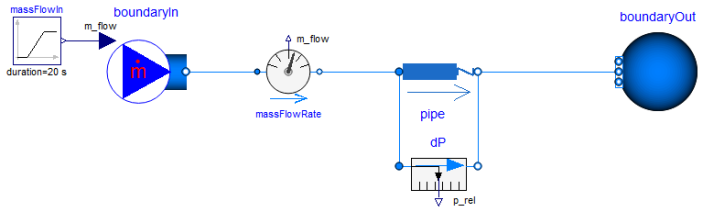

Figure 4.1: Implementation of the pressure drop calculation in the pipe segment model.

Pressure drops in pipes can be categorized into major and minor losses. Major losses occur in straight pipes due to friction while minor losses occur in components which affect the flow, such as elbows, T-junctions, hand shut-off valves and reducers. The major and minor losses are shown in equation (4.1) and equation (4.2) respectively [42].

$$\Delta p = \frac{8fl}{\rho\pi^2 d^5}\dot{m}^2 \tag{4.1}$$

$$\Delta p = \frac{8K_{tot}}{\rho\pi^2 d^4}\dot{m}^2 \tag{4.2}$$

Combining equations (4.1) and (4.2), the pressure drop as a function of mass flow rate across the pipe segment model can be calculated by equation (4.3).

$$\Delta p = \frac{8\left(K_{tot} + \frac{fl}{d}\right)}{\rho\pi^2 d^4}\dot{m}^2 \tag{4.3}$$

K_{tot} is in turn the sum of the different components loss coefficients and is shown in equation (4.4).

$$K_{tot} = K_{E_{tot}} + K_{R_{tot}} + K_{T_{tot}} + K_{V_{tot}} \tag{4.4}$$

A comparison between the model results and the mathematical results is depicted in Figure 4.2, where the solid curve shows the results from the simulation and the dashed curve shows the results from the mathematical approach.

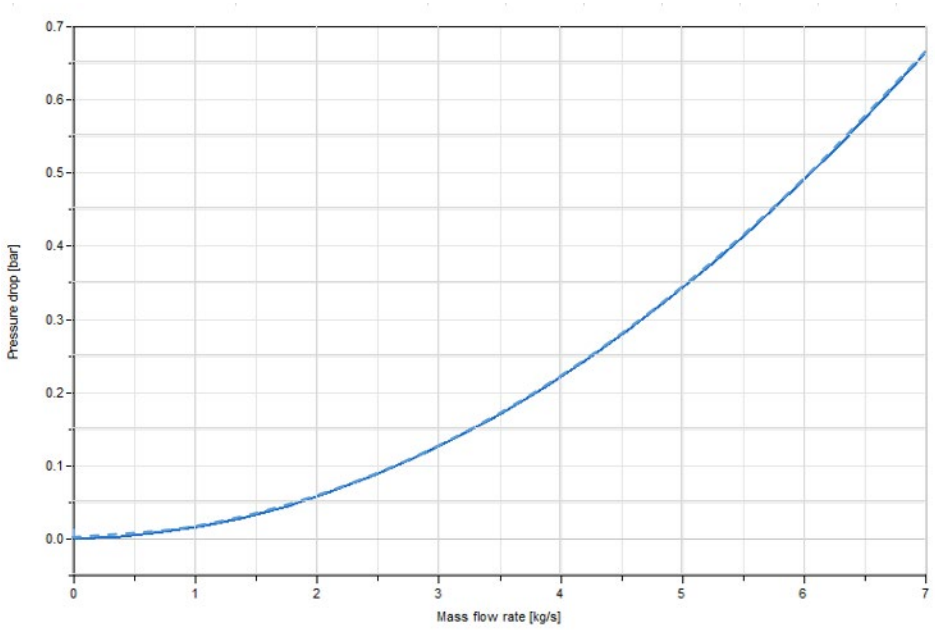

Figure 4.2: Comparison of the pressure drop obtained from the pipe segment model and the mathematical calculations, where the solid curve shows the model result and the dashed curve shows the result from the mathematical calculation.

4.1.2 Heat transfer verification

The temperatures of the pipe wall and the medium in the pipe segment model as a function of time is verified. The inlet fluid temperature is increased from 20 to 30 °C in a step and the temperatures of the pipe wall and the medium is calculated as a function of time. The implementation of the heat transfer calculation in the pipe segment model is shown in Figure 4.3 while the initial and boundary conditions are listed in Table 4.1.

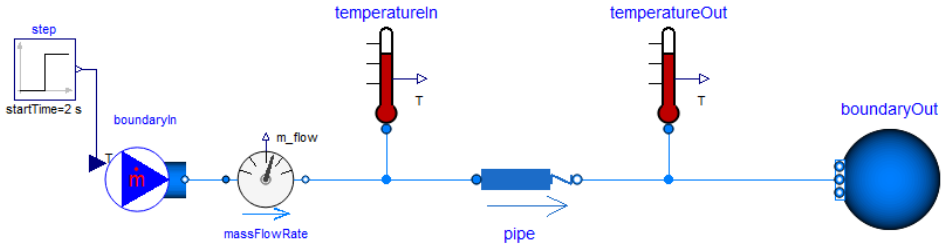

Figure 4.3: Implementation of the heat transfer calculation in the pipe segment model.

Table 4.1: Initial and boundary conditions of the implemented pipe segment model for the heat transfer calculation.

Initial conditions	**Value**
Starting temperature of pipe wall [°C]	20
Starting temperature of water [°C]	20
Boundary conditions	
Inlet temperature [°C]	30
Inlet mass flow rate [kg/s]	4

The energy balance of the liquid is shown in equation (4.5), while the energy balance of the solid is shown in equation (4.6).

$$m_l c_{p_l} \frac{dT_l}{dt} = \dot{m} c_{p_l}(T_{in} - T_l) - h_i A_i (T_l - T_s) \tag{4.5}$$

$$m_s c_{p_s} \frac{dT_s}{dt} = h_i A_i (T_l - T_s) - h_o A_o (T_s - T_{amb}) \tag{4.6}$$

With the initial conditions $T_s(0) = T_{s_0}$ and $T_l(0) = T_{l_0}$, a solution to the system of differential equations (4.5) and (4.6), is found and shown in equation (4.7).

$$\begin{pmatrix} T_s \\ T_l \end{pmatrix} = B_1 e^{\lambda_1 t} \begin{pmatrix} \eta_1 \\ \eta_2 \end{pmatrix}^{[1]} + B_2 e^{\lambda_2 t} \begin{pmatrix} \eta_1 \\ \eta_2 \end{pmatrix}^{[2]} + \begin{pmatrix} a_1 \\ a_2 \end{pmatrix} \tag{4.7}$$

The temperature of the pipe walls and the medium in the pipe segment model is plotted as a function of time in Figure 4.4, where the solid curves from the model are compared to the dashed curves from the mathematical calculations. The red curves show the temperature in the pipe walls while the blue curves show the temperature in the medium.

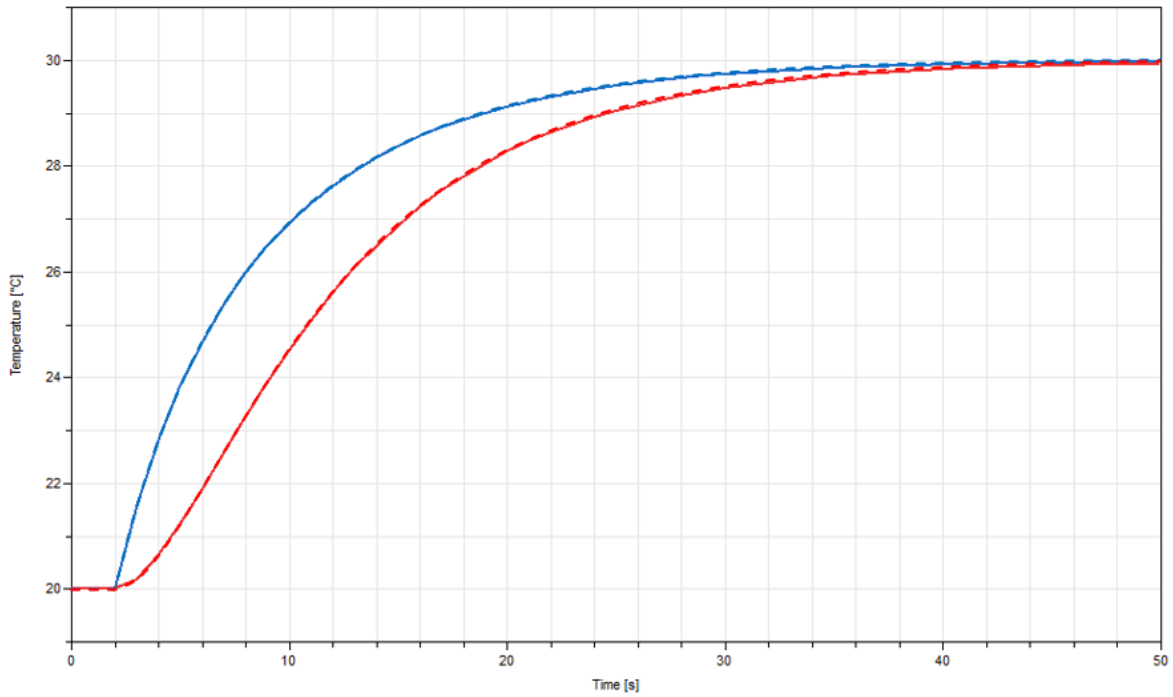

Figure 4.4: Temperature of the pipe walls and the medium in the pipe segment model as a function of time, where the solid curves are from the model and the dashed curves are from the mathematical calculations. The red curves show the temperature in the pipe walls while the blue curves show the temperature in the medium.

4.2 Gas and liquid separation tank

First the pressures at the port inlet and outlet are verified for a set tank pressure and water level, thereafter, the temperatures of the tank wall and the medium as a function of time are verified.

4.2.1 Port pressure verification

The implementation of the model used to simulate the tank port pressures for a set tank pressure and water level is depicted in Figure 4.5. The model results are then compared to the results obtained from the mathematical calculations, which are explained in the following paragraphs.

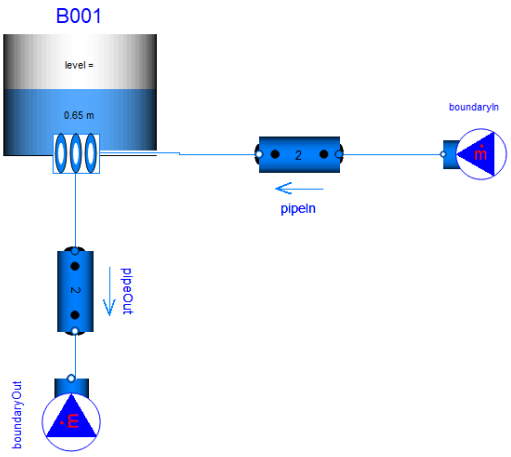

Figure 4.5: Implementation of the tank port pressures calculation in the gas and liquid separation tank model.

The port pressures are determined by equation (4.8).

$$p_{port} = p_{tank} + \rho g H \tag{4.8}$$

A comparison between the model results and the mathematical results regarding the port pressures is depicted in Figure 4.6, where the solid curves show the results from the simulation and the dashed curves show the results from the mathematical approach. The blue curves represent the inlet port pressure while the red curves represent the outlet port pressure.

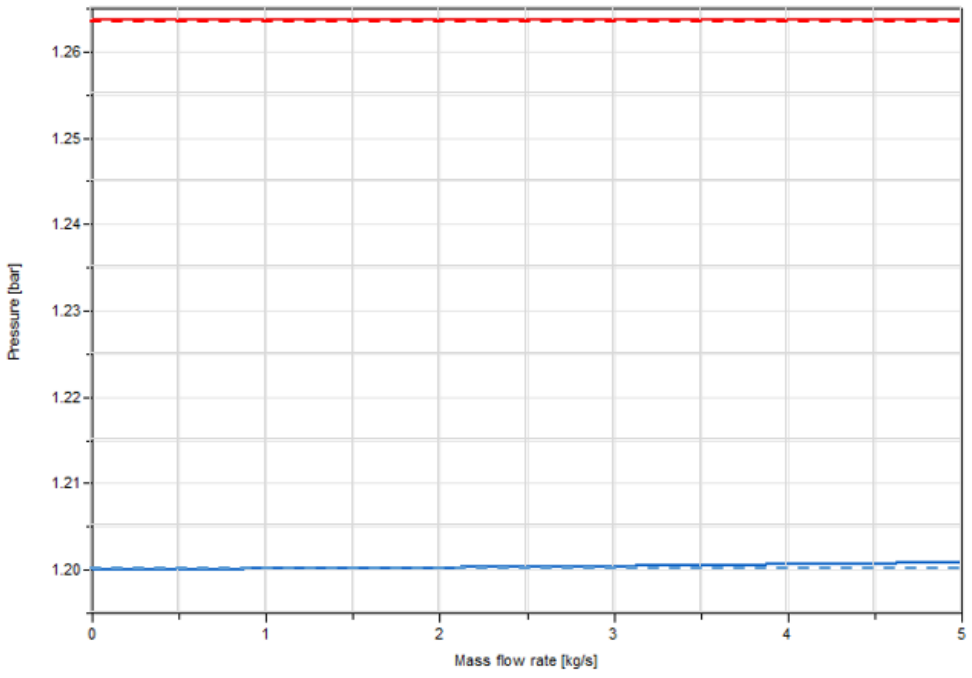

Figure 4.6: Comparison between the model results and the mathematical results regarding the port pressures, where the solid curves show the results from the simulation and the dashed curves show the results from the mathematical approach. The blue curves represent the inlet port pressure while the red curves represent the outlet port pressure.

4.2.2 Heat transfer verification

The temperatures of the pipe wall and the medium in the GLS tank as a function of time is verified. The inlet fluid temperature is increased from 20 to 28.3 °C in a step and the temperatures of the pipe wall and the medium is calculated as a function of time. The implementation of the heat transfer calculation in the GLS tank test model is shown in Figure 4.7 while the initial and boundary conditions are listed in Table 4.2.

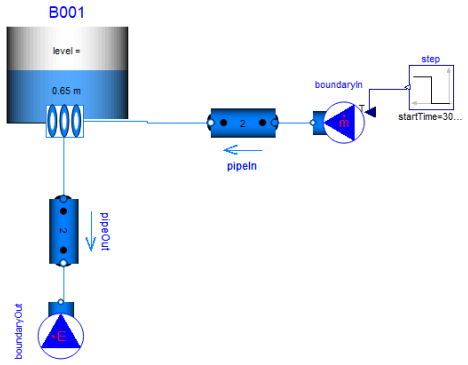

Figure 4.7: Implementation of the heat transfer calculation in the GLS tank model.

Table 4.2: Initial and boundary conditions of the implemented GLS tank model for the heat transfer calculation.

Initial conditions	**Value**
Starting temperature of pipe wall [°C]	20
Starting temperature of water [°C]	20
Boundary conditions	
Inlet temperature [°C]	28.3
Inlet mass flow rate [kg/s]	4.8

The energy balance of the liquid is shown in equation (4.9), while the energy balance of the solid is shown in equation (4.10).

$$m_l c_{p_l} \frac{dT_l}{dt} = \dot{m} c_{p_l}(T_{in} - T_l) - h_i A_i (T_l - T_s) \tag{4.9}$$

$$m_s c_{p_s} \frac{dT_s}{dt} = h_i A_i (T_l - T_s) - h_o A_o (T_s - T_{amb}) \tag{4.10}$$

With the initial conditions $T_s(0) = T_{s_0}$ and $T_l(0) = T_{l_0}$, a solution to the system of differential equations (4.9) and (4.10), is found and shown in equation (4.11).

$$\begin{pmatrix} T_s \\ T_l \end{pmatrix} = B_1 e^{\lambda_1 t} \begin{pmatrix} \eta_1 \\ \eta_2 \end{pmatrix}^{[1]} + B_2 e^{\lambda_2 t} \begin{pmatrix} \eta_1 \\ \eta_2 \end{pmatrix}^{[2]} + \begin{pmatrix} a_1 \\ a_2 \end{pmatrix} \tag{4.11}$$

The temperature of the pipe walls and the medium in the pipe segment model is plotted as a function of time in Figure 4.8, where the solid curves from the model are compared to the dashed curves from the mathematical calculations. The red curves show the temperature in the pipe walls while the blue curves show the temperature in the medium.

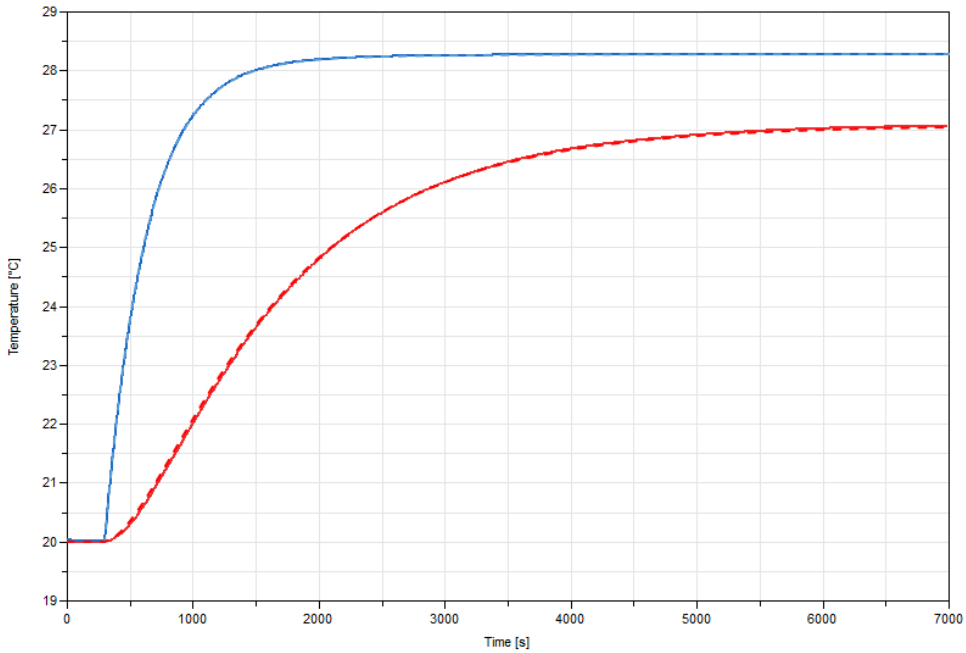

Figure 4.8: Temperature of the pipe walls and the medium in the GLS tank model as a function of time, where the solid curves are from the model and the dashed curves are from the mathematical calculations. The red curves show the temperature in the pipe walls while the blue curves show the temperature in the medium.

4.3 Delay tank

The pressure drop as a function of mass flow rate and the temperatures of the walls and medium of the delay tank as a function of time are verified.

4.3.1 Pressure drop verification

The implementation of the model used to simulate the pressure drop across the delay tank as a function of mass flow rate is depicted in Figure 4.9. The model results are then compared to the results obtained from the mathematical calculations. The pressure drop across the delay tank is calculated by equation (4.3).

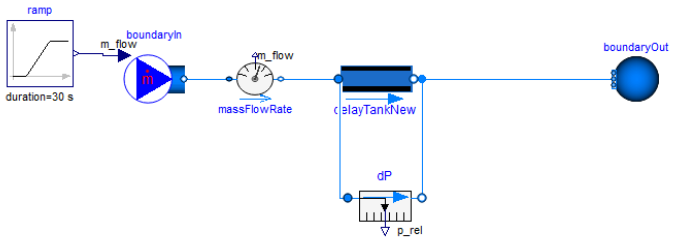

Figure 4.9: Implementation of the pressure drop calculation in the delay tank model.

A comparison between the model results and the mathematical results is depicted in Figure 4.10, where the solid curve shows the results from the simulation and the dashed curve shows the results from the mathematical approach.

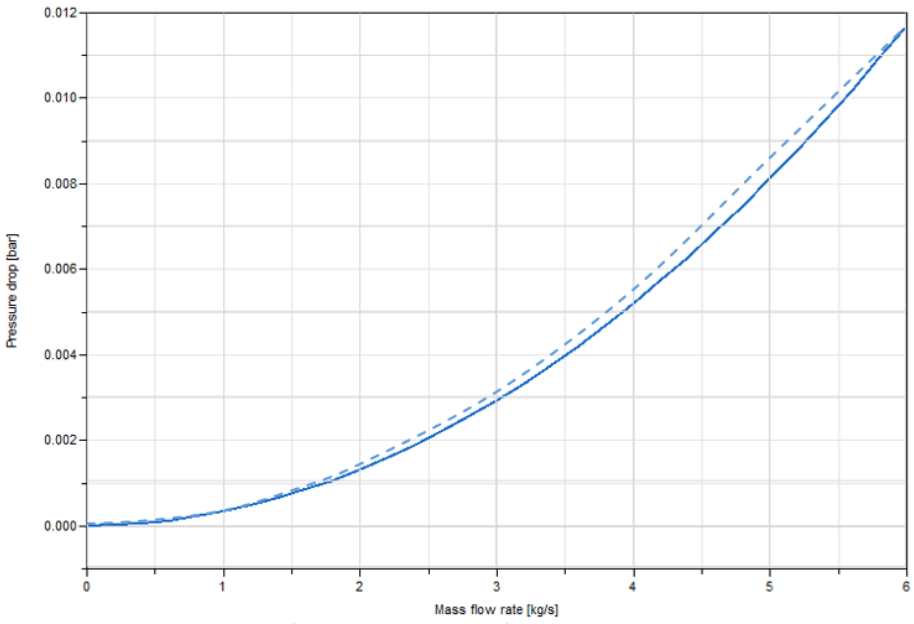

Figure 4.10: Comparison of the pressure drop obtained from the pipe segment model and the mathematical calculations, where the solid curve shows the model result and the dashed curve shows the result from the mathematical calculation.

4.4 Heat exchanger

The pressure drop and the outlet temperatures as a function of mass flow rate in the hot side of the heat exchanger are verified. The test model results are validated with data from the manufacturer, the data is however only available for nominal conditions and thus other conditions are hard to verify. The test model is depicted in Figure 4.11, while the boundary conditions of the test model are shown in Table 4.3.

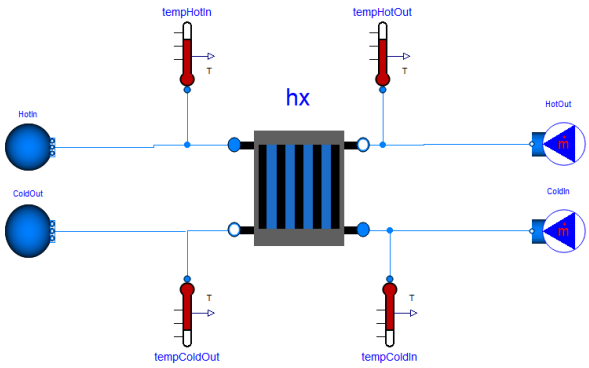

Figure 4.11: Heat exchanger test model.

Table 4.3: Boundary conditions of the heat exchanger test model.

Boundary conditions	**Value**
Hot side	
Inlet temperature [°C]	28.5
Inlet pressure [bar]	1.5
Cold side	
Inlet temperature [°C]	15
Outlet pressure [bar]	1
Mass flow rate [kg/s]	4.8

4.4.1 Pressure drop verification

A comparison between the model results and the manufacturer data regarding the pressure drop as a function of mass flow rate in the hot side of the heat exchanger is depicted in Figure 4.12, where the red curve shows the results from the simulation and the red marker shows the data from the manufacturer.

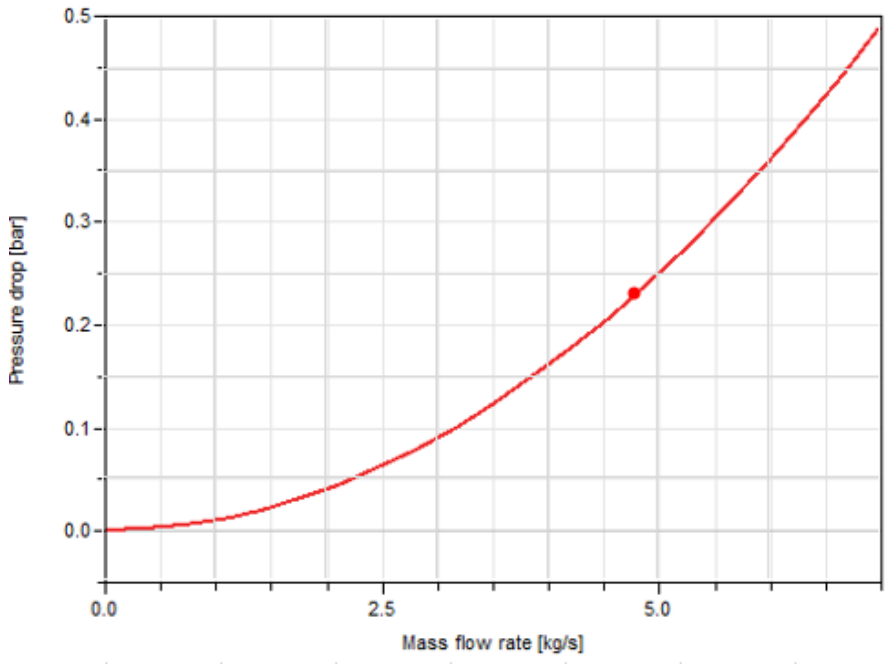

Figure 4.12: Comparison between the model results and the manufacturer data regarding the pressure drop as a function of mass flow rate in the hot side of the heat exchanger, where the red curve shows the results from the simulation and the red marker shows the data from the manufacturer.

4.4.2 Heat transfer verification

A comparison between the model results and the manufacturer data regarding the outlet temperatures as a function of mass flow rate in the hot side of the heat exchanger is depicted in Figure 4.13, where the curves show the results from the simulation and the markers show the data from the manufacturer.

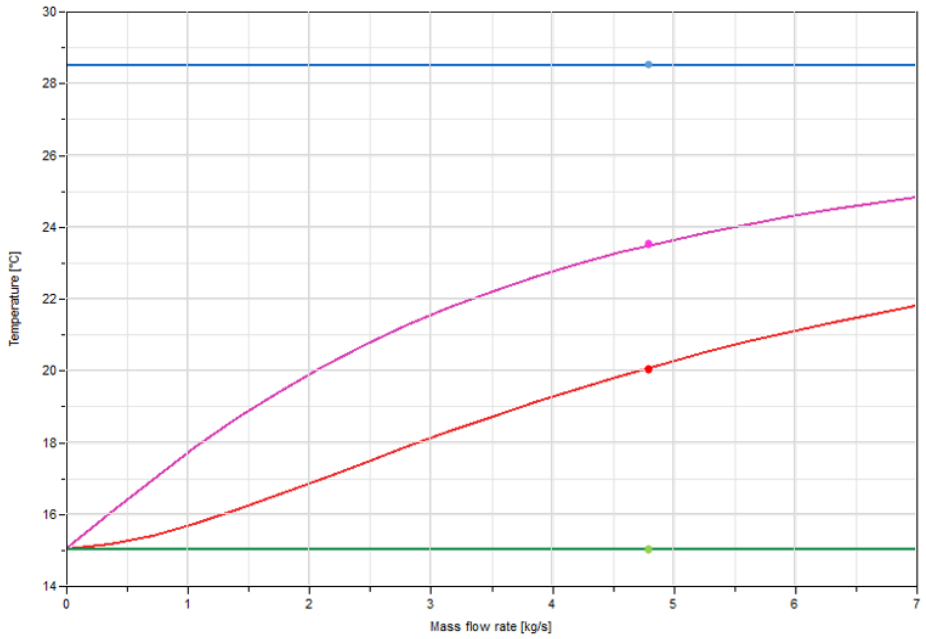

Figure 4.13: Comparison between the model results and the manufacturer data regarding the outlet temperatures as a function of mass flow rate in the hot side of the heat exchanger, where the red curve shows the results from the simulation and the red marker show the data from the manufacturer. The green, red, magenta and blue curves and markers are the cold inlet, hot outlet, cold outlet, and hot inlet temperatures respectively.

4.5 Flow control valve, actuator shut-off valve and flow shut-off valve

The pressure drop as a function of mass flow rate for different valve openings is verified.

4.5.1 Pressure drop verification

The implementation of the valve model used to simulate the pressure drop as a function of mass flow rate for different valve openings is depicted in Figure 4.14. The model results are compared to the results obtained from the mathematical calculations, which are explained in the following paragraphs.

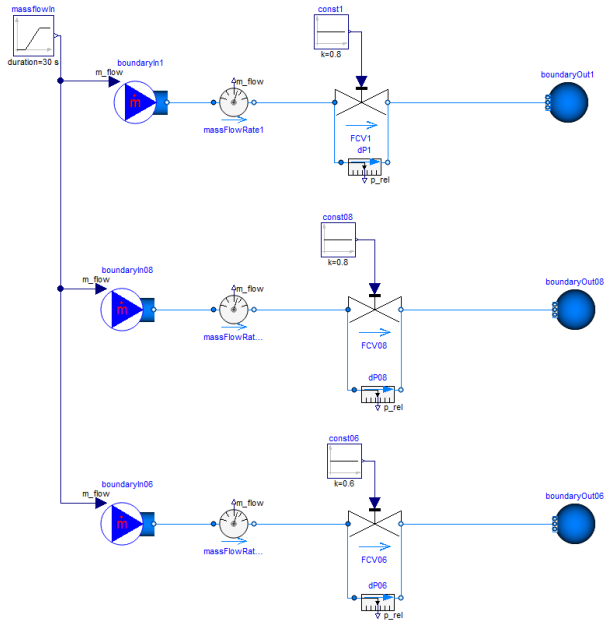

Figure 4.14: The implementation of the valve model used to simulate the pressure drop as a function of mass flow rate for different valve openings.

The k_{vv} value of a valve is determined by equation (4.12) [41].

$$k_{vv} = \dot{V}\sqrt{\frac{\left(\frac{\rho}{\rho_0}\right)}{\Delta p \cdot 10^5}} \tag{4.12}$$

The flow rate $\dot{V}$ is converted into mass flow rate $\dot{m}$ by equation (3.13). With the linear inherent valve characteristics, the opening of the valve can be determined by equation (4.13) [73].

$$opening = \frac{k_{vv}}{k_{vs}} \tag{4.13}$$

Combining equations (4.12), (3.13) and (4.13), allows for the pressure drop to be computed as a function of mass flow rate, as seen in equation (4.14).

$$\Delta p = \frac{3600^2 \cdot 10^5 \dot{m}^2}{\rho_0 {k_{vs}}^2 opening^2 \rho} \tag{4.14}$$

The pressure drop as a function of mass flow rate for different valve openings is shown in Figure 4.15, where the solid curves from the simulation are compared to the dashed curves from the mathematical calculations.

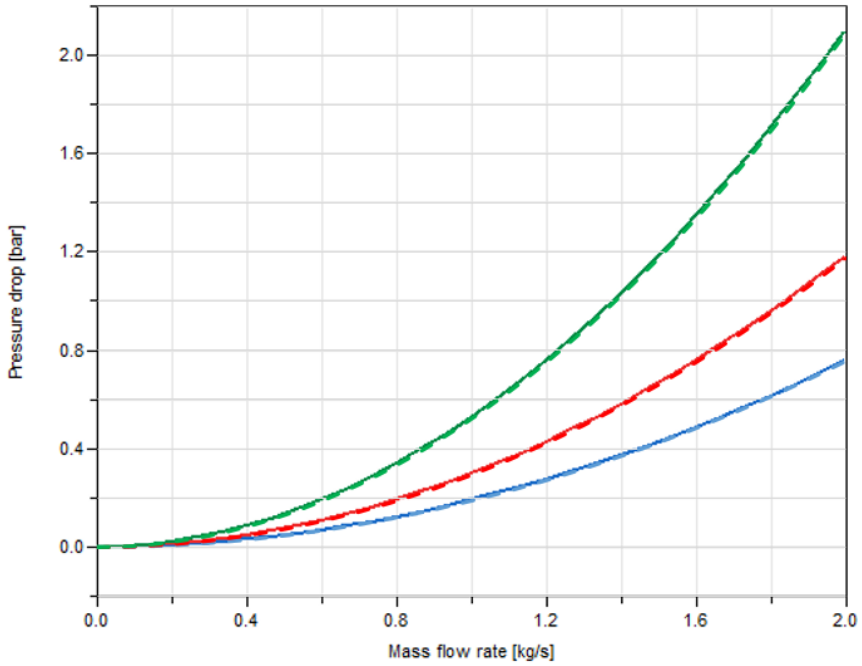

Figure 4.15: Pressure drop as a function of mass flow rate for different valve openings, where the solid curves show the results from the model results while the dashed curves show the results from the mathematical calculations. The blue, red and green curves show the pressure drop at valve openings 1, 0.8 and 0.6 respectively.

4.6 Pump

The pump models in systems 1041 and 1070 are validated with the pump curves delivered by the manufacturer. Both pump models are verified since they are individually calibrated to achieve their respective pump curve as delivered by the manufacturer. Since the pump curves are only available at the nominal pump speed, the pump models can only be verified at this speed. Pump curves at different pump speeds and the pump head as a function of mass flow rate and pump speed are verified with the similarity laws.

4.6.1 Validation of the nominal pump curve

A pump test model for the generation of the nominal pump curve for the pump models in systems 1041 and 1070 is shown in Figure 4.16. The pump curves of the pumps in systems 1041 and 1070 are shown in Figure 4.17 and Figure 4.18 respectively, where the red curves are the model results and the black curves are the pump curves from the manufacturer. The x-axis shows the volume flow rate through the pump while the y-axis shows the pump head in Figure 4.17 and Figure 4.18.

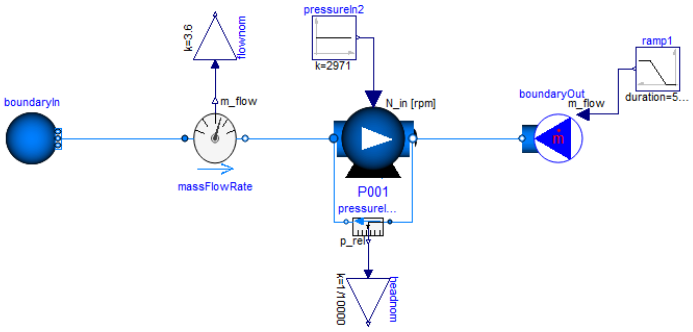

Figure 4.16: Pump test model for the generation of the nominal pump curve for the pump models in systems 1041 and 1070.

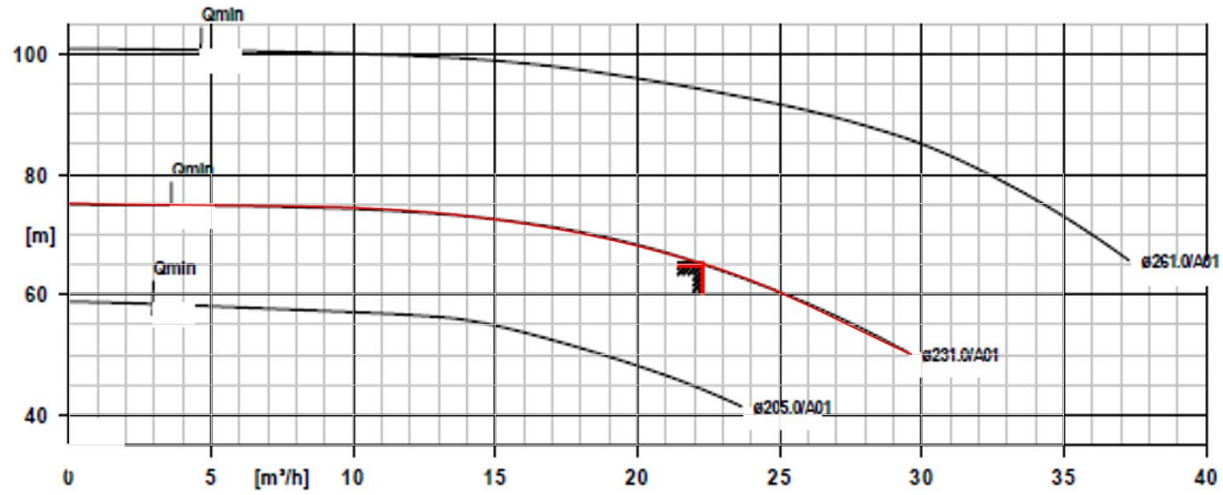

Figure 4.17: Pump curve at nominal speed of the pump in system 1041, where the red curve is the pump curve from the model and the black curve is the pump curve from the manufacturer [70].

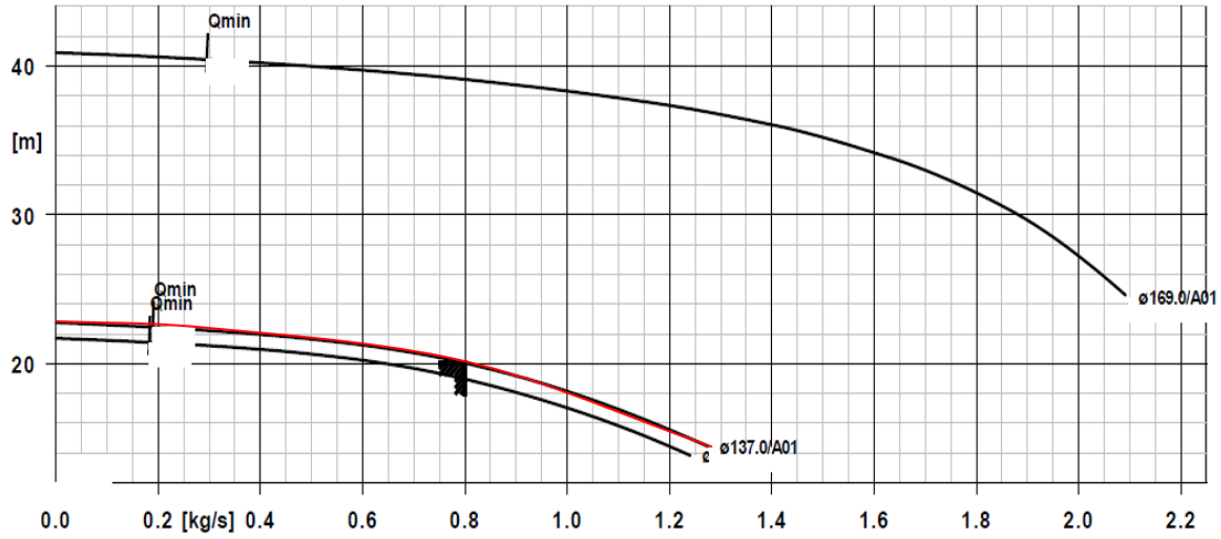

Figure 4.18: Pump curve at nominal speed of the pump in system 1070, where the red curve is the pump curve from the model and the black curve is the pump curve from the manufacturer [71].

4.6.2 Verification of pump curves at different pump speeds

The pump curve at nominal speed can be extrapolated from the maximum allowed operational point rate to larger mass flow rate values. The extrapolation allows for the pump curves at lower speeds to be constructed in the same mass flow rate range as the pump curve at nominal speed. The extrapolation from the maximum allowed operational point to larger points of the nominal pump curve is performed by equation (4.15).

$$Head_1 = Head_0 + f'(\dot{m}_0)(\dot{m}_1 - \dot{m}_0) \tag{4.15}$$

Subscript 0 denotes the maximum operational point of the nominal pump curve and subscript 1 denotes the point extrapolated to.

The pump test model to verify pump curves at different pump speeds is shown in Figure 4.19.

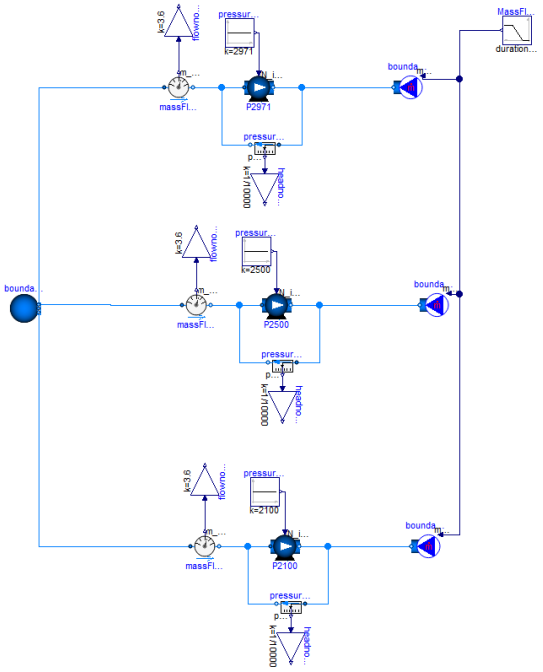

Figure 4.19: Pump test model to verify pump curves at different pump speeds.

With the pump affinity laws, pump curves at different speeds can be calculated for fixed impeller design, diameter and efficiency. At new pump speeds, the pump head and pump volume flow rate can be calculated by equations (4.16) and (4.17) respectively [74].

$$Head_1 = Head_0 \left(\frac{n_1}{n_0}\right)^2 \tag{4.16}$$

$$\dot{V}_1 = \dot{V}_0 \left(\frac{n_1}{n_0}\right) \tag{4.17}$$

Pump curves at different speeds for the pump model in system 1041 is shown in Figure 4.20, where the solid curves from the simulation are compared to the dashed curves from the mathematical calculations. The x-axis shows the volume flow rate through the pump while the y-axis shows the pump head in Figure 4.20.

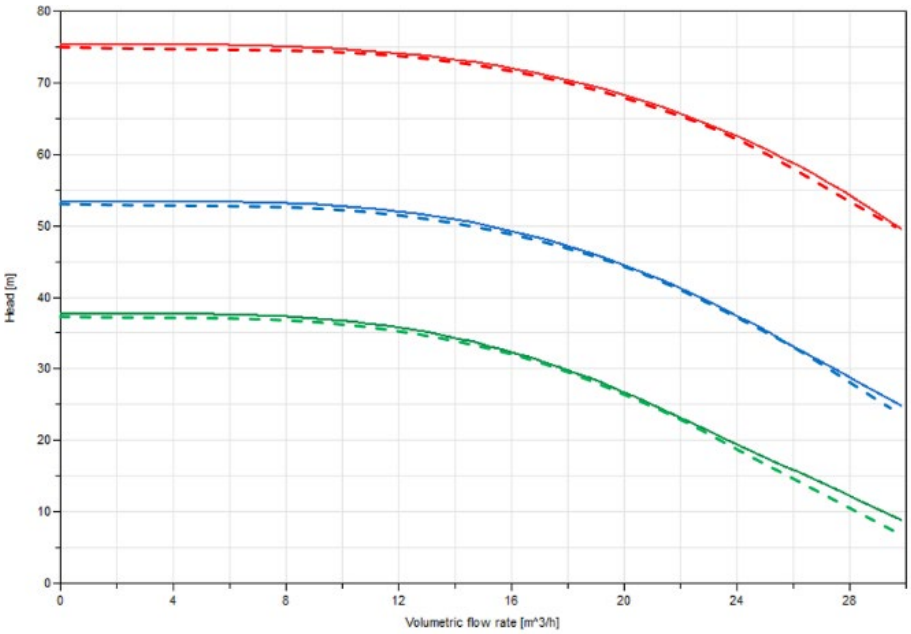

Figure 4.20: Pump curves at different pump speeds for the pump model in system 1041, where the solid curves from the simulation are compared to the dashed curves from the mathematical calculations. The red, blue and green curves are the pump curves at pump speeds of 2971, 2500 and 2100 rpm respectively.

4.7 Heated component

The temperatures of the pipe wall and the medium in the heated component model as a function of time is verified. In the test model the heat input is increased from 0 to 40 kW in a step and the temperatures of the pipe wall and the medium is calculated as a function of time. The heated component test model is shown in Figure 4.21 while the initial and boundary conditions are listed in Table 4.4 .

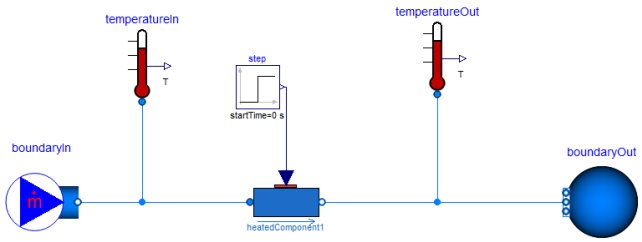

Figure 4.21: Heated component test model, to compute the temperature of the pipe wall and the medium in the heated component model as a function of time.

Table 4.4: Initial and boundary conditions of the heated component test model.

Initial conditions	**Value**

Starting temperature of pipe wall [°C]	20
Starting temperature of water [°C]	20
Boundary conditions	
Inlet temperature [°C]	20
Inlet mass flow rate [kg/s]	1
Heat input [kW]	40

The energy balance regarding the solid is shown in equation (4.18), while the energy balance regarding the liquid is shown in equation (4.19).

$$m_s c_{p_s} \frac{dT_s}{dt} = Q - hA(T_s - T_l) \tag{4.18}$$

$$m_l c_{p_l} \frac{dT_l}{dt} = hA(T_s - T_l) - \dot{m} c_{p_l}(T_l - T_{in}) \tag{4.19}$$

With the initial conditions $T_s(0) = T_{s_0}$ and $T_l(0) = T_{l_0}$, a solution to the system of differential equations (4.18) and (4.19), is found and shown in equation (4.20).

$$\begin{pmatrix} T_s \\ T_l \end{pmatrix} = B_1 e^{\lambda_1 t} \begin{pmatrix} \eta_1 \\ \eta_2 \end{pmatrix}^{[1]} + B_2 e^{\lambda_2 t} \begin{pmatrix} \eta_1 \\ \eta_2 \end{pmatrix}^{[2]} + \begin{pmatrix} a_1 \\ a_2 \end{pmatrix} \tag{4.20}$$

The temperature of the pipe walls and the medium in the heated component is plotted as a function of time in Figure 4.22, where the solid curves from the model are compared to the dashed curves from the mathematical calculations. The red curves show the temperature in the pipe walls while the blue curves show the temperature in the medium.

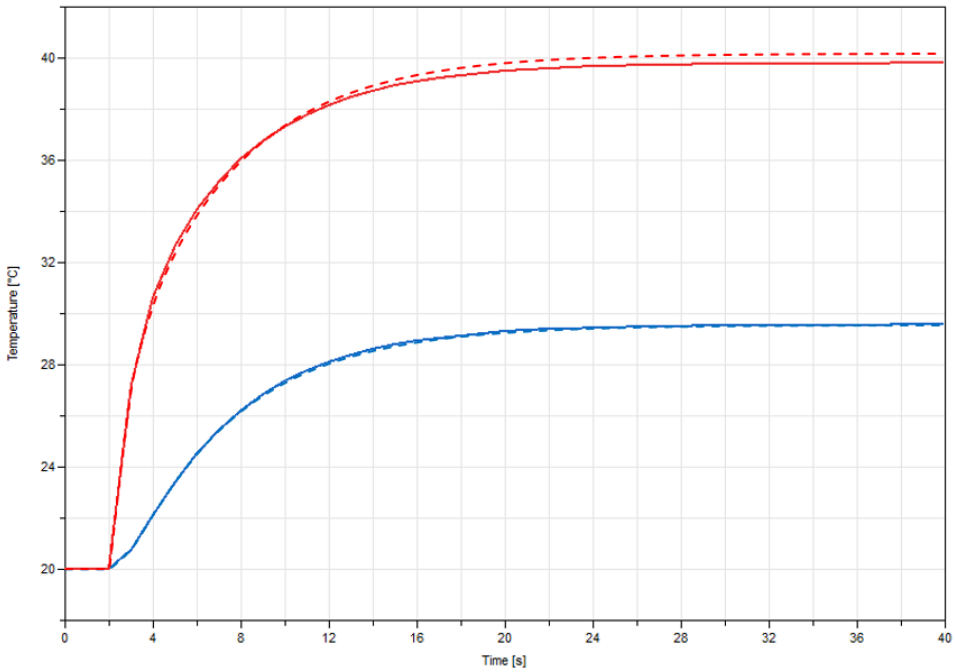

Figure 4.22: Temperature of the pipe walls and the medium in the heated component as a function of time, where the solid curves are from the model and the dashed curves are from the mathematical calculations. The red curves show the temperature in the pipe walls while the blue curves show the temperature in the medium.

4.8 Temperature sensor

The response time of the temperature sensor is verified. In the test model, the temperature at the sensor inlet is increased from 20 to 40 °C in a step for three different inlet mass flow rates. The test model is shown in Figure 4.23 while the input to the test model is listed in Table 4.5. The model results are compared to the results obtained from the mathematical calculations, which are explained in the following paragraphs.

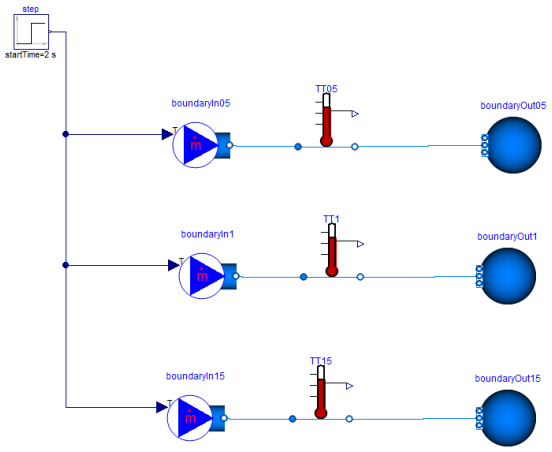

Figure 4.23: Test model of the temperature sensor, for the verification of the response time of the temperature sensor.

Table 4.5: Initial and boundary conditions of the temperature sensor test model.

Initial conditions	**Input**
Starting sensor output temperature [°C]	20
Boundary conditions	
Inlet temperature	40
Mass flow rate in test 1 [kg/s]	0.5
Mass flow rate in test 2 [kg/s]	1
Mass flow rate in test 3 [kg/s]	1.5

The temperature of the sensor is governed by differential equation (4.21).

$$\dot{m}c_p \frac{dT_s}{dt} = hA(T_l - T_s) \tag{4.21}$$

The time constant of the temperature sensor is defined in equation (4.22).

$$\tau = \frac{\dot{m}c_p}{hA} \tag{4.22}$$

A proportional gain is included to take the mass flow rate into account for the sensor time constant and is defined in equation (4.23).

$$k = \frac{\dot{m}}{\dot{m}_{nom}} \tag{4.23}$$

Combining equations (4.21) - (4.23) and solving the differential equation yields the temperature of the sensor as a function of time, as seen in equation (4.24).

$$T_s = T_l + (T_s(0) - T_l)e^{\frac{-kt}{\tau}} \tag{4.24}$$

The temperature of the sensor is plotted as a function of time for different mass flow rates in Figure 4.24, where the solid curves from the test model are compared to the dashed curves from the mathematical calculations.

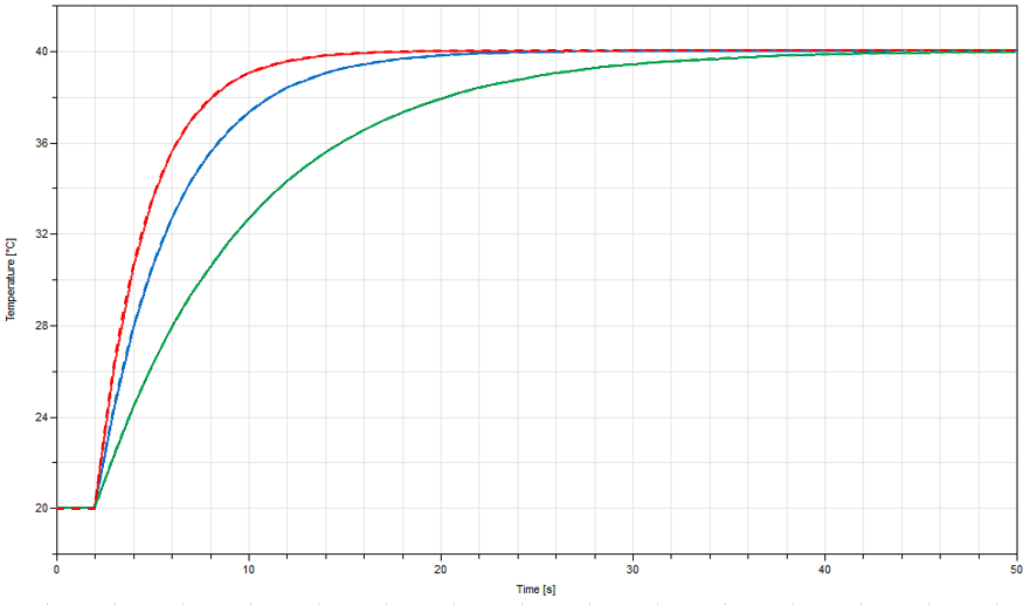

Figure 4.24: Temperature of the sensor as a function of time, where the solid curves from the test model are compared to the dashed curves from the mathematical calculations. The red, blue and green curves show the sensor temperature for mass flow rates of 1.5, 1 and 0.5 kg/s respectively.

5 Simulation set-up

Before the simulations can start, the initial values of the continuous variables such as pressure, temperature and mass flow rate are assigned for most components in the cooling system. The initial values can either be fixed or guessed. The formulation of the energy, mass and momentum balances are also determined before the simulations.

The four different formulations that can be set for the balance equations are:

- `DynamicFreeInitial`
- `FixedInitial`
- `SteadyStateInitial`
- `SteadyState`

For the `DynamicFreeInitial` setting, dynamic balance equations are formulated with initial guess values. For the `FixedInitial` setting, dynamic balance equations are formulated with fixed initial values. The `FixedInitial` setting should be used cautiously since this setting can cause fast transients at the start of the simulation which will in turn create numerical difficulties for the solver [20]. For the `SteadyStateInitial` setting, dynamic balance equations are formulated while the simulations are initialized at steady state with initial guess values. For the `SteadyState` setting, steady state balance equations are formulated with initial guess values.

The formulations of the balance equations chosen in the cooling system, together with the balance equation conditions and initial conditions are shown in Table 5.1 [75]. The energy dynamics and mass balance are set to `FixedInitial` since this gives the user the most control in how the cooling system will initialize. The `SteadyState` formulation of the momentum balance is chosen since the system model does not converge with the dynamic formulations.

Table 5.1: Formulations, balance equation conditions and the initial conditions of the balance equations.

Balance equation	**Formulation**	**Balance equation condition**	**Initial condition**
Energy balance	`FixedInitial`	-	$T(0) = T_{start}$
Mass balance	`FixedInitial`	-	$p(0) = p_{start}$
Momentum balance	`SteadyState`	$\frac{d\dot{m}}{dt} = 0$	-

For the different case studies performed, the same simulation setup is used. The simulation parameters chosen are shown in Table 5.2.

Table 5.2: Simulation parameters chosen for all the case studies.

Simulation parameter	**Parameter selection**
Solver	`ESDIRK45a`
Tolerance	1e-5
Output Interval length	1 s

When testing different solvers `ESDIRK45a` was the most stable solver and it required a tolerance of 1e-5 for the simulations to be able to converge. `ESDIRK45a` is an explicit singly diagonal implicit Runge-Kutta integration method of the 5^{th} order and the tolerance defines the order of accuracy of the solution [76][77]. The output interval length is set to 1 s which is chosen to approximately correspond to the sampling rate of the monitored process variables and the simulation time is set to assure that steady state is achieved before and after the introduced disturbance.

6 Results

The case studies performed is arranged into five different categories: normal operation, disturbance of system 1044, disturbance of system 1041 and disturbance of system 1070. In order to achieve convergence in the simulations, the case studies cannot be initialized at stationary conditions. The case studies are initialized with a pump speed of approximately 10% of operational speed for pump 1041-P-001. As the simulation procedure will vary slightly for the different case studies a simulation procedure table will be shown for each category. All the warning and alarm limits of the sensors, if not otherwise specified, are retrieved from [28]. For the tables in the present chapter with the time until warning and alarm limits are reached, the specified seconds after the positive sign regards the time delay of the sensors from when a warning or alarm limit is reached until the sensor is triggered and sends a signal to the operator.

6.1 Normal operation

During the normal operation, the start-up procedure is performed until steady-state is reached in the cooling systems, thereafter the shut-down procedure is performed. The objective of the case study is to quantify the process variables in the cooling system and compare the results during steady-state to respective cooling systems Process Flow Diagrams (PFD). With the depiction of the normal operation process variables before the disturbance case studies, a greater understanding is gained on how the cooling systems are affected by the different disturbances. The simulation procedure during normal operation is shown in Table 6.1.

Table 6.1: Simulation procedure during normal operation.

Simulation time [s]	**Action**
0-30	The intermediate flow through the heat exchanger 1041-W-001 ramps up linearly from 0-100% of operational flow.
35	The opening of the flow control valves 1041-FCV-125, 1041-FCV-125, 1041-FCV-129, 1041-FCV-130 go from fully open to the manually set opening that will allow for 0.5 kg/s to flow through each flow control valve at reduced pump speed of pump 1041-P-001. The opening of the flow control valve 1041-FV-114 is regulated from fully closed position. The opening of the flow control valve is regulated to assure that a minimum of 0.8 kg/s flows through the flow sensor 1041-FE-113.
35-50	The speed of pump 1041-P-001 ramps up linearly from 10-50% of operational speed. The flow to the purification system is ramped up linearly from 0-100% of operational flow

55-85	The speed of pump 1070-P-026 ramps up linearly from 0-100% of operational speed.
385-397	The speed of pump 1041-P-001 ramps up linearly from 50-100% of operational speed, allowing for 1 kg/s to flow through control valves 1041-FCV-125, 1041-FCV-125, 1041-FCV-129 and 1041-FCV-130.
460	The proton beam is on. The heat transfer to each pipeline entering the moderator in system 1110 is increased linearly to 40 kW in one second. The heat transfer to the proton beam window in system 1065 is increased linearly to 5.2 kW in one second. The heat transfer to the proton beam window flanges in system 1065 is increased linearly to 1 kW in one second.
4060	The proton beam is off The heat transfer to each pipeline entering the moderator in system 1110 is decreased to 20 kW in a step and subsequently decreased linearly to 0 kW in one hour. The heat transfer to the proton beam window in system 1065 is decreased to 2.6 kW in a step and subsequently decreased linearly to 0 kW in one hour. The heat transfer to the proton beam window flanges in system 1065 is decreased to 0.5 kW in a step and subsequently decreased linearly to 0 kW in one hour.
4060-4072	The speed of pump 1041-P-001 ramps down linearly from 100-50% of operational speed.
7660	Residual heat becomes zero after an hour of beam off
11300	One hour of inaction in order for steady-state to be reached.

The temperatures, pressures and mass flow rates at different locations in the cooling system are plotted as a function of time in Figure 6.1, Figure 6.2 and Figure 6.3 respectively.

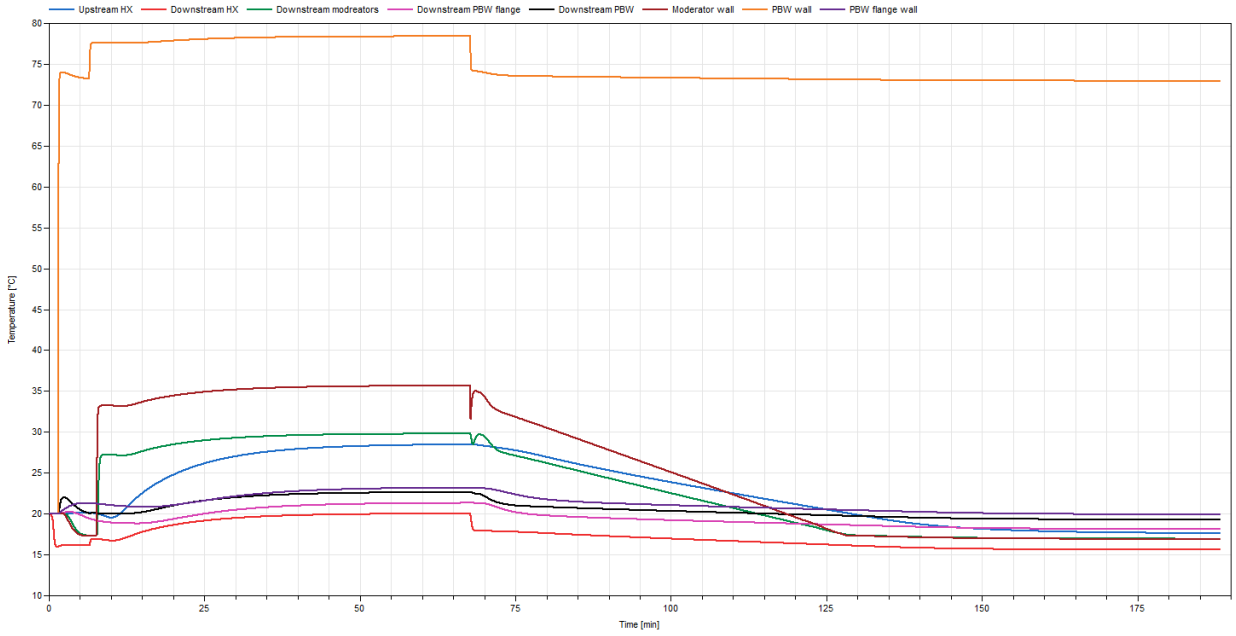

Figure 6.1: Temperature as a function of time at temperature sensors and at walls of the moderators, PBW and PBW flanges.

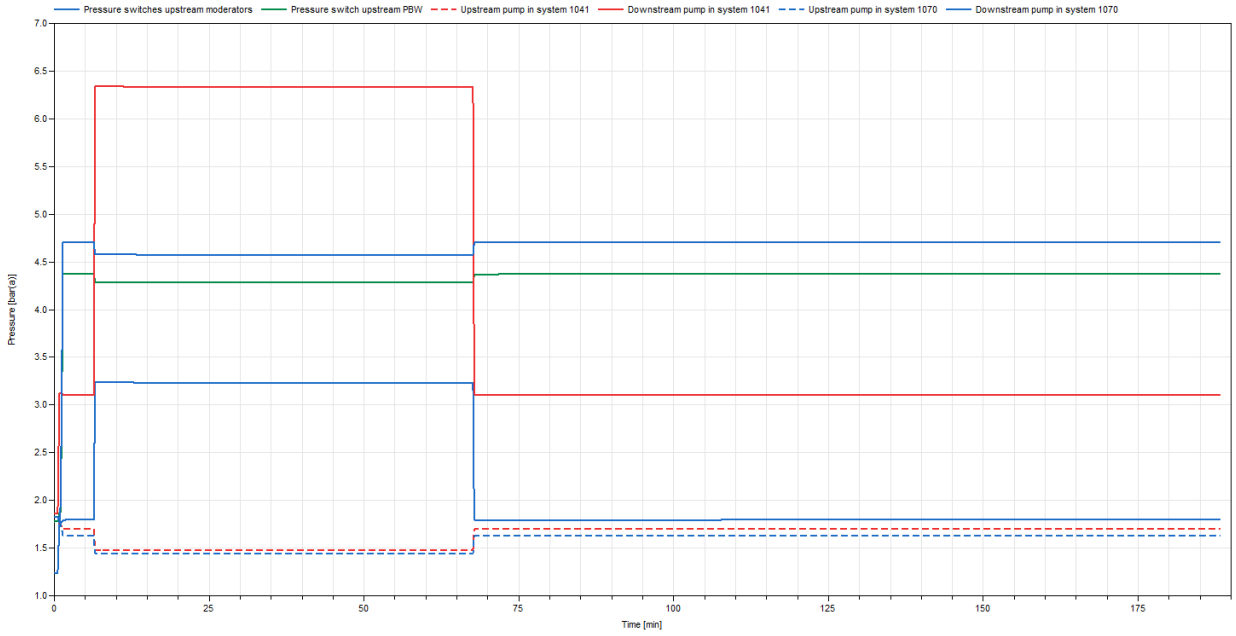

Figure 6.2: Pressure as a function of time at pressure switches and upstream and downstream the pumps.

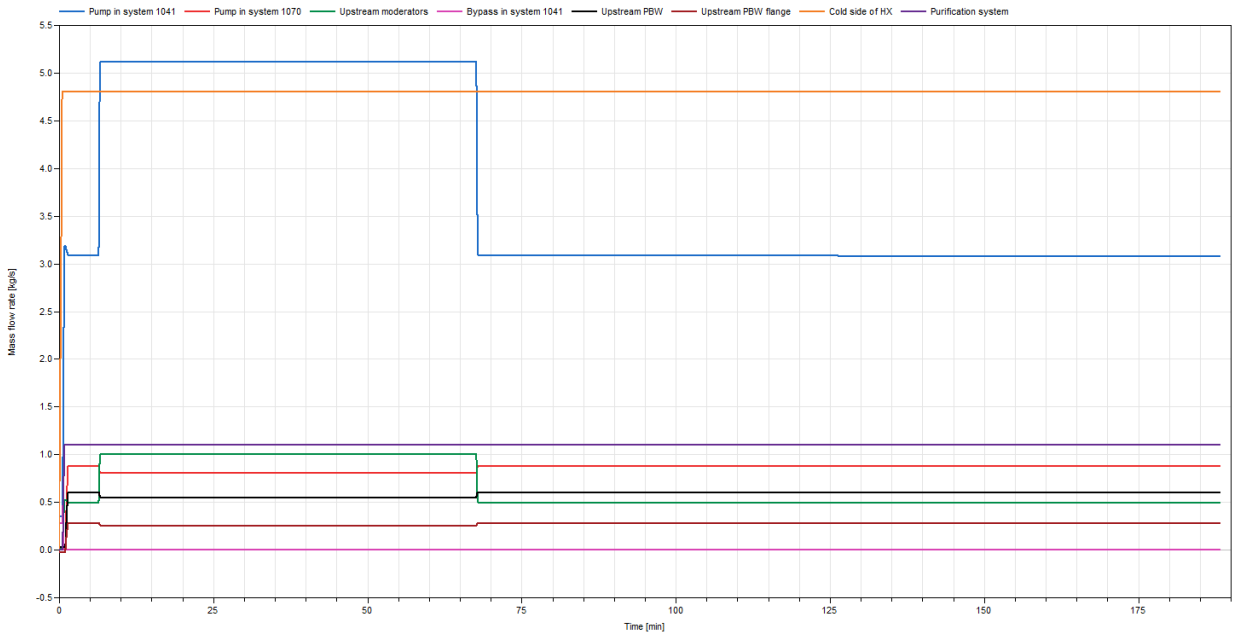

Figure 6.3: Mass flow rates at different locations in the cooling systems.

6.2 Disturbance in system 1044

A disturbance is introduced to system 1044 during steady-state. A transient is developed and the process variables will alter until a new steady-state is reached. The objective of each simulation is to investigate if one of the process values will exceed any alarm limits during the transient. If an alarm limit is exceeded it is of interest to determine the duration between the introduction of the disturbance and the triggering of the alarm. When an alarm is triggered the operator must intervene to get the process values within safety limits again. The start-up procedure will be simplified since the interest is to analyze how the cooling system behaves after a disturbance is introduced.

6.2.1 Reduced intermediate flow

The pump in the intermediate cooling system gets damaged resulting in a sudden decrease in pump speed and thereby a decrease in flow through heat exchanger 1041-W-001. The disturbance is introduced as a one second ramp with a decreased intermediate flow from its previous operational flow. This will result in an increase in temperature downstream heat exchanger 1041-W-001. The simulation procedure of the case study is shown in Table 6.2.

Table 6.2: Simulation procedure of the reduced intermediate flow case study.

Simulation time [s]	**Action**
0	The intermediate flow into the heat exchanger 1041-W-001 is at nominal flow.

5-35	The speed of pumps 1041-P-001 ramps up linearly from 0-100% of nominal speed.
40-70	The speed of pump 1070-P-026 ramps up linearly from 0-100% of nominal speed.
90-91	The proton beam is on. The heat transfer to each pipeline entering the moderator in system 1110 is increased linearly to 40 kW. The heat transfer to the proton beam window in system 1065 is increased linearly to 5.2 kW. The heat transfer to the proton beam window flanges in system 1065 is increased linearly to 1 kW.
3600-3601	The intermediate flow through heat exchanger 1041-W-001 is decreased linearly to a smaller flow.
10800	2 hours of inaction to discern if alarm limits have been exceeded.

The operational intermediate mass flow rate and the operational temperature of sensor 1041-TE-109 are shown in Table 6.3 while the simulations performed are listed in Table 6.4.

Table 6.3: Operational intermediate mass flow rate and operational temperature of sensor 1041-TE-109.

Operational intermediate mass flow rate [kg/s]	**Operational temperature of 1041-TE-109 [°C]**
4.8	20.0

Table 6.4: Simulations performed for the reduced intermediate flow case study with times until the warning and alarm of sensor 1041-TE-109 have been triggered.

Mass flow rate relative to nominal intermediate mass flow rate	**Intermediate mass flow rate [kg/s]**	**Time until warning by 1041-TE-109 (T=1.1·20.0°C) [s]**	**Time until alarm by 1041-TE-109 (T=1.2·20.0°C) [s]**
80%	3.84	-	-
60%	2.88	14 + 10	-
40%	1.92	6 + 10	60 + 10

The intermediate mass flow rate as a function of time is shown in the upper part of Figure 6.4 while and the temperature of 1041-TE-109 as a function of time is shown in the lower part of Figure 6.4.

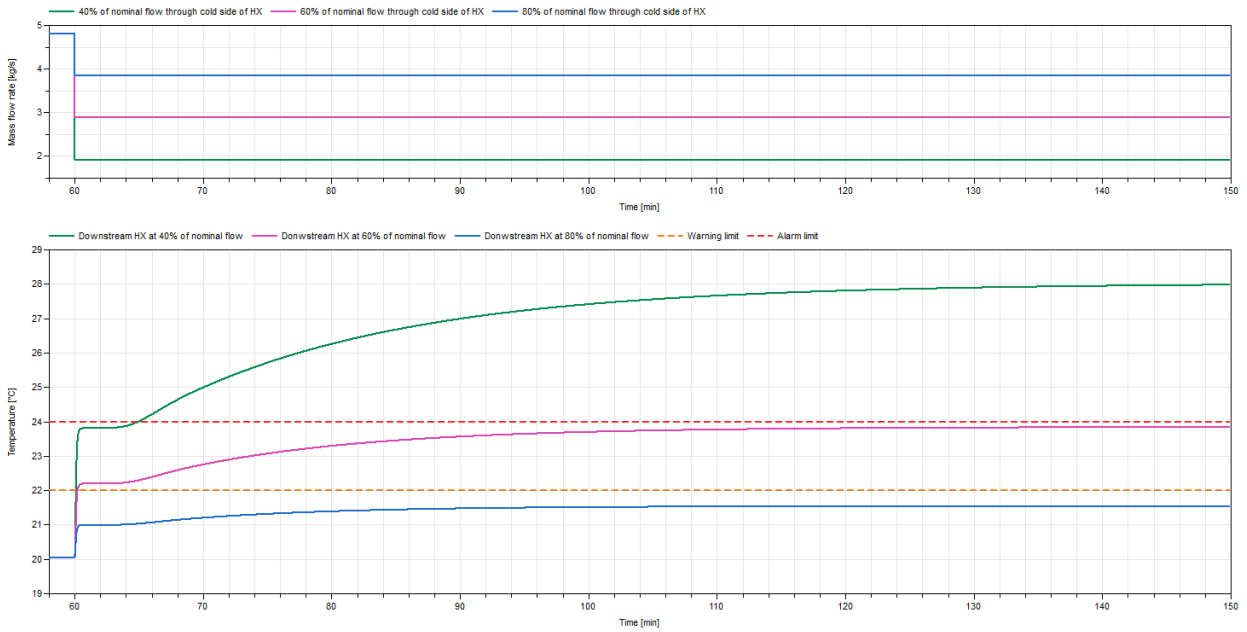

Figure 6.4: The intermediate mass flow rate as a function of time is shown in the upper part of the figure while the temperature of 1041-TE-109 as a function of time is shown in the lower part of the figure.

In Figure 6.4, the temperature increases drastically when the intermediate mass flow rate is decreased at 60 min, this is due to the short distance between the heat exchanger and the temperature sensor resulting in a low total heat capacity of the fluid and pipe walls. At 65 min, the temperature increases slowly. As the inlet temperature to the moderators, PBW and PBW flanges increase so will the outlet temperature increase. Due to the large distance and the two tanks between the heated objects and the heat exchanger, the total heat capacity of the fluid and the pipe walls is large, resulting in the delay of 5 min until a new slower temperature increase is registered. A new steady-state is reached when the heat input from the moderators, PBW and PBW flanges and the heat output to the intermediate cooling system and the ambient are equal.

The intermediate mass flow rate as a function of time is shown in the upper part, the PBW wall and PBW flange wall temperatures as a function of time is shown in the middle part while the moderator wall as a function of time is shown in the lower part of Figure 6.5.

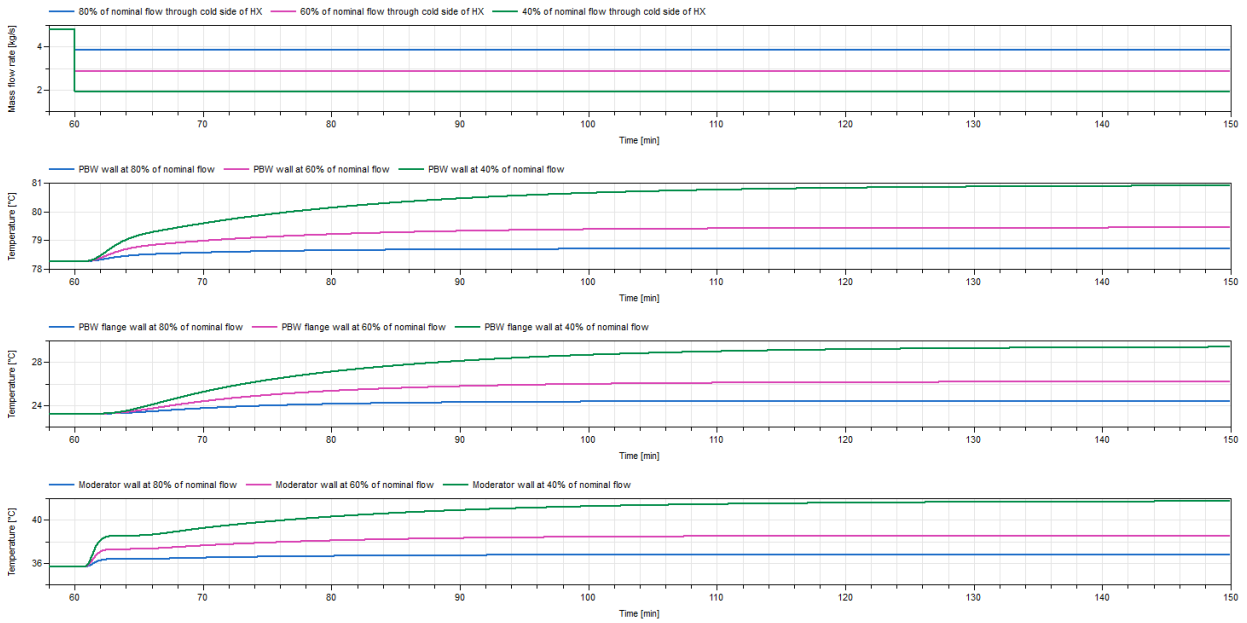

Figure 6.5: The intermediate mass flow rate as a function of time is shown at the top, the PBW wall and PBW flange wall temperatures as a function of time is shown in the upper middle and lower middle part respectively while the moderator wall temperature as a function of time is shown at the bottom of the figure.

6.2.2 Trip of pump 1044-P-007

The pump in system 1044 trips, resulting in a sudden linear decrease of flow from operational flow to zero in five seconds. After a specified duration the pump ramps up to operational flow again. The simulation procedure of the case study is shown in Table 6.5.

Table 6.5: Simulation procedure of the trip of pump 1044-P-007 case study.

Simulation time [s]	**Action**
0	The intermediate flow into the heat exchanger 1041-W-001 is at nominal flow.
5-35	The speed of pumps 1041-P-001 ramps up linearly from 0-100% of nominal speed.
40-70	The speed of pump 1070-P-026 ramps up linearly from 0-100% of nominal speed.
90	The proton beam is on. The heat transfer to each pipeline entering the moderator in system 1110 is increased linearly to 40 kW. The heat transfer to the proton beam window in system 1065 is increased linearly to 5.2 kW. The heat transfer to the proton beam window flanges in system 1065 is increased linearly to 1 kW.

3600-3605	The intermediate flow through heat exchanger 1041-W-001 decreases linearly from operational flow to zero.
3605-z	Specified amount of time when flow is zero.
z-(z+30)	The pump ramps up linearly to operational flow.
10800	Simulate for 2 hours after introduction of the disturbance to discern if alarm limits have been exceeded.

The operational intermediate mass flow and the operational temperature of sensor 1041-TE-109 are shown in Table 6.6 while the simulations performed are shown in Table 6.7.

Table 6.6: Operational intermediate mass flow rate and operational temperature of sensor 1041-TE-109.

Operational intermediate mass flow rate [kg/s]	**Operational temperature of 1041-TE-109 [°C]**
4.8	20.0

Table 6.7: Simulations performed for the pump trip of pump 1044-P-007 case study with times until the warning and alarm of sensor 1041-TE-109 have been triggered.

Time when the intermediate flow is zero [s]	**Time until warning by 1041-TE-109 (T=1.1·20°C) [s]**	**Time until alarm by 1041-TE-109 (T=1.2·20°C) [s]**
5	6 + 5	8 + 5
10	6 + 5	8 + 5
15	6 + 5	8 + 5

The intermediate mass flow rate as a function of time is shown in the upper part of Figure 6.6 while and the temperature of 1041-TE-109 as a function of time is shown in the lower part of Figure 6.6.

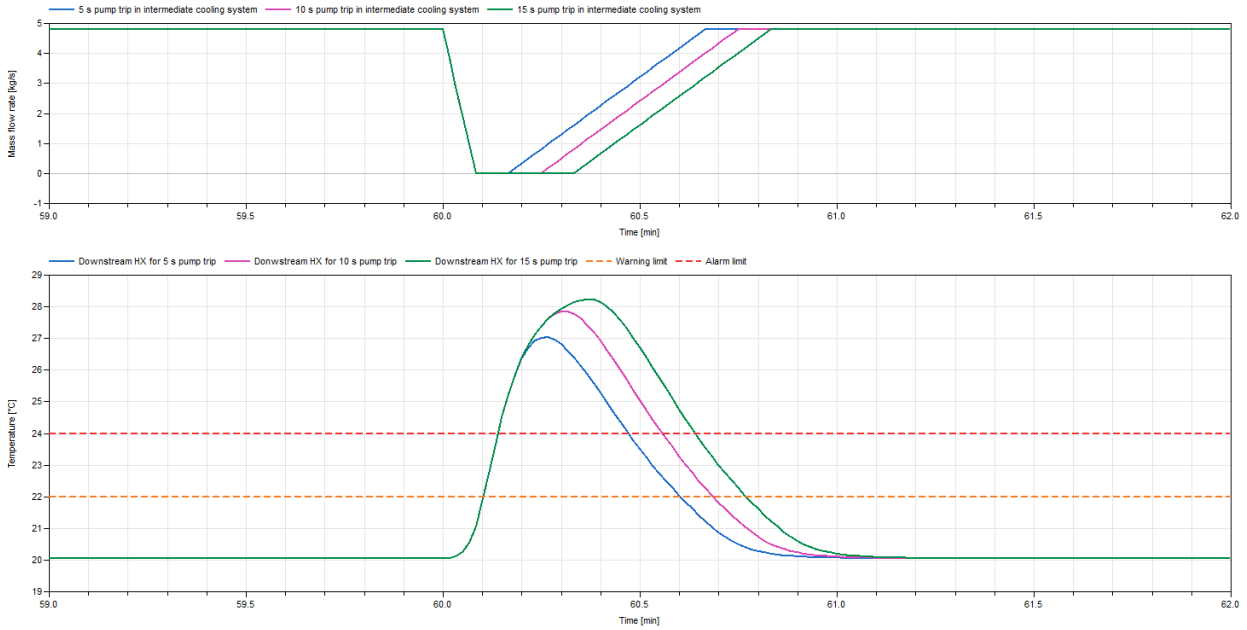

Figure 6.6: The intermediate mass flow rate as a function of time is shown in the upper part of the figure while the temperature of 1041-TE-109 as a function of time is shown in the lower part of the figure.

As seen in Figure 6.6, shorter pump trips results in smaller maximum values. The temperature increase is similar for all three curves in the beginning which is due to the zero intermediate mass flow rate and the nominal mass flow rate through pump 1041-P-001 for all three cases.

The intermediate mass flow rate as a function of time is shown in the upper part, the PBW wall and PBW flange wall temperatures as a function of time is shown in the middle part while the moderator wall as a function of time is shown in the lower part of Figure 6.7.

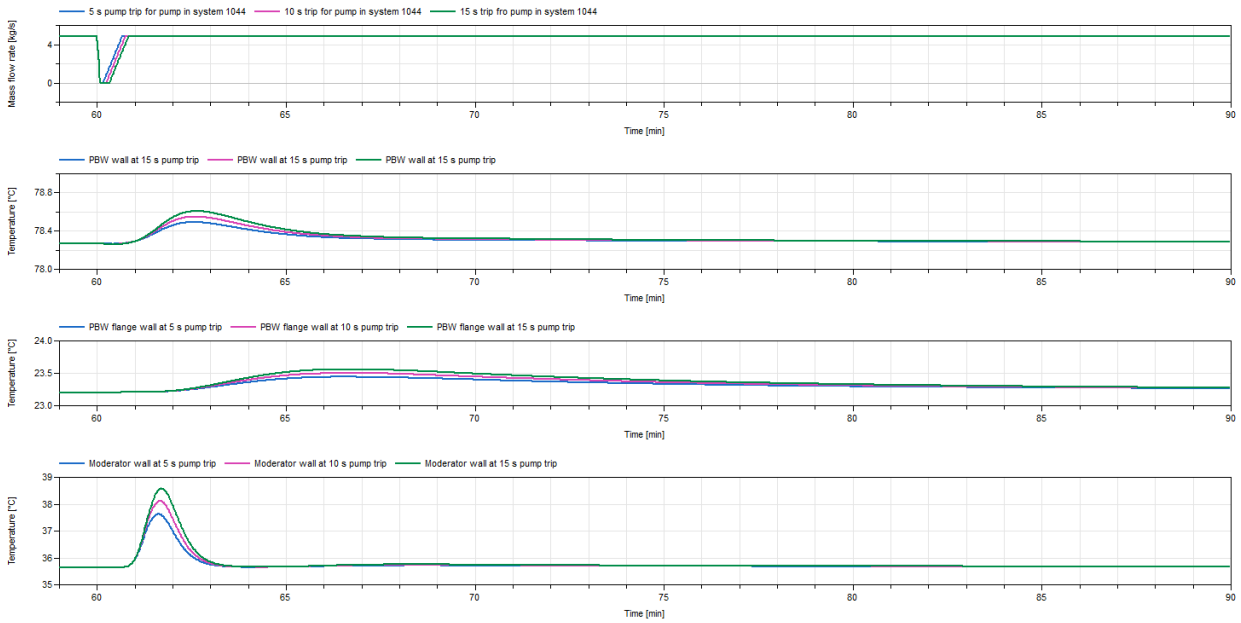

Figure 6.7: The intermediate mass flow rate as a function of time is shown in the upper part, the PBW wall and PBW flange wall temperatures as a function of time is shown in the upper middle and lower middle part respectively while the moderator wall temperature as a function of time is shown in the lower part of the figure.

6.3 Disturbance in system 1041

A disturbance is introduced to cooling system 1041 during steady-state. A transient is developed and the process variables will alter until a new steady-state is reached. The objective of each simulation is to investigate if one of the process values will exceed any alarm limits during the transient. If an alarm limit is exceeded it is of interest to determine the duration between the introduction of the disturbance and the triggering of the alarm. When an alarm is triggered the operator must intervene to get the process values within safety limits again. The start-up procedure will be simplified since the interest is to analyze how the cooling system behaves after a disturbance is introduced.

6.3.1 Increased speed of pump 1041-P-001

The speed of pump 1041-P-001 is increased until the alarm limit of a pressure switch is triggered. The simulation procedure is shown in Table 6.8.

Table 6.8: Simulation procedure of the increased speed of pump 1041-P-001 case study.

Simulation time [s]	**Action**
0	The intermediate flow into the heat exchanger 1041-W-001 is at operational flow.
5-32	The speed of pump 1041-P-001 ramps up linearly from 0-100% of operational speed.

40-70	The speed of pump 1070-P-026 ramps up linearly from 0-100% of operational speed.
90	The proton beam is on. The heat transfer to each pipeline entering the moderator in system 1110 is increased linearly to 40 kW. The heat transfer to the proton beam window in system 1065 is increased linearly to 5.2 kW. The heat transfer to the proton beam window flanges in system 1065 is increased linearly to 1 kW.
3600-z	Speed of pump 1041-P-001 is increased linearly until a pressure switch is triggered.
3610	Ten minutes of inaction to discern if alarm limits have been exceeded.

The operational speed of pump 1041-P-001 and the alarm limit of pressure switch 1041-PSZ-104 are shown in Table 6.9 while the simulation performed is shown in Table 6.10.

Table 6.9: Operational speed of pump 1041-P-00 and alarm limit of pressure switch 1041-PSZ-104.

Operational speed of pump 1041-P-001 [rpm]	**Assumed alarm limit of 1041-PSZ-104 [bar(a)]**
2542	4.9 [78]

Table 6.10: Simulations performed for the increased speed of pump 1044-P-007 case study with time until the alarm of pressure switch 1041-PSZ-104 has been triggered.

Speed of pump 1041-P-001 at fault [rpm]	**Time duration from introduction of disturbance to fault [s]**
3442	10

The speed of pump 1041-P-001 and the pressure at the pressure switch 1041-PSZ-104 are shown in the upper and lower part of Figure 6.8 respectively. It shall be noted that the pressure increase due to the increase in pump speed is calculated for a steady-state momentum balance, due to this there is no fluid acceleration or pressure surges present in the results.

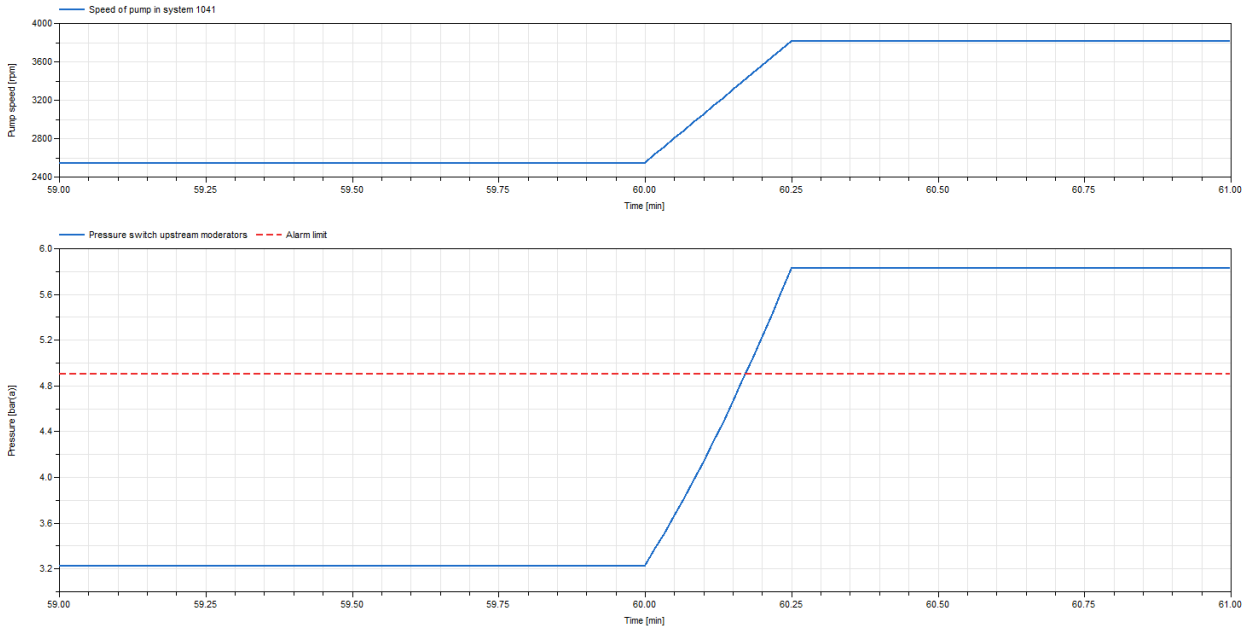

Figure 6.8: The speed of pump 1041-P-001 as a function of time is shown in the upper part of the figure while the pressure at pressure switch of 1041-PSZ-104 as a function of time is shown in the lower part of the figure.

6.3.2 Reduced speed of pump 1041-P-001

Pump 1041-P-001 gets damaged resulting in a decrease in speed from its nominal speed in a one second ramp, resulting in a decrease in flow and pressure in the cooling system. Due to the decrease in flow through the moderator lines the temperature downstream each moderator line will increase. The simulation procedure for the disturbance case study is shown in Table 6.11.

Table 6.11: Simulation procedure of the reduced speed of pump 1041-P-001 case study.

Simulation time [s]	**Action**
0	The intermediate flow into the heat exchanger 1041-W-001 is at nominal flow.
5-35	The speed of pumps 1041-P-001 ramps up linearly from 0-100% of nominal speed.
40-70	The speed of pump 1070-P-026 ramps up linearly from 0-100% of nominal speed.
90-91	The proton beam is on. The heat transfer to each pipeline entering the moderator in system 1110 is increased linearly to 40 kW. The heat transfer to the proton beam window in system 1065 is increased linearly to 5.2 kW. The heat transfer to the proton beam window flanges in system 1065 is increased linearly to 1 kW.

3600-3601	The speed of pump 1041-P-001 is decreased linearly.
10800	2 hours of inaction to discern if alarm limits have been exceeded.

The operational speed of pump 1041-P-001 and the operational temperature of sensor 1041-TE-101 are shown in Table 6.12 while the simulations performed are shown in Table 6.13.

Table 6.12: Operational speed of pump 1041-P-001 and operational temperature of sensor 1041-TE-101.

Operational speed of pump 1041-P-001 [rpm]	**Operational temperature of 1041-TE-101 [°C]**
2542	29.8

Table 6.13: Simulations performed for the reduced speed of pump 1041-P-001 case study with times until the warning and alarm of sensor 1041-TE-101 have been triggered.

Pump speed relative to operational pump speed	**Pump speed [rpm]**	**Time until warning by 1041-TE-101(T=1.05·29.8) [s]**	**Time until alarm by 1041-TE-101(T=1.1·29.8°C) [s]**
90%	2288	-	-
80%	2034	22 + 5	-
70%	1779	20 + 5	29 + 5

The speed of pump 1041-P-001 as a function of time is shown in the upper part of Figure 6.9 while the temperature of sensor 1041-TE-101 as a function of time is shown in the lower part of Figure 6.9.

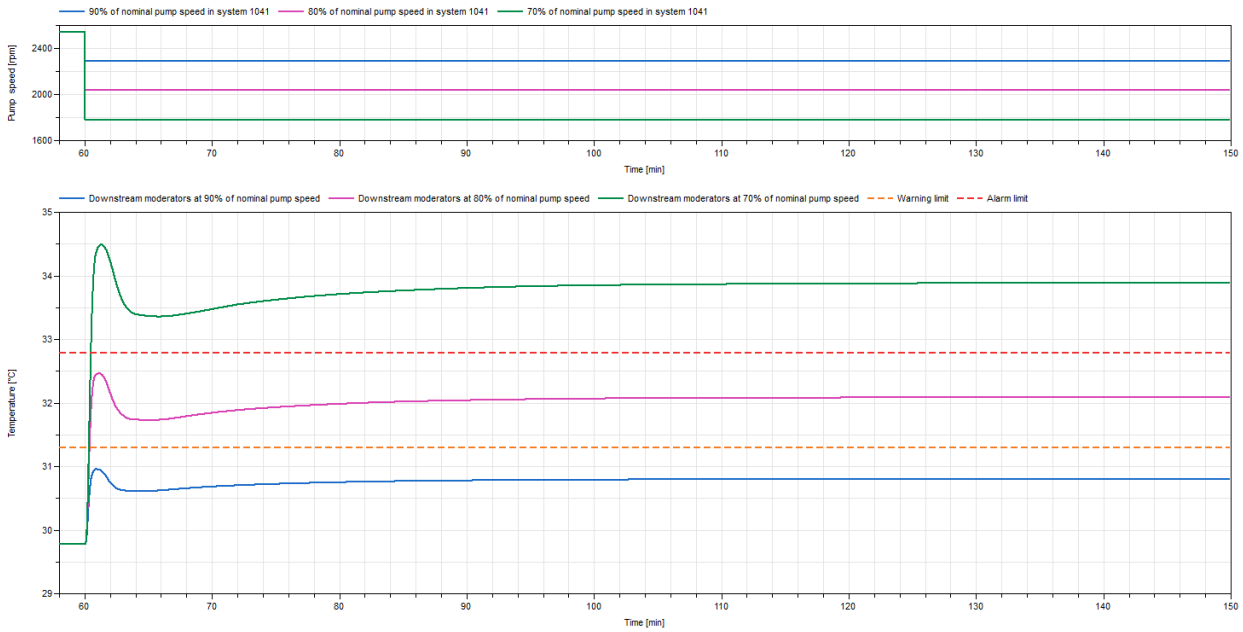

Figure 6.9: The pump speed as a function of time is shown in the upper part of the figure while the temperature of sensor 1041-TE-109 as a function of time is shown in the lower part of the figure.

In Figure 6.9, the temperature increases drastically downstream the moderators at 60 min, this is due to the decrease in mass flow rate through the moderators and the close proximity of the temperature sensors downstream the moderators. The temperature reaches a maximum eventually before it decreases. As the temperature of the flow entering the heat exchanger on the hot side increases, a larger heat transfer to the intermediate cooling system occurs and along with the smaller mass flow rate, a larger temperature difference between the inlet and outlet of the heat exchanger occurs. The cooler inlet temperature to the moderators increases the heat transfer from the moderator walls to the fluid, resulting in a decrease in temperature downstream the moderators. With a decrease of inlet temperature to the heat exchanger the heat transfer decreases resulting in a temperature increase at the heat exchanger outlet. The now hotter inlet temperature to the moderators will result in a temperature increase downstream the moderators until steady-state is reached.

The speed of pump 1041-P-001 as a function of time is shown in the upper part, the PBW wall and PBW flange wall temperatures as a function of time is shown in the middle part while the moderator wall as a function of time is shown in the lower part of Figure 6.10.

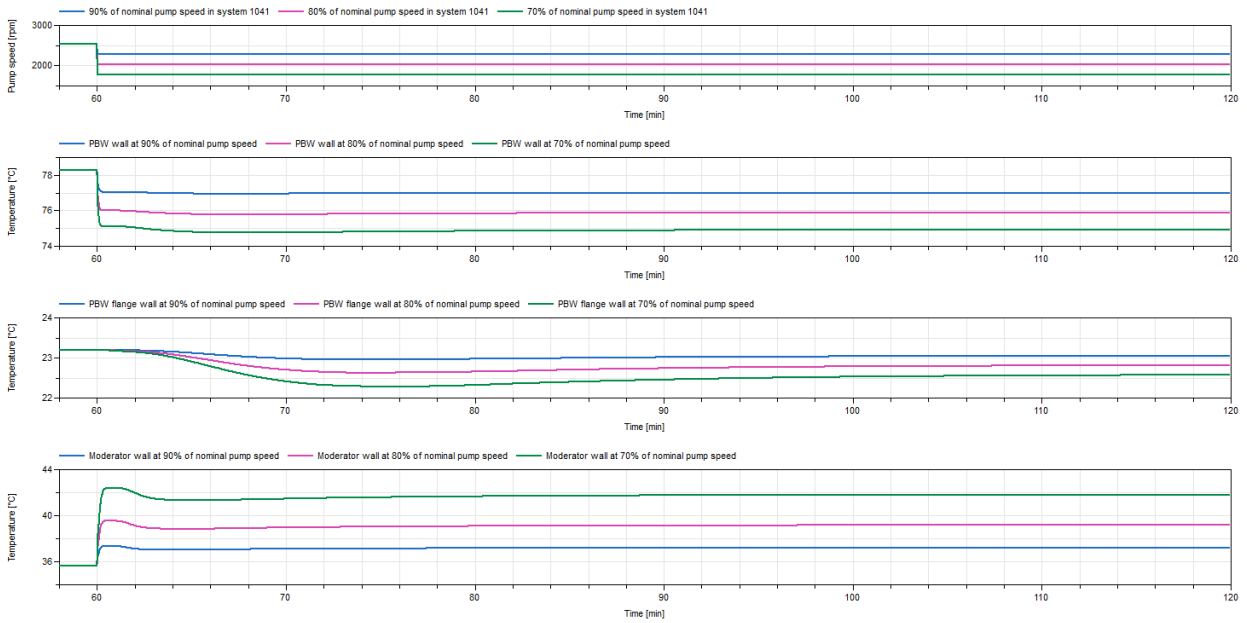

Figure 6.10: The speed of pump 1041-P-001 as a function of time is shown in the upper part, the PBW wall and PBW flange wall temperatures as a function of time is shown in the upper middle and lower middle part respectively while the moderator wall temperature as a function of time is shown in the lower part of the figure.

6.3.3 Trip of pump 1041-P-001

The pump in system 1041 trips, resulting in a sudden decrease of pump speed from operational speed to zero in five seconds. After a specified duration the pump ramps up to operational speed again. The simulation procedure for the disturbance case study is listed in Table 6.14.

Table 6.14: Simulation procedure of the trip of pump 1041-P-001 case study.

Simulation time [s]	**Action**
0	The intermediate flow into the heat exchanger 1041-W-001 is at nominal flow.
5-35	The speed of pumps 1041-P-001 ramps up linearly from 0-100% of nominal speed.
40-70	The speed of pump 1070-P-026 ramps up linearly from 0-100% of nominal speed.
90	The proton beam is on. The heat transfer to each pipeline entering the moderator in system 1110 is increased linearly to 40 kW. The heat transfer to the proton beam window in system 1065 is increased linearly to 5.2 kW. The heat transfer to the proton beam window flanges in system 1065 is increased linearly to 1 kW.

3600-3605	The speed of pump 1041-P-001 decreases linearly from operational speed to zero.
3605-z	Specified amount of time when flow is zero.
z-(z+30)	The pump ramps up linearly to operational pump speed.
10800	Simulate for 2 hours after introduction of the disturbance to discern if alarm limits have been exceeded.

The operational speed of pump 1041-P-001 and the operational temperature of sensor 1041-TE-101 is shown in Table 6.15 while the simulations performed are shown in Table 6.16.

Table 6.15: Operational intermediate mass flow rate and operational temperature of sensor 1041-TE-109.

Operational speed of pump 1041-P-001 [rpm]	**Operational temperature of 1041-TE-101 [°C]**
2542	29.8

Table 6.16: Simulations performed for the trip of pump 1041-P-001 case study with times until the warning and alarm of sensor 1041-TE-101 have been triggered.

Time when flow through 1041-P-001 is zero [s]	**Time until warning by 1041-TE-101 (T=1.05·29.8°C) [s]**	**Time until H2 of TE-101-104 (T=1.1·29.8°C) [s]**
5	25 + 5	27 + 5
10	29 + 5	31 + 5
15	33 + 5	35 + 5

The speed of pump 1041-P-001 as a function of time is shown in the upper part of Figure 6.11 while the temperature of sensor 1041-TE-101 as a function of time is shown in the lower part of Figure 6.11.

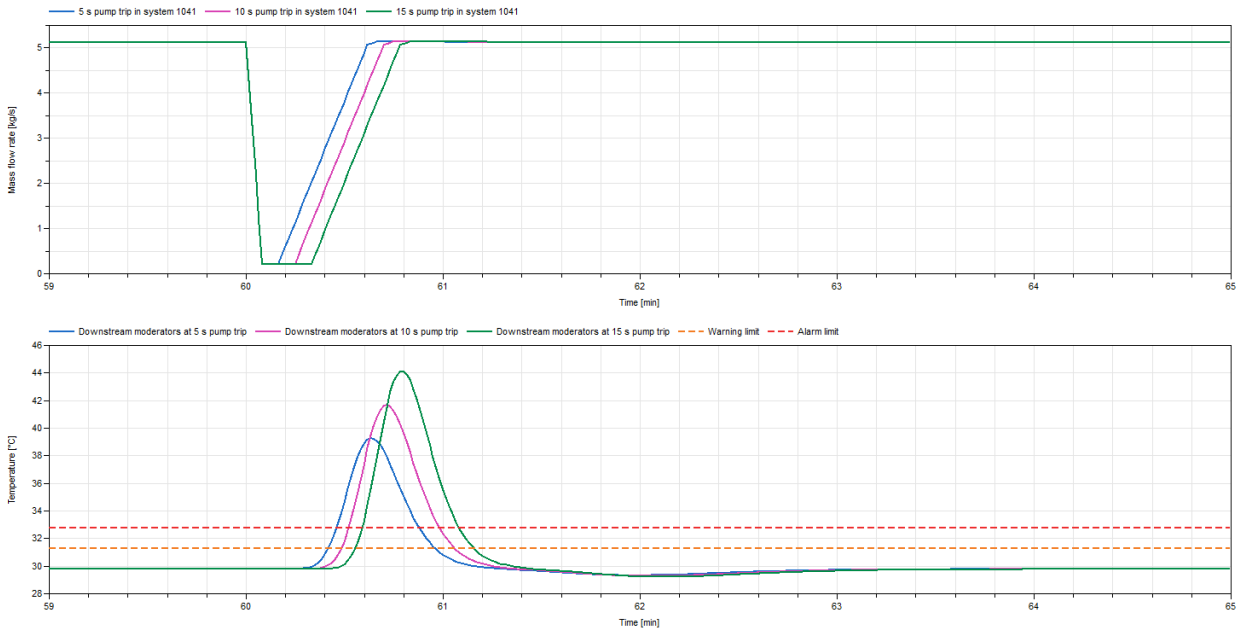

Figure 6.11: The pump speed as a function of time is shown in the upper part of the figure while the temperature of sensor 1041-TE-101 as a function of time is shown in the lower part of the figure.

As seen in Figure 6.11, shorter pump trips results in smaller maximum values and the temperature curve is shifted to the left for shorter pump trips. There are delays of the temperature increase downstream the moderators after the introduced disturbances. As there is zero mass flow rate through the moderators at pump stand-still, the immediate temperature increase will only occur in the moderators, but as the mass flow rate increases later on the sensor is able to monitor the temperature increase of the fluid upstream.

The mass flow rate through pump 1041-P-001 as a function of time is shown in the upper part, the PBW wall and PBW flange wall temperatures as a function of time is shown in the middle part while the moderator wall as a function of time is shown in the lower part of Figure 6.12.

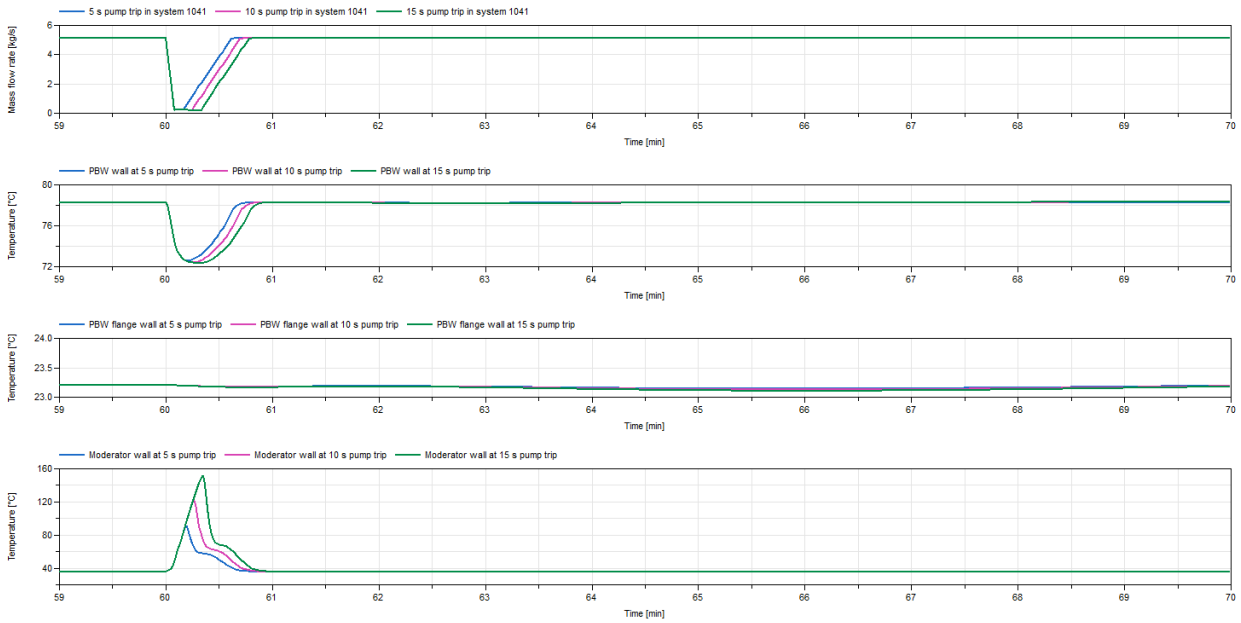

Figure 6.12: The mass flow rate through pump 1041-P-001 as a function of time is shown in the upper part, the PBW wall and PBW flange wall temperatures as a function of time is shown in the upper middle and lower middle part respectively while the moderator wall temperature as a function of time is shown in the lower part of the figure.

6.4 Disturbance in system 1070

A disturbance is introduced to cooling system 1070 during steady-state. A transient is developed and the process variables will alter until a new steady-state is reached. The objective for each simulation is to investigate if one of the process values will exceed any alarm limits during the transient. If an alarm limit is exceeded it is of interest to determine the duration between the introduction of the disturbance and the triggering of the alarm. When an alarm is triggered the operator must intervene to get the process values within safety limits again. The start-up procedure will be simplified since the interest is to analyze how the cooling systems behave after a disturbance is introduced.

6.4.1 Increased speed of pump 1070-P-026

The speed of pump 1070-P-026 is increased until the alarm limit of a pressure switch is triggered. The simulation procedure is shown in Table 6.17.

Table 6.17: Simulation procedure of the increased speed of pump 1070-P-026 case study.

Simulation time [s]	**Action**
0	The intermediate flow into the heat exchanger 1041-W-001 is at operational flow.
5-32	The speed of pump 1041-P-001 ramps up linearly from 0-100% of operational speed.

40-70	The speed of pump 1070-P-026 ramps up linearly from 0-100% of operational speed.
90	The proton beam is on. The heat transfer to each pipeline entering the moderator in system 1110 is increased linearly to 40 kW. The heat transfer to the proton beam window in system 1065 is increased linearly to 5.2 kW. The heat transfer to the proton beam window flanges in system 1065 is increased linearly to 1 kW.
3600-z	Speed of pump 1070-P-0026 is increased linearly until a pressure switch is triggered.
3610	Ten minutes of inaction to discern if alarm limits have been exceeded.

The operational speed of pump 1070-P-026 and the alarm limit of pressure switch 1070-PSZ-101 is shown in Table 6.18 while the simulation performed is shown in Table 6.19.

Table 6.18: Operational speed of pump 1070-P-026 and alarm limit of pressure switch 1070-PSZ-101.

Operational speed of pump 1070-P-026 [rpm]	**Assumed alarm limit of 1070-PSZ-101 [bar(a)]**
3613	5.0 [6]

Table 6.19: Simulations performed for the increased speed of pump 1070-P-026 case study with time until the alarm of pressure switch 1070-PSZ-101 has been triggered.

Speed of pump 1070-P-026 at fault [rpm]	**Time duration from introduction of disturbance to fault [s]**
4100	4

The speed of pump 1070-P-026 and the pressure at the pressure switch 1070-PSZ-101 are shown in the upper and lower part of Figure 6.13 respectively. It shall be noted that the pressure increase due to the increase in pump speed is calculated for a steady-state momentum balance, due to this there is no fluid acceleration or pressure surges present in the results.

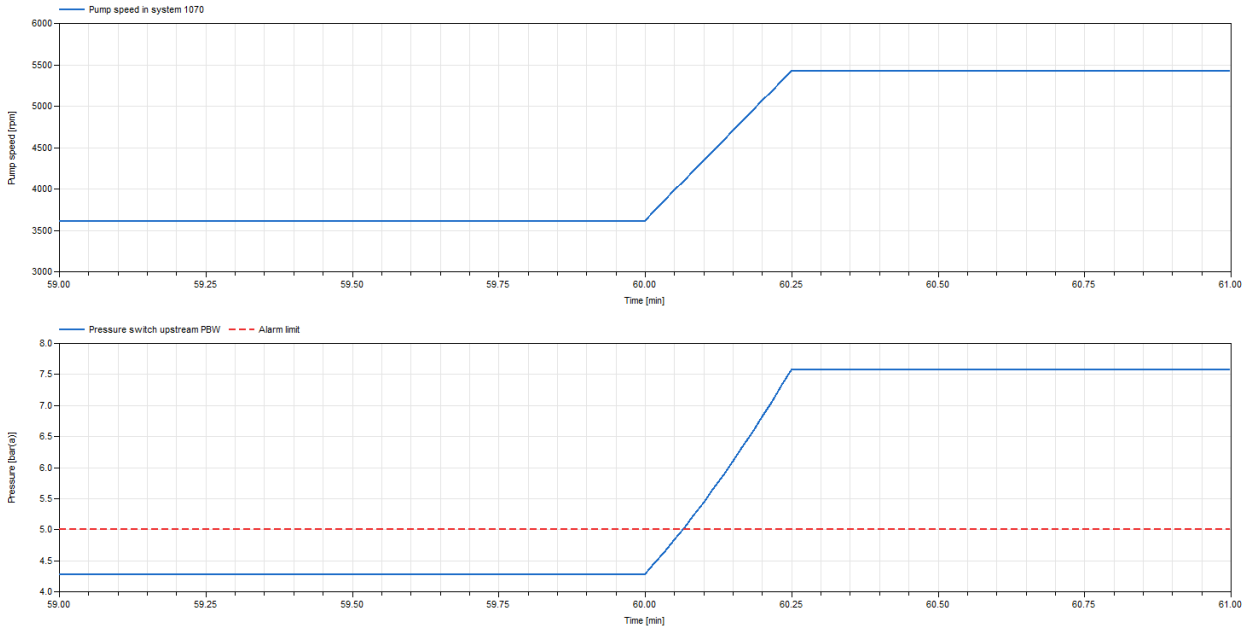

Figure 6.13: The speed of pump 1070-P-026 as a function of time is shown in the upper part of the figure while the pressure at pressure switch of 1070-PSZ-101 as a function of time is shown in the lower part of the figure.

6.4.2 Reduced speed of pump 1070-P-026

Pump 1070-P-026 gets damaged resulting in a decrease in speed from operational speed in a one second ramp, resulting in a decrease in flow and pressure in the cooling system. Due to the decrease in flow through the proton beam window and proton beam window flanges, the temperatures downstream will increase. The simulation procedure for the disturbance case study is shown in Table 6.20.

Table 6.20: Simulation procedure of the reduced speed of pump 1070-P-026 case study.

Simulation time [s]	**Action**
0	The intermediate flow into the heat exchanger 1041-W-001 is at nominal flow.
5-35	The speed of pumps 1041-P-001 ramps up linearly from 0-100% of nominal speed.
40-70	The speed of pump 1070-P-026 ramps up linearly from 0-100% of nominal speed.
90-91	The proton beam is on. The heat transfer to each pipeline entering the moderator in system 1110 is increased linearly to 40 kW. The heat transfer to the proton beam window in system 1065 is increased linearly to 5.2 kW.

	The heat transfer to the proton beam window flanges in system 1065 is increased linearly to 1 kW.
3600-3601	The speed of pump 1070-P-026 is decreased linearly.
10800	2 hours of inaction to discern if alarm limits have been exceeded.

The operational speed of pump 1070-P-026 and the operational temperatures of 1070-TE-102 and 1070-TE-104 are shown in Table 6.21 while the simulations performed are shown in Table 6.22.

Table 6.21: Operational speed of pump 1070-P-026 and the operational temperatures of sensors 1070-TE-102 and 1070-TE-104.

Operational speed of pump 1070-P-026 [rpm]	**Operational temperature of 1070-TE-104 [°C]**	**Operational temperature of 1070-TE-102 [°C]**
3613	21.3	22.6

Table 6.22: Simulations performed for the reduced speed of pump 1070-P-026 case study with times until the warning and alarm of sensors 1070-TE-102 and 1070-TE-104 have been triggered.

Pump speed relative to operational pump speed	**Pump speed [rpm]**	**Time until warning by 1070-TE-104 (T=1.05·21.3 °C) [s]**	**Time until alarm by 1070-TE-104 (T=1.1·21.3 °C) [s]**	**Time until warning by 1070-TE-102 (T=1.05·22.6 °C) [s]**	**Time until alarm by 1070-TE-102 (T=1.1·22.6 °C) [s]**
80%	2890	-	-	-	-
70%	2529	-	-	42 + 5	-
60%	2168	-	-	33 + 5	67 + 5

The speed of pump 1070-P-026 as a function of time is shown in the upper part, the temperature of sensor 1070-TE-102 as a function of time is shown in the middle part and the temperature of sensor 1070-TE-104 as a function of time is shown in the lower part of Figure 6.14.

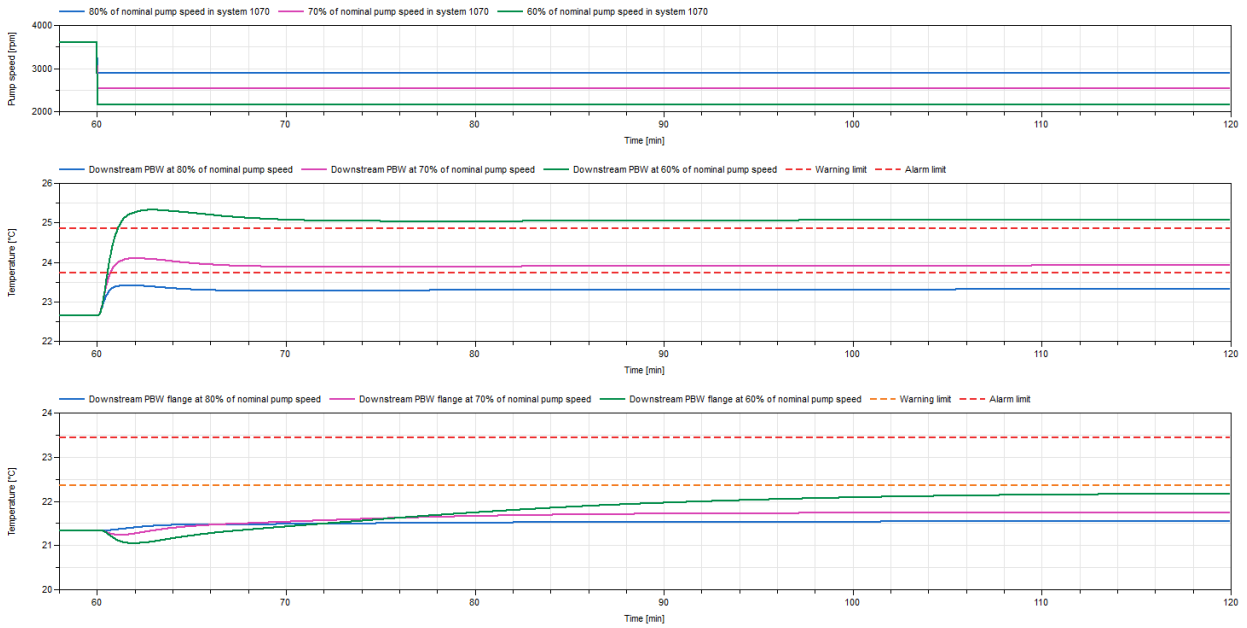

Figure 6.14: The speed of pump 1070-P-026 as a function of time is shown in the upper part, the temperature of sensor 1070-TE-102 as a function of time is shown in the middle part and the temperature of sensor 1070-TE-104 as a function of time is shown in the bottom part of the figure.

In Figure 6.14, the temperature downstream the PBW increases until it reaches a maximum, thereafter only a small decrease of temperature occurs until steady-state is reached compared to Figure 6.9, this is due to the smaller drop in mass flow rate through the heat exchanger and the smaller resulting temperature difference between the inlet and outlet of the heat exchanger. When looking at the temperature downstream the PBW flange in Figure 6.14, the temperature increases directly for the blue curve while the temperature decreases before increasing for the pink and green curve. For the pink and green curve, the convective heat transfer coefficient between the PBW flange wall and the fluid decreases drastically due to the decrease in flow and the temperature increases relatively slow in the PBW flange wall due to the heat capacity, resulting in a smaller heat transfer rate between the PBW flange and the fluid. A few seconds later the heat transfer rate between the PBW flange and fluid increases, due to the increase in temperature of the PBW flange wall, that finally increases the temperature of the fluid.

The speed of pump 1070-P-026 as a function of time is shown in the upper part, the PBW wall and PBW flange wall temperatures as a function of time is shown in the middle part while the moderator wall as a function of time is shown in the lower part of Figure 6.15.

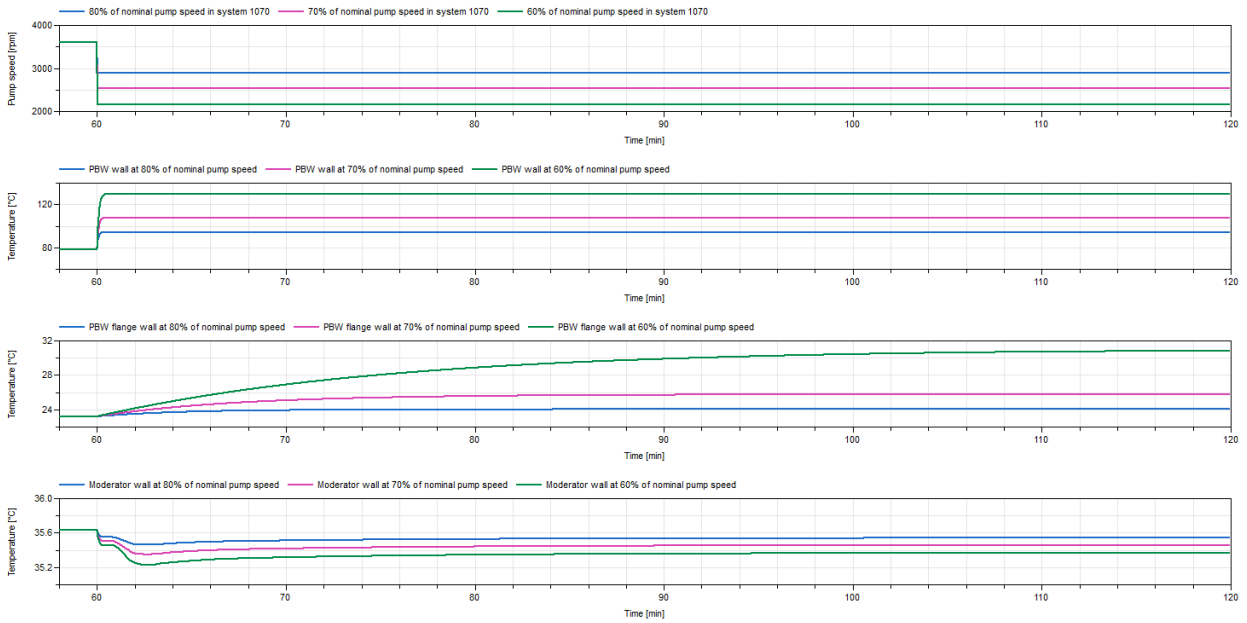

Figure 6.15: The speed of pump 1070-P-026 as a function of time is shown in the upper part, the PBW wall and frame temperature as a function of time is shown in the upper middle and lower middle part respectively while the moderator wall temperature as a function of time is shown in the lower part of the figure.

6.4.3 Trip of pump 1070-P-026

The pump in system 1070 trips, resulting in a sudden linear decrease of flow from operational flow to zero in five seconds. After a specified duration the pump ramps up to operational flow again. The simulation procedure for the disturbance case study is listed in Table 6.23.

Table 6.23: Simulation procedure of the trip of pump 1070-P-026 case study.

Simulation time [s]	**Action**
0	The intermediate flow into the heat exchanger W-001 is at nominal flow.
5-35	The speed of pumps 1041-P-001 ramps up linearly from 0-100% of nominal speed.
40-70	The speed of pump 1070-P-026 ramps up linearly from 0-100% of nominal speed.
90	The proton beam is on. The heat transfer to each pipeline entering the moderator in system 1110 is increased linearly to 40 kW. The heat transfer to the proton beam window in system 1065 is increased linearly to 5.2 kW. The heat transfer to the proton beam window flanges in system 1065 is increased linearly to 1 kW.

3600-3605	The speed of pump 1070-P-026 decreases linearly from operational speed to zero.
3605-z	Specified amount of time when flow is zero.
z-(z+30)	The pump ramps up linearly to operational pump speed.
10800	Simulate for 2 hours after introduction of the disturbance to discern if alarm limits have been exceeded.

The operational pump speed and the operational temperatures of 1070-TT-102 and 1070-TT-104 are shown in Table 6.24 while the simulations performed are shown in Table 6.25.

Table 6.24: The operational speed of pump 1070-P-026 and the operational temperatures of sensors 1070-TE-102 and 1070-TE-104.

Nominal speed of pump 1070-P-026 [rpm]	**Operational temperature of 1070-TE-104 [°C]**	**Operational temperature of 1070-TE-102 [°C]**
3613	21.3	22.6

Table 6.25: Simulations performed for the trip of pump 1070-P-026 case study with times until the warning and alarm of sensors 1070-TE-102 and 1070-TE-104 have been triggered.

Time when flow through 1070-P-026 is zero [s]	**Time until warning by 1070-TE-104 (T=1.05·21.3 °C) [s]**	**Time until alarm by 1070-TE-104 (T=1.1·21.3 °C) [s]**	**Time until warning by 1070-TE-102 (T=1.05·22.6 °C) [s]**	**Time until alarm by 1070-TE-102(T=1.1·22.6 °C) [s]**
5	-	-	31	-
10	-	-	35 + 5	40 + 5
15	-	-	40 + 5	43 + 5

The speed of pump 1070-P-026 as a function of time is shown in the upper part, the temperature of sensor 1070-TE-102 as a function of time is shown in the middle part and the temperature of sensor 1070-TE-104 as a function of time is shown in the lower part of Figure 6.16.

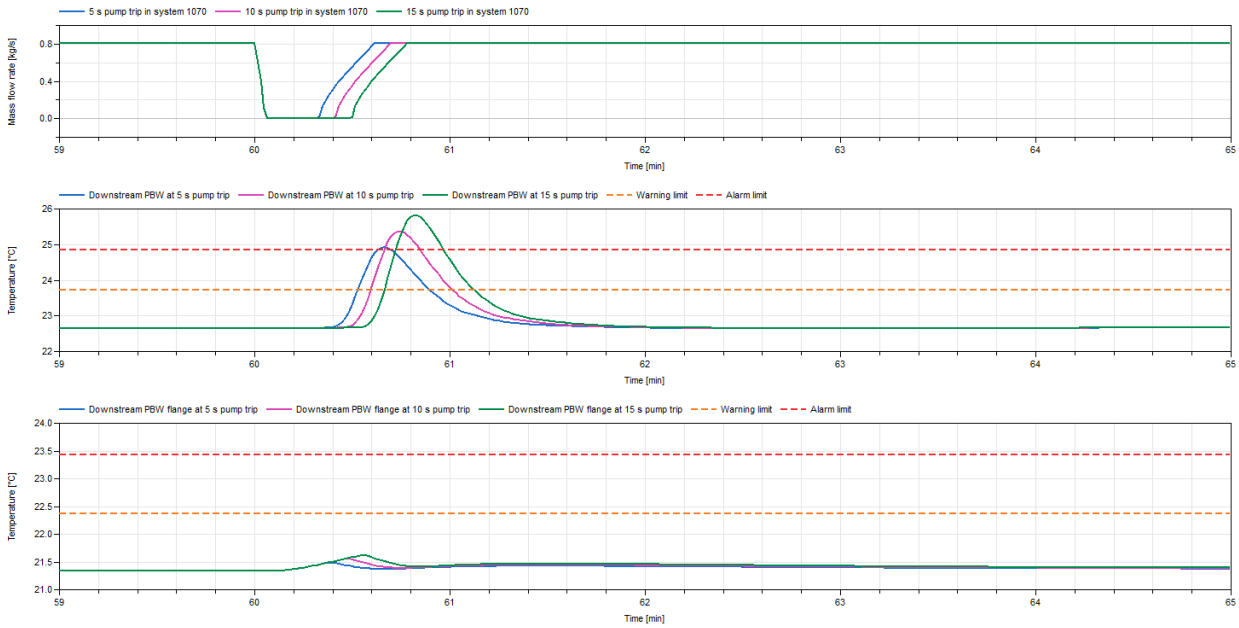

Figure 6.16: The speed of pump 1070-P-026 as a function of time is shown in the upper part, the temperature of sensor 1070-TE-102 as a function of time is shown in the middle part and the temperature of sensor 1070-TE-104 as a function of time is shown in the bottom part of the figure.

As seen in Figure 6.16, shorter pump trips results in smaller maximum values and the temperature curve is shifted to the left for shorter pump trips. There are delays of the temperature increase downstream the PBW and the PBW flange after the introduced disturbances. As there is zero mass flow rate through the PBW and PBW flange at pump stand-still, the immediate temperature increase will only occur in the components, but as the mass flow rate increases later on the sensor is able to monitor the temperature increase of the fluid upstream. For the blue curve in the middle part of Figure 6.16, the alarm limit is reached but since the temperature is over the alarm limit for a duration shorter than the on-delay time the sensor is not triggered.

The mass flow rate through pump 1070-P-026 as a function of time is shown in the upper part, the PBW wall and PBW flange wall temperatures as a function of time is shown in the middle part while the moderator wall as a function of time is shown in the lower part of Figure 6.17.

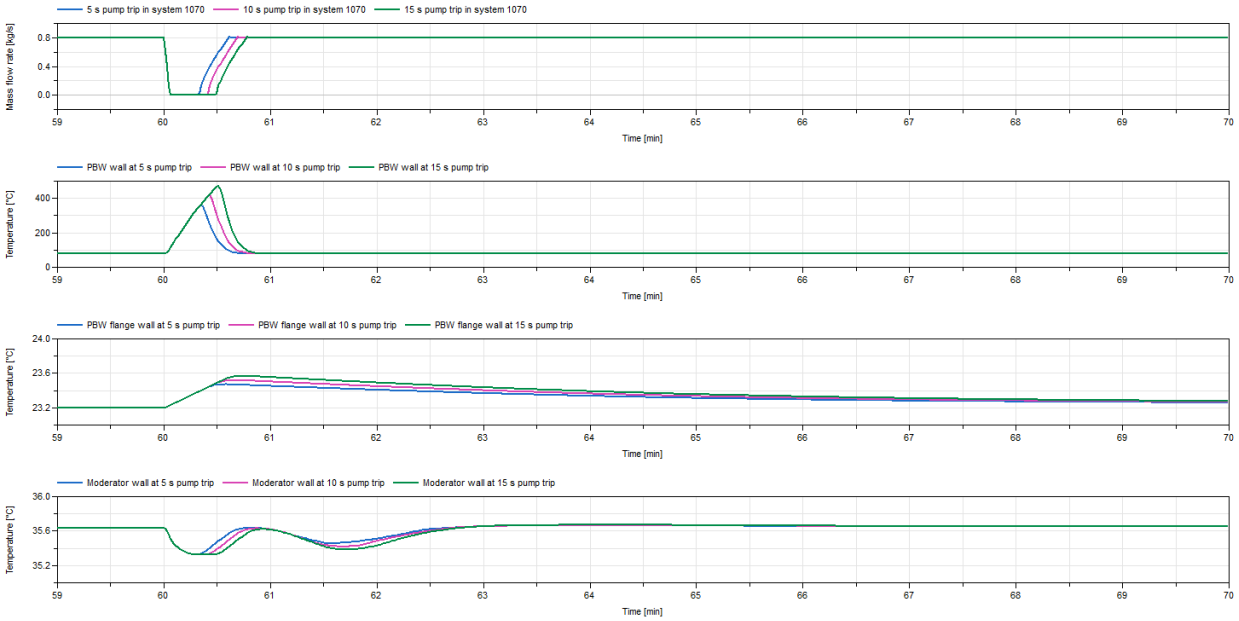

Figure 6.17: The mass flow rate through pump 1070-P-026 as a function of time is shown in the upper part, the PBW wall and PBW flange wall temperatures as a function of time is shown in the upper middle and lower middle part respectively while the moderator wall temperature is shown in the lower part of the figure.

7 Discussion

For disturbances such as lower mass flow rates in the cooling systems simulated, higher steady-state temperatures occurred. If the mass flow rates in the simulated cooling systems could not be altered, the intermediate mass flow rate through the heat exchanger could be increased to decrease the fluid temperatures in the cooling systems simulated.

For disturbances such as lower mass flow rates through the moderators, PBW window and PBW flange, the temperatures downstream the components increased until a maximum was reached. The temperatures later decreased due to the larger temperature differences between the inlet and outlet of the heat exchanger, which was due to the lower mass flow rate through the heat exchanger, this resulted in a cooler inlet temperature to the components and thus larger heat transfer between the heated components and the fluid.

For pump trips in systems 1044 and 1041, the alarms were triggered before 20 seconds, the triggering of the alarms would then occur before the stand-by pumps would have reached their operational speed.

As the steady-state momentum balances had to be set, the pressure surges and the acceleration and deceleration of the fluid was not simulated. For the simulations when the pump speeds decreased, the deceleration of the fluid would cool the heated components more during the first seconds compared to the simulations performed with the sudden decreased mass flow rates.

7.1 Challenges

During the course of the thesis challenges arose which affected the defined objective and the progress of the thesis. During the thesis there were different levels of design maturity for the different cooling systems. All data needed for accurate modeling and simulation of the cooling systems were therefore not available. Undetermined data included system and component data as well as control logic data. Undetermined data resulted in more assumptions and simplifications being made to the models.

The most challenging part of the thesis was the initialization of the system model. Several starting values of process variables had to be set manually in each component model and they needed to be close to the real values in order for the system model to initialize and converge. In many cases, trial and error was performed to set the starting values of the process variables and the tolerance and solver used for the simulations. The simulations did not initialize at zero pump speeds in the system model, starting pump speeds of at least 10 % of nominal operation were needed for the simulation to initialize, resulting in cooling system start-ups not being properly modeled.

8 Conclusions

The main goal of the project was to have a cooling system model constructed by free library component models and with the model simulate normal operation and disturbance cases. The goal has been partly achieved. Early in the project it was concluded that the number of cooling systems to be modeled had to be decreased. The temperature transients in the cooling system could be simulated, however the pressure transients could not due to convergence issues.

A pipe segment model has been created to include pressure drops across elbows, reducers, T-junctions and hand shut-off valves. The pipe and tank walls have been modelled as heat capacitors and the heat transfer between the fluid and the walls and between the walls and the ambient have been included to model the temperature dynamics of the cooling systems. Components such as a delay tank, a gas and liquid separation tank and a cooled component have been modeled.

A wide-proven commercially available software, Dymola, and the Modelica Standard Library and Buildings Library, developed and tested by developers around the world, were chosen to guarantee the correctness of the underlying equations and component models in the libraries. The component models that have been developed in Dymola are verified with manufacturer data or known and proven mathematical calculations performed in Excel. The system model could not be validated with data from the actual cooling systems since the actual cooling systems are yet to be in operation.

The disturbance case studies have been performed in order to analyze what operating conditions will trigger an alarm and also discern the duration from the introduction of a disturbance to the triggering of an alarm.

9 Future work

When the cooling systems are fully defined, the assumptions previously made should be altered to the new defined values. When the cooling systems are in operation, the process values obtained from the cooling systems should be used to calibrate component models and validate component and system models.

More controllers can, if possible, be implemented in the system model to properly model the control logic of the cooling systems. It should be noted that the computational time will increase and the system model will be more susceptible to convergence failures.

Pressure transients can possibly be simulated, for this to succeed the system model may need to be simplified or better starting values may need to be set in the components models. The inertia of the pumps should then be implemented.

Other cooling systems can be modeled with the component models used for this thesis and be connected to the modeled cooling system.

10 References

[1] ESS. The ESS Mandate | ESS [Internet]. Lund: ESS; [date unknown] [cited 2021 Jan 7]. Available from: https://europeanspallationsource.se/ess-mandate

[2] ESS. European Spallation Source | ESS [Internet]. Lund: ESS; [date unknown] [cited 2020 Feb 12]. Available from: https://europeanspallationsource.se/about

[3] ESS. Home | ESS [Internet]. Lund: ESS; [date unknown] [cited 2020 Feb 12]. Available from: https://europeanspallationsource.se/

[4] ESS. ESS Organisation | ESS [Internet]. Lund: ESS; [date unknown] [cited 2020 Feb 12]. Available from: https://europeanspallationsource.se/ess-organisation#vision

[5] Nordeng P. Aerial view over ESS Construction Site 5 March 2021 [Internet]. 2021 [cited 2021 Apr 13]. Available from: https://dam.esss.lu.se/asset-bank/action/viewAsset?id=11148&index=6&total=23&view=viewSearchItem

[6] ESS internal report (ESS-0049053).

[7] ESS. How It Works | ESS [Internet]. Lund: ESS; [date unknown] [cited 2021 Jan 7]. Available from: https://europeanspallationsource.se/accelerator/how-it-works

[8] ESS. Accelerator | ESS [Internet]. Lund: ESS; [date unknown] [cited 2021 Jan 7]. Available from: https://europeanspallationsource.se/accelerator

[9] ESS. Machine Systems Advance at Bilbao as Spain Makes a Move Toward Full ERIC Membership | ESS. A cutaway view of the Monolith, showing Target System components in the Monolith and the connection cell above it. [Internet]. Lund: ESS; 2018 [cited 2021 Apr 13]. Available from: https://europeanspallationsource.se/article/2018/01/15/machine-systems-advance-bilbao-spain-makes-move-toward-full-eric-membership

[10] Lawrence Berkeley National Laboratory. Modelica.Fluid.UsersGuide.ComponentDefinition [Internet]. Berkeley: Lawrence Berkeley National Laboratory; [date unknown] [cited 2021 Jun 22]. Available from: https://simulationresearch.lbl.gov/modelica/releases/msl/3.2/help/Modelica_Fluid_UsersGuide_ComponentDefinition.html

[11] Dassault Systèmes. Dymola - Dassault Systèmes® [Internet]. Vélizy-Villacoublay: Dassault Systèmes; [date unknown] [cited 2021 Jan 7]. Available from: https://www.3ds.com/products-services/catia/products/dymola/

[12] Modelica Association. The Modelica Association — Modelica Association [Internet]. Modelica Association; [date unknown] [cited 2021 Jan 7]. Available from: https://modelica.org/

[13] Lawrence Berkeley National Laboratory. Modelica Buildings library [Internet]. Berkeley: Lawrence Berkeley National Laboratory; [date unknown] [cited 2021 Jan 7]. Available from: https://simulationresearch.lbl.gov/modelica/index.html

[14] ESS internal report (ESS-0012527).

[15] ESS internal report (ESS-0040858).

[16] ESS internal report (ESS-0040861).

[17] ESS internal report (ESS-0040860).

[18] ESS internal report (ESS-0043291).

[19] ESS internal report (ESS-0040874).

[20] ESS internal report (ESS-0046901).

[21] ESS. Machine Systems Advance at Bilbao as Spain Makes a Move Toward Full ERIC Membership | ESS [Internet]. Lund: ESS; 2018 [cited 2021 Apr 13]. Available from: https://europeanspallationsource.se/article/2018/01/15/machine-systems-advance-bilbao-spain-makes-move-toward-full-eric-membership

[22] ESS internal report (ESS-0026363).

[23] ESS internal report (ESS-0018268).

[24] ESS internal report (ESS-0040856).

[25] ESS internal report (ESS-0062444).

[26] ESS internal report (ESS-0040857).

[27] ESS internal report (ESS-0115530).

[28] ESS internal report (ESS-2501109).

[29] Gallarotti M. How to avoid computationally expensive fluid networks in Dymola - Claytex [Internet]. Leamington Spa: Claytex; 2016 [cited 2021 Jan 7]. Available from: https://www.claytex.com/blog/how-to-avoid-computationally-expensive-fluid-networks-in-dymola/

[30] Open Source Modelica Consortium. Modelica.Fluid.Examples.HeatingSystem [Internet]. Open Source Modelica Consortium; [date unknown] [cited 2021 Apr 28]. Available from: https://build.openmodelica.org/Documentation/Modelica.Fluid.Examples.HeatingSystem.html

[31] Lawrence Berkeley National Laboratory. 2. Best Practice — Buildings Library User Guide [Internet]. Berkeley: Lawrence Berkeley National Library; [date unknown] [cited 2021 Jan 7]. Available from: https://simulationresearch.lbl.gov/modelica/userGuide/bestPractice.html

[32] ESS internal report (ESS-0105544).

[33] ESS internal report (ESS-3048832).

[34] ESS internal report (ESS-0120692).

[35] Idelchik IE. Handbook of Hydraulic Resistance. 1st ed. Barouch A, translator. Jerusalem: Isreal Program for Scientific Translations; 1966.

[36] Lawrence Berkeley National Laboratory. Modelica.Fluid.Fittings.SimpleGenericOrifice [Internet]. Berkeley: Lawrence Berkeley National Library; [date unknown] [cited 2021 May 13]. Available from: https://build.openmodelica.org/Documentation/Modelica.Fluid.Fittings.SimpleGenericOrifice.html

[37] Crane Co. Flow of fluids through valves, fittings and pipe. New York: Crane Co; 1982.

[38] ESS internal report (ESS-2713050).

[39] ESS internal report (ESS-2767489).

[40] Grundfos. Kv and Kvs values [Internet]. Bjerringbro: Grundfos; [date unknown] [cited 2021 Jan 27]. Available from: https://www.grundfos.com/ww/learn/research-and-insights/kv-and-kvs-values

[41] Native Dynamics. Pressure Loss Cv and Kv Method | Neutrium [Internet]. Native Dynamics; 2012 [cited 2021 Apr 30]. Available from: https://neutrium.net/fluid-flow/pressure-loss-cv-and-kv-method/

[42] Young DF, Munson BR, Okiishi TH, Huebsch WW. Introduction to Fluid Mechanics. 5th ed. John Wiley & Sons Inc; 2011.

[43] ThyssenKrupp AG. Stainless Steel 316L - 1.4404 Data Sheet - thyssenkrupp Materials (UK) [Internet]. Essen: ThyssenKrupp AG; [date unknown] [cited 2021 Jan 27]. Available from: https://www.thyssenkrupp-materials.co.uk/stainless-steel-316l-14404.html

[44] Sundén B. Introduction to Heat Transfer. Southampton: WIT Press; 2012.

[45] Kosky P, Balmer R, Keat W, Wise G. Exploring Engineering [Internet]. 3rd ed. New York: Elsevier Inc; 2013 [cited 2021 Feb 8]. Available from: https://linkinghub.elsevier.com/retrieve/pii/B9780124158917000121

[46] ESS internal report (ESS-2713052).

[47] AutomationForum. Control valve characteristics | Instrumentation and Control Engineering [Internet]. AutomationForum; [date unknown] [cited 2021 Feb 3]. Available from: https://automationforum.co/control-valve-characteristics/

[48] ESS internal report (ESS-3212459).

[49] Ventim Ventil & Instrument AB. Strainer VM6312 [Internet]. Kalmar: Ventim Ventil & Instrument AB; 2015 [cited 2021 Jan 19]. Available from: https://www.ventim.se/smutsfilter/smutsfilter-vm6312

[50] Planetcalc LLC. Online calculator: Circular segment [Internet]. Moscow: Planetcalc LLC;

[date unknown] [cited 2021 Jan 29]. Available from: https://planetcalc.com/1421/

[51] ESS internal report (ESS-1074941).

[52] Page JD. Area and height of a circle segment with calculator- Math Open Reference [Internet]. Unknown: Math Open Reference; [date unknown] [cited 2021 May 6]. Available from: https://www.mathopenref.com/segmentareaht.html

[53] ESS internal report (ESS-1074942).

[54] ESS internal report (ESS-1074935).

[55] ESS internal report (ESS-1729722).

[56] ESS internal report (ESS-1729723).

[57] ESS internal report (ESS-1729719).

[58] ESS internal report (ESS-1074936).

[59] Variohm Eurosensor Limited. How Does an RTD Work? [Internet]. Towcester: Variohm Eurosensor Limited; 2019 [cited 2021 Apr 21]. Available from: https://www.variohm.com/news-media/technical-blog-archive/how-does-an-rtd-work-

[60] Barani J. Difference between sensor response time and sensor time constant τ (tau) 63.2%. — BARANI DESIGN Technologies [Internet]. Bratislava: BARANI DESIGN technologies; 2019 [cited 2021 Feb 3]. Available from: https://www.baranidesign.com/faq-articles/2019/5/6/difference-between-sensor-response-time-and-sensor-time-constant-tau

[61] ESS. 01 System Introduction - Moderator & Reflector Systems - ESS Inside [Internet]. Lund: ESS; [date unknown] [cited 2021 Apr 21]. Available from: https://confluence.esss.lu.se/display/MRS/01+System+Introduction?preview=/209977634/209977649/WP3 Moderator and Reflector.pdf

[62] ESS internal report (ESS-0111269).

[63] ESS internal report (ESS-0066480).

[64] ESS internal report (ESS-0110608).

[65] ESS internal report (ESS-0464441).

[66] ESS internal report (ESS-0067142).

[67] ESS internal report (ESS-0066872).

[68] The World Material. AL 6061-T6 Aluminum Alloy Properties, Density, Tensile & Yield Strength, Thermal Conductivity, Modulus of Elasticity, Welding [Internet]. The World Material; [date unknown] [cited 2021 Feb 4]. Available from: https://www.theworldmaterial.com/al-6061-t6-aluminum-alloy/

[69] 1041-W-001 specification (ESS-2126668).

[70] ESS internal report (ESS-2127048).

[71] ESS internal report (ESS-1103126).

[72] ESS internal report (ESS-0036510).

[73] Emerson Automation Solutions. CONTROL VALVE HANDBOOK. 5th ed. Marshalltown: Emerson Automation Solutions; 2019.

[74] KSB. Pump affinity laws | KSB [Internet]. Frankenthal: KSB; [date unknown] [cited 2021 May 13]. Available from: https://www.ksb.com/centrifugal-pump-lexicon/pump-affinity-laws/191832/

[75] Open Source Modelica Consortium. Modelica.Fluid.Types.Dynamics [Internet]. Open Source Modelica Consortium; [date unknown] [cited 2021 Apr 23]. Available from: https://build.openmodelica.org/Documentation/Modelica.Fluid.Types.Dynamics.html

[76] Kristensen MR, Jørgensen JB, Thomsen PG, Jørgensen SB. An ESDIRK method with sensitivity analysis capabilities. Comput Chem Eng. 2004 Nov 15;28(12):2695–707.

[77] Dassault Systèmes AB. Dymola User Manual Volume 1. Lund: Dassault Systèmes AB; 2018.

[78] ESS internal report (ESS-0034299).